



TECHNISCHE UNIVERSITÄT MÜNCHEN

III. Medizinische Klinik und Poliklinik

Klinikum rechts der Isar

und

Lehrstuhl für Systembiologie der Pflanzen

The role of the SCF^{Fbxo9} ubiquitin ligase in the pathogenesis and therapy of multiple myeloma

Bianca-Sabrina Targosz, M.Sc.

Vollständiger Abdruck der von der Fakultät Wissenschaftszentrum Weihenstephan für Ernährung, Landnutzung und Umwelt der Technischen Universität München zur Erlangung des akademischen Grades eines *Doktors der Naturwissenschaften* genehmigten Dissertation.

Vorsitzender: Univ.- Prof. Dr. B. Küster
Prüfer der Dissertation: 1. Priv.-Doz. Dr. F. Chr. Bassermann
2. Univ.- Prof. Dr. C. Schwechheimer

Die Dissertation wurde am 30.01.2013 bei der Technischen Universität München eingereicht und durch die Fakultät Wissenschaftszentrum Weihenstephan für Ernährung, Landnutzung und Umwelt am 29.04.2013 angenommen.

Table of contents

Table of contents.....	1-2
1 Abstract.....	1-6
2 Abbreviations	2-7
3 Introduction	3-10
3.1 Multiple Myeloma.....	3-10
3.1.1 Molecular characteristics.....	3-10
3.1.2 Clinical manifestations.....	3-11
3.1.3 Current treatment.....	3-13
3.1.4 FBXO9 locus in MM patients	3-14
3.2 The ubiquitin proteasome system.....	3-15
3.2.1 Ubiquitin	3-15
3.2.2 The Proteasome	3-16
3.2.3 Ubiquitylation	3-18
3.2.4 Deubiquitylating enzymes.....	3-21
3.3 The mTOR pathway	3-23
3.3.1 mTOR.....	3-23
3.3.2 mTOR complex 1	3-24
3.3.3 mTOR complex 2.....	3-25
3.3.4 mTORC1 and mTORC2 – feedback inhibition.....	3-26
3.3.5 Tti1/Tel2.....	3-27
3.4 Aim of the study	3-28
4 Materials and Methods	4-29
4.1 Materials.....	4-29
4.1.1 Chemicals.....	4-29
4.1.2 Media and supplements for cell culture	4-31
4.1.3 Antibiotics.....	4-31
4.1.4 Transfection reagents	4-31
4.1.5 Enzymes	4-31
4.1.6 Inhibitors	4-32
4.1.7 Molecular weight standards for DNA and proteins.....	4-32
4.1.8 Molecular biological Kits.....	4-32
4.1.9 Buffers.....	4-32

4.1.10	Antibodies	4-35
4.1.11	Plasmids	4-36
4.1.12	Oligonucleotides.....	4-38
4.1.13	Lentiviral particles.....	4-41
4.1.14	Patient samples	4-41
4.1.15	Mice.....	4-41
4.1.16	Bacteria	4-41
4.1.17	Cell lines.....	4-42
4.1.18	Cell culture dishes	4-42
4.1.19	Membrane	4-42
4.1.20	Machinery and equipment.....	4-43
4.1.21	Software and Databases	4-43
4.2	Methods	4-44
4.2.1	Molecular biology	4-44
4.2.2	Protein biochemistry	4-46
4.2.3	Antibody production	4-49
4.2.4	Murine liver cell extraction.....	4-50
4.2.5	Eukaryotic cell culture	4-50
4.2.6	Insect cell culture	4-55
4.2.7	Bacteria cell culture.....	4-56
4.2.8	Data mining.....	4-56
5	Results	5-57
5.1	Fbxo9 mediates degradation of Tel2 and Tti1 proteins in response to serum withdrawal to regulate mTOR abundance and function.....	5-57
5.1.1	Fbxo9 interacts with Tel2 and Tti1	5-57
5.1.2	SCF ^{Fbxo9} ubiquitylates Tel2/Tti1.....	5-60
5.1.3	Tel2/Tti1 protein levels decrease upon serum withdrawal.....	5-62
5.1.4	Fbxo9 loss impairs proteasomal degradation of Tel2/Tti1 under serum deprivation..	5-65
5.1.5	The function of Tel2/Tti1 in serum deprivation is modulated by loss of Fbxo9.....	5-67
5.1.6	Tti1/Tel2 degradation and its impact on mTOR functions upon serum withdrawal...	5-68
5.2	Phospho-degron dependent ubiquitylation of Tel2/Tti1 via Fbxo9 regulates mTOR signalling	5-71
5.2.1	Identification of the degrons	5-71
5.2.2	Biological relevance of Fbxo9-specific phospho-degrons in Tel2/Tti1 in the context of serum deprivation.....	5-74

5.2.3	Ubiquitylation is dependent on phospho-degrons of Tel2/Tti1.....	5-76
5.3	CK2 associates with Tel2 and Tti1 upon growth factor withdrawal to mediate degra- n-specific phosphorylation and Fbxo9-dependent degradation.....	5-78
5.3.1	Identification of CK2 as kinase for Fbxo9-specific degrons in Tel2/Tti1.....	5-78
5.3.2	Regulation of CK2 activity towards Tel2/Tti1 under serum deprivation.....	5-80
5.3.3	Depletion of CK2 impacts on Tel2/Tti1 degradation upon serum withdrawal.....	5-81
5.3.4	Phospho-mimic of Tel2 degron co-localises with Fbxo9.....	5-83
5.4	Fbxo9 preferentially targets mTORC1-bound Tel2/Tti1, thereby activating mTORC2 signalling.....	5-83
5.4.1	Fbxo9 targets mTORC1 associated Tel2/Tti1.....	5-83
5.4.2	Overexpression of Fbxo9 and CK2 enhances mTORC2 signalling.....	5-86
5.4.3	Tel2/Tti1 degradation is relevant for mTOR signalling in vivo.....	5-88
5.5	Fbxo9 is overexpressed in MM to promote survival.....	5-89
6	Discussion.....	6-96
6.1	CK2 and SCF ^{Fbxo9} regulate mTOR signalling in response to serum deprivation via targeted proteasomal degradation of Tel2/Tti1.....	6-97
6.2	Fbxo9 dependent degradation of Tel2/Tti1 is deregulated in MM to promote survival via asymmetric activation of mTOR pathways.....	6-102
6.3	Summary.....	6-107
7	Literature.....	7-108
8	List of figures and tables.....	8-119
8.1	Figures.....	8-119
8.2	Tables.....	8-122
9	Publications.....	9-123
10	Danksagung.....	10-124

Für meine Großmütter

Danke für die Gene

1 Abstract

Multiple myeloma (MM) is the second most common hematologic neoplasm in Europe. This incurable blood malignancy is characterised by a high incidence of genomic instability and high clinical response rates to treatment with proteasomal inhibitors. The ubiquitin proteasome system (UPS) comprises a large and conserved network of processes that accurately regulate protein levels, turnover and functions in both spatial and timely manner, to ensure balanced metabolism, genomic stability and controlled proliferation of the cell. Major components of this system are the proteasome, which proteolytically degrades proteins marked by polyubiquitin, and the ubiquitin ligases (E3), which at the end of an enzymatic activation cascade target-specifically transfer ubiquitin. Prominent E3 ligases are the Skp1/Cullin/F-box protein (SCF)-complexes, of which only handfuls have been matched to specific targets and functions. To date, even though proteasome inhibition has been established as a successful treatment strategy, the identity of underlying deregulated UPS-dependent events in MM has remained unknown. In search of potential candidates, analyses of comparative genomic hybridisation arrays in MM identified a significant amplification of the FBXO9 locus, coding for the orphan F-box protein defining the SCF^{Fbxo9} (SCF defined by the F-box protein Fbxo9) ubiquitin ligase of unknown function. In an unbiased screen, this study identified Tel2 (Telomere maintenance 2) and Tti1 (Tel2 interacting protein 1) proteins as ubiquitylation substrates of SCF^{Fbxo9}, which adjusts mTOR (mammalian Target of Rapamycin) signalling to growth factor availability. When deprived of nutrients and mitogens, cells restrain resource-consuming processes to favour pro-survival pathways by a yet poorly understood mechanism. The PIKK (Phosphoinositide 3-kinase [PI3K]-related kinase) family member mTOR governs cell growth and protein translation via the multimeric mTOR complex 1 (mTORC1) and survival via mTORC2. Tel2 and Tti1 control the cellular abundance of mammalian PIKKs and are integral components of both mTORC1 and mTORC2. Presented experiments show that selective degradation of Tel2/Tti1 within mTORC1 is procured by CK2 (Casein kinase 2), which upon growth factor withdrawal translocates to the cytoplasm, to phosphorylate Tel2 and Tti1 degrons. mTORC1 inactivation prompts activation of the PI3K/mTORC2/Akt pathway via relief of feedback inhibition on mTORC2. This mechanism restrains the resource-consuming processes of cellular growth and protein translation, yet sustains survival upon growth factor withdrawal. Significantly, primary human multiple myelomas display high expression levels of Fbxo9. In this setting, PI3K/mTORC2/Akt signalling and survival of MM cells is shown to be dependent on Fbxo9 expression. Thus, this study defined mTORC1-specific degradation of Tel2 and Tti1 proteins as a central mTOR regulatory mechanism with clinical implications in MM, both in predicting the patient response to proteasomal inhibition and in providing novel targets - Fbxo9, CK2 - for the specific treatment of MM.

2 Abbreviations

(γ)ATP	([γ -32P])Adenosine triphosphate	DMSO	Dimethyl sulfoxide
³⁵ S	Radioactive sulfur	DNA.....	Desoxyribonucleic acid
4E-BP1.....	eIF4E binding protein 1	DNA-PKcs	DNA protein kinase
AGC.....	related to PKA, PKG, and PKC	dNTP.....	Deoxynucleotide triphosphate
APS.....	Ammonium persulfate	DUB(s).....	Deubiquitylating enzyme(s)
ATM	Ataxia telangiectasia mutated	E,Glu.....	Glutamic acid
ATR.....	ATM and RAD5 related	E1	Ubiquitin activating enzyme
b,bp	basepairs	E2.....	Ubiquitin conjugating enzyme
BES.....	N,N-Bis(2-hydroxyethyl)-2- aminoethanesulfonic acid	E3.....	Ubiquitin ligase
BMM	Bone marrow microenvironment	EDTA.....	Ethylendiamintetraacetic acid
BrdU	Bromodesoxyuridin	eIF4E.....	eukaryotic Initiation factor 4E
BSA	Albumin fraction V	Em.....	Emission
C, Cys	Cysteine	ERK1/2	Extracellular-signal-regulated kinase 1/2
CaCl ₂	Calcium chloride	EV	Empty vector
cAMP.....	cyclic Adenosine monophosphate	Ex.....	Excitation
CaPO ₄	Calcium phosphate	FACS	Fluorescence Activated Cell Sorting
CDK.....	Cell cycle dependent kinase	FAT.....	FRAP, ATM, TRRAP
cDNA.....	complementary DNA	FBP	F-box protein
CGH.....	Comparative genomic hybridization	FGFR3	fibroblast growth factor receptor 3
cGMP.....	cyclic Guanine monophosphate	FRB	FKBP12-rapamycin binding
CK2.....	Casein kinase 2	FSC	Forward scatter
CP	Catalytic particle	G, Gly.....	Glycin
CRL	Cullin-Rbx1/Roc1-Ligases	G2P ..	Glycerol 2-phosphate disodium salt hydrate
C-terminus(al).....	Carboxy-terminus(al)	GAP	GTPase-activating protein
Cul1	Cullin1	GEO	Gene Expression Omnibus
D, Asn.....	Aspartic acid	Grb10 ...	Growth factor receptor-bound protein 10
Da	Dalton	GTP.....	Guanine triphosphate
DDR.....	DNA-damage response	HCl.....	Hydrochloric acid
Deptor	DEP domain containing mTOR- interacting protein	HEAT	Huntington, Elongation Factor 3, PR65/A, TOR
dH ₂ O	Distilled water	HECT	Homologous to the E6-AP carboxy terminus
DMEM.....	Dulbecco's Modified Eagle's Medium		

HEPES	4-(2-hydroxyethyl)-1-piperazineethanesulfonic acid	NFκB	Nuclear Factor 'kappa-light-chain-enhancer' of activated B-cells
hr(s).....	hour(s)	Noc.....	Nocodazole
IκKβ.....	IκB kinase β	N-terminus(al).....	Amino terminus(al)
IFNγ.....	Interferon γ	Ntn	N-terminal nucleophile
IGF.....	Insulin-like growth factors	OD ₆₀₀	Optical Density at 600nm
IgH.....	Immuno-globulin heavy-chain	PBS	Phosphate Buffered Saline
IL-6.....	Interleukin 6	PCR.....	Polymerase chain reaction
IMDM.....	Iscove's Modified Dulbecco's Media	PDCD 4.....	Programmed cell death protein 4
IMiDs.....	Immunomodulators	PFA.....	Paraformaldehyde
IPTG	Isopropyl β-D-1-thiogalactopyranoside	p-HH3	phosphorylated Histone H3
IRS	Insulin receptor substrate	PI3K.....	phosphoinositide 3-kinase
K, Lys	Lysine	PIKK.....	phosphoinositide 3-kinase related kinase
LTR.....	Long terminal repeats	PKA	cAMP-dependent protein kinase 1
M.....	Molar	PKB.....	Protein kinase B
M, Met	Methionine	PKCa.....	Protein kinase Ca
MCS.....	Multiple Cloning Site	PKG	cGMP-dependent protein kinase
MgCl ₂	Magnesium chloride	Plk1	Polo-like-kinase 1
MGUS.....	Monoclonal gammopathy of undetermined significance	PML	Promyelocytic leukemia protein
MHC I.....	major histocompatibility complex I	PMSF	Phenylmethylsulfonyl fluoride
min.....	minute(s)	PPTase	Phosphatase
mLST8.....	Lethal with sec-13 protein 8	PRAS40	Proline-rich Akt substrate 40 kDa
MM.....	Multiple myeloma	Protor1/2	Protein observed with rictor 1 and 2
MS	Mass spectrometry	PTM	Post-translational modification
mSin1 ...	mammalian Stress-activated map kinase-interacting protein 1	qPCR.....	Quantitative PCR
mTOR	mammalian Target of rapamycin	Raptor.....	Regulatory associated protein of mTOR
mTORC1/2	mTOR complex 1 and 2	Rheb	Ras homologue enriched in brain
MW.....	Molecular weight	Rictor	Rapamycin-insensitive companion of mTOR
Na ₃ VO ₄	Sodium orthovanadate	RING.....	Really Interesting New Gene
NaCl.....	Sodium chloride	RNA.....	Ribonucleic acid
NaOH.....	Sodium hydroxid	RP.....	regulatory particle
		RT	Room temperature

RTK	Receptor Tyrosine Kinase	TEMED.....	Tetramethylethylenediamine
S	Serum	Thy	Thymidine
S, Ser.....	Serine	TLCK	Tosyl-L-lysyl-chloromethyl ketone hydrochloride
S6K1	p70-S6 kinase 1	TNF α	Tumor necrosis factor α
SA	Serum addition	TPCK ...	Tosyl-phenylalanyl-chloromethyl ketone
SCF	Skp1/Cullin/F-box	Tris	Tris(hydroxymethyl)aminomethane
sd.....	Standard deviation	TRRAP....	Transformation/ transcription domain– associated protein
SD	Serum deprivation	TSC1/2.....	Tuberous sclerosis 1/2
SDS.....	Sodium dodecylsulfate	Tti1	Tel2 interacting protein 1
sec	second(s)	TU	Titer Units
SGK ..	Serum and glucocorticoid-inducible kinase	Ub.....	Ubiquitin
shRNA	small hairpin RNA	Ubc.....	Ubiquitin conjugating enzyme
siRNA	small interfering RNA	UPS	Ubiquitin proteasome system
SMG1 ..	Suppressor with morphological effect on genitalia 1	VCAM	Vascular cell adhesion molecule
SSC	Sideward scatter	VEGF	Vascular endothelial growth factor
T, Thr.....	Threonine	VLA-4	Very late antigen-4
TAP.....	Tandem Affinity Purification	vol	volumes (unit)
TBB	4,5,6,7-tetrabromobenzotriazole	WB	Washing Buffer
TBE.....	Tris/Borate/EDTA	WCE.....	Whole cell extracts
TBS.....	Tris Buffered Saline	WT	wildtype
TCA	Trichloroacetic acid	β -TrCP	β -transducin repeat containing protein
Tel2.....	Telomere maintenance 2		

3 Introduction

3.1 Multiple Myeloma

Multiple myeloma (MM) is a clonal disease of plasma cells, which accounts for ~1% of all cancers and for ~13% of hematological neoplasms, making it the second most common hematologic malignancy². Annual incidence of MM in Europe is 6.0 cases per 100,000 persons with a median age at diagnosis between 63 and 70 years³. To date MM remains an incurable disease, still associated with poor prognosis and mortality rates of 4.1 cases per 100,000 persons³. Thus, there is an urgent need for more effective treatment strategies, which require fundamental research and better understanding of the causative factors involved in pathogenesis of MM.

3.1.1 Molecular characteristics

Plasma cells are long-lived antibody producing cells important for the response of the adaptive immune system⁴. Originally derived from B-cells, which undergo immunoglobulin gene recombination, class switching and somatic hypermutation during the differentiation process in the germinal centres of lymphoid tissues, to ensure optimal pathogen and antigen recognition⁵, plasma cells maintain a phenotype of high genetic variability. Once terminally differentiated, plasma cells remain quiescent, unable to proliferate⁶ and localise to the bone marrow, which is referred to as “homing”⁷. Within the tightly balanced bone marrow microenvironment (BMM), the interactions with adhesion molecules of stromal cells and extracellular matrix proteins, and the stimulation of various cytokines cooperate to maintain plasma cells⁸.

MM cells are malignantly transformed plasma cells, which proliferate uncontrollably, resulting in abnormally high numbers of MM cells in the bone marrow. Originating from plasma cells, they also produce and secrete a large amount of antibodies. In case of MM cells, these antibodies are monoclonal and often dysfunctional, and also referred to as M protein or paraprotein⁸. On the genetic level, mainly two types of primary chromosomal aberrations are thought to cause the malignant transformation of plasma cells⁹⁻¹⁰. Frequently, primary translocations involve the immuno-globulin heavy-chain (IgH) locus on chromosome 14, which is juxtaposed to chromosomal loci coding for known oncogenes such as cyclin D1 (*CCND1* (t[11;14][q13;q32.33])) and FGFR3 (Fibroblast growth factor receptor 3) (*FGFR3* (t[4;14][p16.3;q32.33])). In another subset of MM cells, karyotypes display a hyperdiploid state with occurrence of multiple trisomies². It is assumed that this pre-malignant state allows for enhanced oncogene expression and thus facilitates a subsequent accumulation of multiple secondary mutations, which eventually result in malignant transformation. As such, high incidence of chromosomal instability is a hallmark of MM¹¹. Furthermore, distinct genetic aberrations have been differentially correlated with prognosis, disease progression and resistance to therapy^{2, 12-13}, which

makes characterization and treatment of MM a difficult task. Homing of the myeloma cells to the BMM additionally promotes their clonal expansion through growth stimulating interactions⁸. Cell adhesion mediated signaling activates several pro-survival pathways, cell cycle progression and secretion of cytokines. For example, binding of the cell surface molecule VLA-4 (Very late antigen-4) of MM cells to the VCAM (vascular cell adhesion molecule) surface receptor of the bone marrow stromal cells activates the pro-survival NF- κ B (Nuclear factor 'kappa-light-chain-enhancer' of activated B-cells) pathway and hence production of the growth and survival factor IL-6 (Interleukin 6) in the stromal cells, which subsequently activates MM cells to secrete pro-angiogenic VEGF (Vascular endothelial growth factor)⁸. In a paracrine loop, VEGF expression further stimulates IL-6 secretion¹⁴, vastly changing the balanced composition of the microenvironment to favour proliferation and expansion. Another late-stage effect of this imbalance lies in the aberrant neo-angiogenesis within the BMM, promoted by an excess of pro-angiogenic factors, which further promotes spreading of the MM cells¹⁵.

Together, the pathogenesis of MM results mainly from the distinct cellular context from which tumor cells originate. The susceptibility for genetic rearrangements and the homing to a growth factor rich microenvironment, which are characteristic for plasma cells, represent major disease promoting factors. Similarly distinct as the underlying molecular aspects of MM, are its clinical manifestations that will be introduced in the following.

3.1.2 Clinical manifestations

MM is a slowly progressing malignancy with a proliferative rate of less than 1%¹³. Diagnosis is based on the electrophoretic detection of monoclonal protein in either blood or urine, depicting the secretory activity of MM cells. Quantifying serum levels of the different immunoglobulins (IgG, IgA and IgM) may show aberrantly high levels, depending on the type of MM, and detection of immunoglobulin derived light chains in urine can also be indicative of the excess secretory activity of MM cells^{3, 8}. However, there are also non-secretory forms of MM¹⁶. Of further value are analyses of bone marrow aspirates and biopsies, to monitor infiltration rates, cell morphology, karyotype aberrations, and abnormally high density of blood vessels^{3, 8}. In addition, due to the altered microenvironment in the bone marrow, bone remodelling is severely imbalanced⁸. Inhibition of the bone-forming osteoblasts and concomitant activation of osteoclasts responsible for bone resorption leads to lytic bone lesions, detectable in more than 90% of myeloma cases by medical imaging^{3, 12, 17}. Further, calcium usually retained in the mineral storage of the bones is released to body fluids, which may lead to hypocalcaemia and renal insufficiency⁸. Deregulation of the BMM may also interfere with lymphocyte assisted red blood cell maturation and clinically manifest in anaemia¹². While the massive overproduction of monoclonal protein primarily reduces the capacity of the immune response,

secondary effects may be hyperviscosity in the blood stream or renal failure². Impairment of kidney function is thought to be caused by the toxic effects of excess monoclonal light chains and their aggregated precipitates that may form casts in the renal tubules¹⁸. Due to its high genomic variability, not all diagnostic markers for MM can be found in each patient at all times. As such, to confidently diagnose MM, combined knowledge of all possible examinations is required. Subsequently, for an unified prognosis, the international staging system (ISS) can be utilised¹⁹.

Different stages of MM are defined according to the severity of symptoms and progression of the disease² (s. Figure 1). Generally, tumor cells rarely occur *de novo*, but evolve from a premalignant state called monoclonal gammopathy of undetermined significance (MGUS), which is defined by a serum monoclonal protein level of less than 3 g/100 ml and less than 10% monoclonal plasma cells in the bone marrow as well as absence of disease associated symptoms and end-organ damage²⁰. The risk of progression from MGUS to MM is ~ 1% per year²¹. MM is defined by elevated serum levels of monoclonal protein and more than 10% bone marrow infiltration²⁰. In asymptomatic or smouldering myeloma, disease associated symptoms and/or end-organ damage cannot be detected, while the

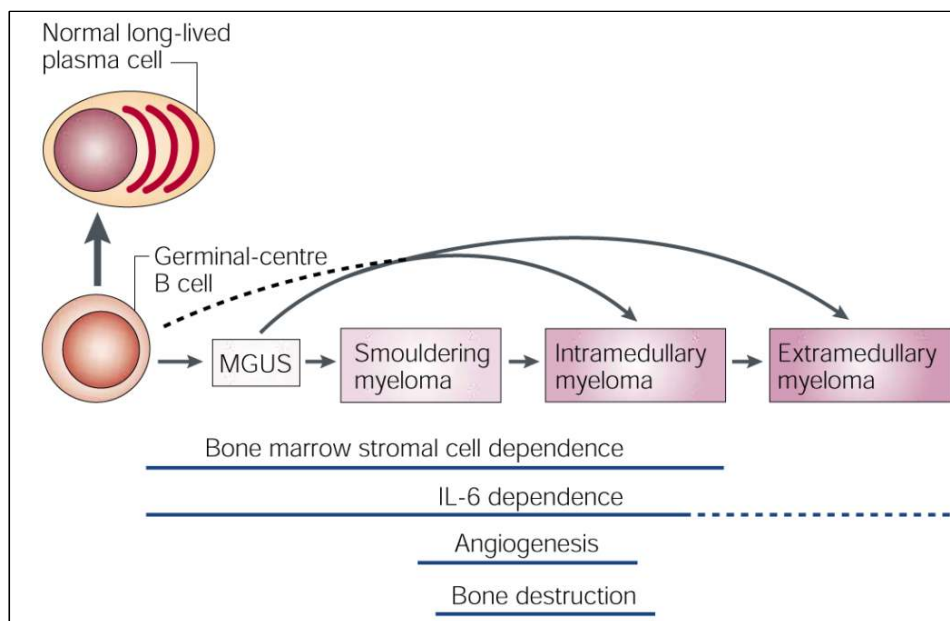


Figure 1: Different stages of MM. Myeloma arises from a normal germinal-centre B cell, which normally differentiates into a plasma cell. In most cases MM arises from the pre-malignant plasma cell neoplasm monoclonal gammopathy of undetermined significance (MGUS). The dashed line indicates rare *in situ* generation of MM. MGUS does not always pass through a period of smouldering myeloma. Initially, multiple myeloma is confined to the bone marrow (intramedullary), but with time the tumor can acquire the ability to grow in extramedullary locations. The transition of MGUS to intramedullary multiple myeloma is manifested by increased numbers of MM cells at multiple foci, and also associated angiogenesis and osteolytic bone destruction (adapted from Kuehl & Bergsagel²²)

symptomatic MM presents with medical conditions. Intramedullary MM is most common, since survival of the myeloma cells is dependent on the homing to the BMM; however, more aggressive forms of MM become bone marrow independent. Common extramedullary sites include blood, pleural fluid, and skin²³. MM can further progress to become plasma cell leukaemia, which is defined by absolute plasma cell count of more than 2×10^9 cells/l or on the presence of more than 20% circulating plasma cells in the peripheral blood²⁴.

In summary, MM can present with several distinctive manifestations. Whereas progression from MGUS to MM is a slow process, once the development of MM has reached a certain threshold, diagnosis is associated with poor prognosis, with a median survival of 6 years and a 10-year survival of only 18%, demanding intensive medical care²⁵.

3.1.3 Current treatment

Even though recent therapies have greatly improved the frequency and duration of remissions in patients with MM, it remains an incurable hematologic cancer²⁶. The protective anti-apoptotic signalling within the BMM is often responsible for relapse of the disease and resistance to treatment⁷. First-line therapy involves combination of effective chemotherapeutics and, if advisable, autologous hematopoietic stem-cell transplantation². Until recently, conventional treatment included administration of DNA-damaging chemo-therapeutics, such as Vincristin and Adriamycin, and immunosuppressing steroids, e.g. Dexamethasone, which in combination produced response rates of 52–63%¹³. Introduction of the novel agents Bortezomib – a proteasome inhibitor –, and the immunomodulators (IMiDs) Thalidomide and Lenalidomide for MM treatment has dramatically improved survival for patients from before 3 years to now over 6 years²⁷⁻²⁸. For example, in a clinical trial, Bortezomib treatment improved response to 38% compared to 18% of conventional treatment with Dexamethasone²⁹. Initially administered to relapsing patients or those developing drug resistance, the novel compounds are now, often in combination with the above mentioned conventional chemotherapeutic drugs, widely used for first-line therapy of MM patients either eligible, or not, for transplantation¹³. Their major advantage compared to conventional drugs is their capability to induce MM cell death despite the action of BMM, and to counteract the negative symptoms of BMM deregulation³⁰. As such, administration of Bortezomib stimulates osteoblasts and inhibits osteoclasts, thereby increasing bone formation³¹, and further reduces VEGF driven angiogenesis⁸. So far, the exact underlying causes for these beneficial features have remained largely elusive. Noteworthy, single-agent activity for each of these novel drugs is only 25% to 50% when administered alone, and despite extended relapse-free intervals the majority of patients continue to suffer recurrent disease relapse and increasing degrees of drug resistance³². Continuing research therefore needs to focus on delineating the

pathophysiological mechanisms of MM in more detail to develop additional targeted treatments to enhance anti-tumor efficacy, avoid drug resistance, and improve patient outcome¹².

3.1.4 FBXO9 locus in MM patients

As mentioned in the former paragraph, proteasome inhibition seems to be a beneficial strategy for treatment of MM. Its effectiveness is striking, considering that universal blockage of proteasomal degradation simultaneously and unspecifically inhibits all mechanisms connected with the action of the ubiquitin proteasome system (UPS) (s. chapter 3.2) thus posing the question if distinct UPS pathways with essential implications in myelomagenesis exist. With this respect, in a comparative genomic hybridization (CGH) analysis in MM patients, which annotated frequent amplifications and deletions of a series of gene loci, just a handful of individual genes related to the UPS could be identified³³. One of those genes is FBXO9, which is encoded by the frequently amplified 6p21.1 locus (7.25×10^6 basepairs [7.25 Mb], 53 genes), coding for a so far uncharacterised F-box protein (FBP) (s. chapter 3.2.3.3). Fbxo9 is a protein of 447 amino acids (aa) with a predicted size of 53 kilo Dalton (kDa), which was initially identified as a tumor antigen in renal cell carcinoma³⁴. Fbxo9 is highly conserved from yeast to plants³⁵⁻³⁶, indicative for an important, if not indispensable role within the cell.

In summary, further research is required to fully understand the processes of malignant transformation in MM, which is a plasma cell malignancy, characterised by a slow but persistent progression and at the molecular level by a high incidence of genomic instability. The most frequent clinical presentations are bone lesions, immunodeficiency, renal failure, and anaemia, and additionally MM patients often suffer from relapse and increasing resistance to therapy. In an attempt to refine the treatment strategies for this hematologic neoplasm, elucidating the pathophysiological background of MM is of extreme importance. To this end, considering the evidently good responsiveness to proteasome inhibitor treatment, the role of UPS specific components could provide further clues as to the pathogenesis and therapy of MM.

3.2 The ubiquitin proteasome system

Initially identified as the major degradation pathway in cell cycle progression³⁷⁻³⁸, energy-dependent break-down of proteins by the ubiquitin proteasome system (UPS) has emerged to be important for a variety of cellular processes such as DNA damage response³⁹⁻⁴⁰, immune system⁴¹, mitochondrial life cycle⁴², apoptosis⁴³, and ageing⁴⁴. Vitality of the cell generally depends on a functional UPS, and its deregulation is found in numerous diseases, such as cancer⁴⁵, neurodegenerative disorders⁴⁶⁻⁴⁷, ischaemia⁴⁸, muscle wasting⁴⁹, fibrosis⁵⁰, renal diseases⁵¹, obesity⁵², and diabetes⁵².

Since its discovery in the 1970s and 1980s, the UPS has been extensively studied and its identification entailed the awarding of the Nobel Prize in Chemistry in 2004 to Aaron Ciechanover, Avram Hershko, and Irwin Rose⁵³. The following will introduce the main members of the UPS, their specific characteristics, functions, and how they are tightly regulated to adapt to various cellular processes.

3.2.1 Ubiquitin

Ubiquitin (Ub) is a protein of 76 aa and 8 kDa that was first identified in a screen for lymphocyte-differentiating polypeptides⁵⁴⁻⁵⁵. Adequately named for its ubiquitous expression in all tissues and high conservation in all eukaryotes⁵⁴⁻⁵⁵, ubiquitin was soon identified to be a key component of the UPS⁵⁶.

In a process called ubiquitylation, ubiquitin, via its carboxy-terminal (C-terminal) glycine (G), is covalently linked to the ϵ -amino group of lysine (K) in the target protein. For polypeptide sequences without lysine, this bond formation may occur to the amino-terminus (N-terminus) of the substrate⁵⁷. This post-translational modification (PTM) of proteins acts as a recognition signal and activates various processes in the cell. Attachment of a single ubiquitin molecule is generally considered to have regulatory functions, for example in remodelling of chromatin, DNA damage response (DDR), and receptor localisation⁵⁸⁻⁶⁰. However, additionally to mono-ubiquitylation, ubiquitin can also form polypeptide chains of several moieties. Basically, this polyubiquitylation can occur at each of the seven lysine residues (K6, K11, K27, K29, K33, K48, and K63) present in ubiquitin, as well as on its N-terminus (Figure 2a). The nature of the formed polymers is highly variable, since besides formation of homotypic chains – comprising only one linkage type – also heterotypic linkages are possible⁶¹. This highly variable “ubiquitin code” gives rise to both structurally and chemically distinct motifs (exemplified in Figure 2b), allowing for specific recognition of interactors by various ubiquitin binding domains⁶². The cellular responses to ubiquitylation are just as versatile, for example, K63-linked polyubiquitin chains have been implicated in regulation of NF- κ B (Nuclear Factor 'kappa-light-chain-enhancer' of activated B-cells) pathway signaling⁶³, while linkage via K11 marks targets for

degradation during mitotic progression⁶⁴. Altogether, amongst all these motifs with yet emerging roles, the most renowned one is K48-linked polyubiquitin chain formation of a minimum of four moieties, directing their targets for degradation by the proteasome⁶⁵⁻⁶⁶.

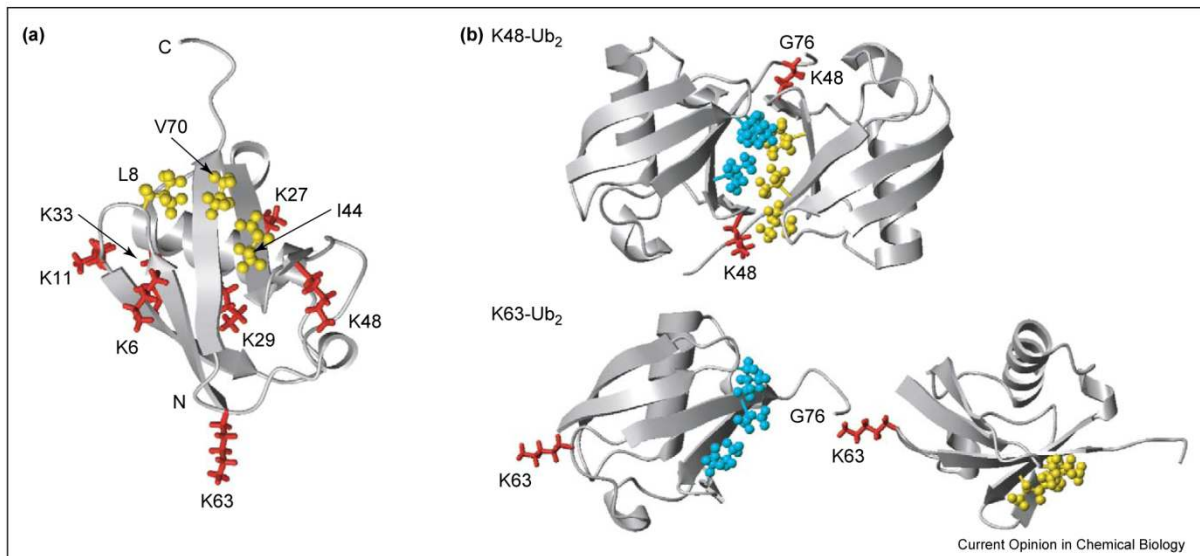


Figure 2: Ribbon diagrams of Ub and two forms of di-ubiquitin. (a) Functionally relevant features of the Ub structure. The seven lysine residues are shown in red and labelled, while the hydrophobic patch is shown in gold ball-and-stick. (b) Solution conformations of K48- (top) and K63-linked di-ubiquitin. The hydrophobic patches on Ub units are shown in ball-and-stick (coloured gold or cyan) along with the side chains of K48 and K63 in stick representation (red). The location of c-terminal Glycine (G76) forming an isopeptide bond with the corresponding lysine is indicated. (Taken from Pickart & Fushman⁶⁷)

3.2.2 The Proteasome

The 26S proteasome is the essential recycle machinery in cells, allowing for processive destruction of damaged, dysfunctional or inapplicable proteins and recovery of free amino acids. Concomitantly to their importance, proteasomes are localised to both nucleus and cytosol⁶⁸. Evolutionary, the structure and the composition of the proteasome are highly conserved in eukaryotes; and simpler forms can also be found in Archaeobacteria and Eubacteria⁶⁹. The 26S proteasome forms an ATP (Adenosine triphosphate)-dependent multimeric protein complex of >2500 kDa, mainly comprising the 20S core subunit and the 19S regulatory subunit. Those components are introduced in the following.

3.2.2.1 20S core subunit

Degradation of proteins takes place in the cylindrical cavity of the 20S core subunit – also called Catalytic particle (CP) – formed by four superimposed seven-membered rings⁷⁰. In higher eukaryotes, the inner two rings consist of seven different homologous β subunits, of which three ($\beta 5$, $\beta 2$, and $\beta 1$) display proteolytic activities at their N-terminal threonine (T) after prosequence processing during assembly⁷¹. This categorises the CP into the rare family of N-terminal nucleophile (Ntn) hydrolases⁷².

Structural analyses revealed that entry to the catalytic centre is sterically restricted by the two outer rings formed by seven different homologous α subunits to prevent non-specific degradation of cellular proteins⁷³. Of note, the 20S composition is highly conserved down to the archaeobacterium *Thermoplasma acidophilum*, where an “Urproteasome” was discovered with heptameric rings of seven identical β or α subunits⁷⁴ (Figure 3), respectively, indicating a functional refinement of the proteasome during evolution. While the catalytic activity of the CP is energy-independent, polyubiquitin chain-specific targeting and gate opening requires ATP breakdown by the 19S regulatory subunit.

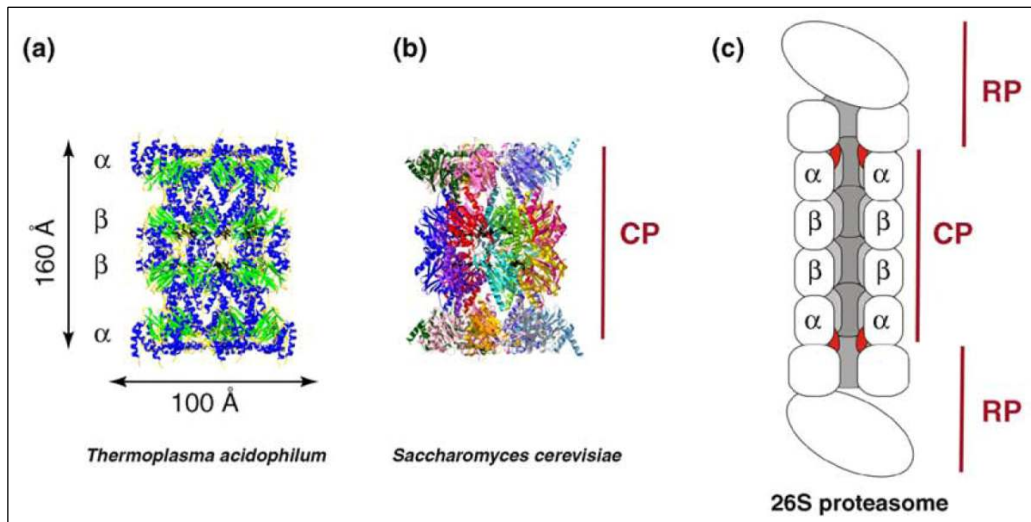


Figure 3: The structure of the proteasome. (a,b) Crystal structures of the 20S proteasome CP showing its cylindrical architecture composed of four stacked heptameric rings. (a) Most archaeobacterial CPs, as illustrated for *T.acidophilum*⁷⁴, contain 14 identical α and β subunits, whereas (b) eukaryotic CPs have seven different α and β subunits⁷⁵ (c) Eukaryotic CPs are ATP-dependently regulated by the 19S RP, here represented as a cartoon, reflecting the lack of high-resolution structural data. The RP recognises, unfolds and translocates Ub-tagged substrates into the active sites of the CP. (taken from Gallastgui & Groll⁷¹)

3.2.2.2 19S regulatory subunit

The 19S regulatory subunit or regulatory particle (RP) (also known as PA700) serves as an opener of the compact CP by a distorting association with the outer α subunits. The RP can be subdivided into the proximal lid and the more distal base⁷⁶. Consisting of a putative ring of six AAA+ ATPases, two ubiquitin receptors and two scaffold proteins, the base is generally thought to drive energy-coupled degradation of ubiquitylated substrates. Whether opening of the gate to the catalytic cavity is energy dependent or if the mere unfolding and translocation of proteins consumes all ATPase activity is subject of current research⁷⁷⁻⁷⁸. In contrast, the components of the lid have not shown ATPase activity, but are thought to be required for binding, recruiting and hydrolytic removal of polyubiquitin chains, as well as unfolding of marked proteins⁷⁹.

3.2.2.3 Immunoproteasome

An important variant of the proteasome is formed, when the three catalytic β subunits of the CP are replaced by analogous Interferon γ (IFN γ) induced subunits. Primarily stimulated by microbial infections, the so-called immunoproteasome functions in the proteolytic processing of foreign proteins into 8-10mer peptides for antigen presentation on the major histocompatibility complex I (MHC I) on the cell surface, ensuring an effective immune response⁴¹. This underscores the universal applicability of the UPS to conduct a broad range of cellular processes, whose regulation and specificity must be ensured.

In summary, proteasomal proteolysis is regulated by a variety of activating proteins that cause CP gate opening and allow specific substrate entry to the active site. However, owing to its complexity, effectiveness of the UPS requires another layer of regulatory enzymatic reactions, which are ubiquitylation and deubiquitylation. The mechanisms and involved enzymes are introduced below.

3.2.3 Ubiquitylation

The enzymes involved in the process of ubiquitylation were first described in 1983 and the mechanism was designated the ubiquitin cascade⁸⁰. The following will discuss how this cascade activates the biochemically unreactive Ub moieties for transfer and enables specific attachment to the substrate.

3.2.3.1 Enzymes of the ubiquitin cascade

Ubiquitylation is a multistep enzymatic process⁸¹. In a first ATP-requiring step, the C-terminus of Ub is activated to form a thioester bond with the cysteine (Cys) of the Ub-activating enzyme (E1). Ub is further transferred to the active site of a so-called Ub-conjugating enzyme (Ubc or E2) independently of energy via the highly energetic thioester. The E2 can specifically bind to the next enzyme in the cascade, which is the ubiquitin-ligase (E3) that aids in transfer of the activated Ub to the substrate⁸². There are only few enzymes of E1, a dozen of E2 and hundreds of E3 ligases known⁷³. Therefore it is assumed that specificity for the substrate is mainly ascertained by E3 ligases⁸³. However, binding preference of E2 enzymes to certain E3 ligases has been observed as well⁸⁴, further underscoring how ubiquitylation specificity is determined on the level of protein-protein interactions. A further attachment of Ub to build polyubiquitin chains can be executed via repetition of the same enzymatic cascade or involve yet another specialised so-called E4 enzyme, which is supposed to recognise and bind to mono-ubiquitylated substrates and mediate chain elongation⁸⁵.

3.2.3.2 Ubiquitin-ligases

Being the main mediators of specificity, E3 ligases must contain structurally distinct domains, which are important for substrate recognition, E2 binding, stability, and proximity of the activated Ub

and its cognate substrate⁸⁶. Ubiquitin ligases are subdivided into two major families: RING (Really Interesting New Gene) and HECT (Homologous to the E6-AP [E6 associated protein] Carboxy Terminus) domain-containing E3s⁸³. Proteins harbouring a HECT domain accept the activated Ub prior to transfer to the substrate, while most RING finger E3s assist the ubiquitylation by sterically coordinating the two reaction partners via a concurrent binding of E2 and substrate⁸⁷ (Figure 4). E3-ligases can identify specific structures in their target proteins, which are called degrons⁸⁸. To avoid constant recognition, ubiquitylation and thus degradation, these degrons are often buried within the structure of the substrate and only exposed upon misfolding or by PTM upon cellular signalling. For

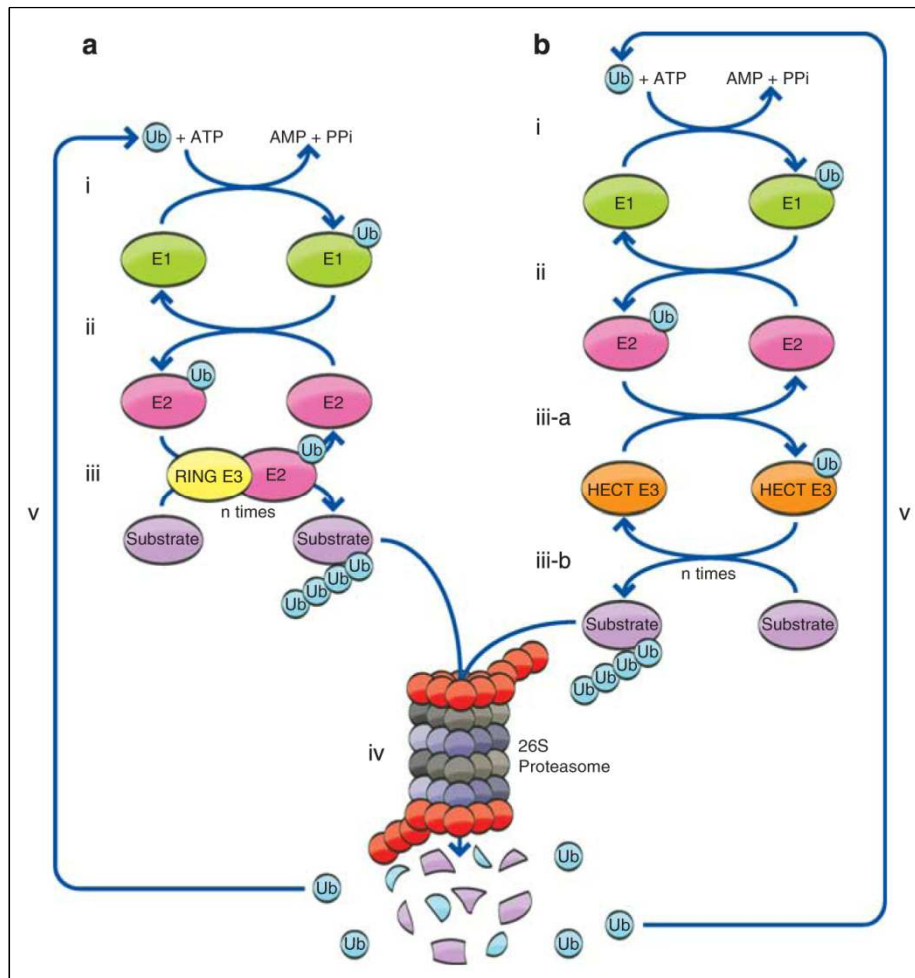


Figure 4: The ubiquitin-proteasome system. Conjugation of ubiquitin catalysed by RING (a) or HECT (b) domain-containing ligases. (ai, bi) ATP-dependent activation of ubiquitin catalysed by the ubiquitin-activating enzyme, E1. (a ii, b ii) Transfer of the activated ubiquitin to an ubiquitin-conjugating enzyme, E2. In the case of a RING ligase, the ubiquitin-charged E2 binds to the E3 and transfers the activated ubiquitin moiety directly to the substrate that is also bound to the E3 (a iii). In the case of a HECT domain ligase, ubiquitin is transferred from the E2 to a Cys residue in the E3 (b iii-a) and then to the substrate (b iii-b). (iv and v) The conjugated substrate is degraded to short peptides by the 26S proteasome (iv) with release of free and reusable ubiquitin mediated by DUB(s) (v). Some of the ubiquitin is degraded in this process along with the substrate (iv) (taken from deBie & Ciechanover⁸³)

example, the cell cycle inhibitor p27 is only polyubiquitylated after growth factor stimulated phosphorylation by Cell cycle dependent kinases (CDKs) at the transition to S-Phase, resulting in proteasomal degradation and hence cell cycle progression⁸⁹. Likewise ubiquitylating activity can be modulated at the level of the E3 for example by phosphorylation⁹⁰, neddylation⁹¹, (auto)ubiquitylation⁹² or activity of small molecules⁹³.

3.2.3.3 The Skp1/Cullin/F-box complex

One of the most prominent members of RING-like E3s is the Skp1/Cullin/F-box (SCF) complex, which was first identified as the main regulator of S-Phase progression⁹⁴. SCF complexes belong to the large superfamily of Cullin-Rbx1/Roc1-Ligases (CRLs) comprising ~200 protein complexes⁹⁵. They are generally composed of a Cullin protein (e.g. Cul1) serving as a scaffold protein bringing activated E2 and the E3-bound substrate in close proximity upon a neddylation-induced conformational change and Rbx1/Roc1 harbouring the catalytic RING subunit that recruits and

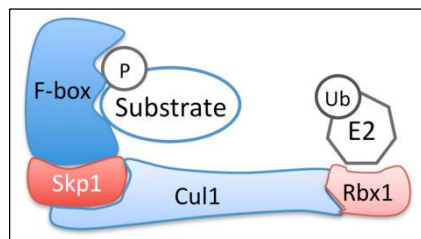


Figure 5: The SCF complex defined by the scaffold proteins Skp1 and Cul1, the RING-domain protein Rbx1 that binds and activates the Ub-bound E2, and an interchangeable F-box protein (FBP) that confers specificity to usually phosphorylated substrates. (adapted from Bassermann & Pagano¹)

activates the E2⁹⁵ (Figure 5). Associating with Cul1 on one side, the other part of Skp1 binds to a conserved motif called the F-box – for its first identification in Cyclin F, a cell cycle regulatory F-box protein⁹⁶. Based on sequence similarity, ~70 proteins have been classified as F-box proteins (FBP), which confer the substrate specificity to the SCF complex⁹⁷. However, most of these FBPs have remained uncharacterised to date. Mostly, specific recognition by FBPs is dependent on phosphorylation of the degron in its target⁸⁷ (Figure 5). FBPs are further categorised according to the binding motifs for their substrates: FBXW proteins display WD40 domains, FBXL proteins harbour leucine-rich repeats, and FBXO proteins contain other diverse domains⁹⁷⁻⁹⁸. While only a few FBP have been designated to substrates and/or cellular functions, each one of them play key roles in cell cycle control and tumorigenesis. For example, SCF^{Fbxw7} can function as a tumor suppressor by targeting positive regulators such as the anti-apoptotic molecule Mcl-1 as well as the cell cycle regulator cyclin E for degradation⁹⁹⁻¹⁰⁰, while Skp2 can function as an oncogene by targeting the cyclin dependent kinase inhibitors p27, p21, and p57⁹⁸. Thus, SCF complexes form defined CRLs with interchanging F-box proteins, whose exact cellular substrates and functions remain to be determined in most cases.

3.2.4 Deubiquitylating enzymes

Similar to other covalent modifications, ubiquitylation is reversible. The human genome harbours ~90 deubiquitylating enzymes (DUBs), which proteolytically cleave Ub off the substrates and terminate ubiquitin-dependent signalling to reverse its particular fate¹⁰¹. DUBs subdivide into five categories, of which four belong to Cys-proteases (USP, UCH, MJD, and OTU), while the remaining JAMM proteins coordinate their active centre via a Zn²⁺-ion, classifying it as a metalloprotease¹⁰². Although only few DUBs have been characterised so far, their implications cover a broad range of cellular processes (Figure 6). Deubiquitylating activity is required for maturation of free mono-ubiquitin, since premature ubiquitin is always transcribed bound to ribosomal proteins or as linear polyubiquitin chains¹⁰³. Other DUBs are crucial for recycling of free Ub at the proteasome, as for example the RP subunit Poh1, which removes polyubiquitin chains from the substrate just prior degradation¹⁰⁴. However, as described above, the most interesting function of DUBs is the specific opposition of ubiquitylation events by E3 ligases. This is exemplified by the action of Usp28 that counteracts the SCF^{Fbw7} mediated polyubiquitylation of c-Myc¹⁰⁵. The DUB and the E3 ligase establish a steady-state equilibrium of de- and ubiquitylated c-Myc which ensures an immediate responsiveness

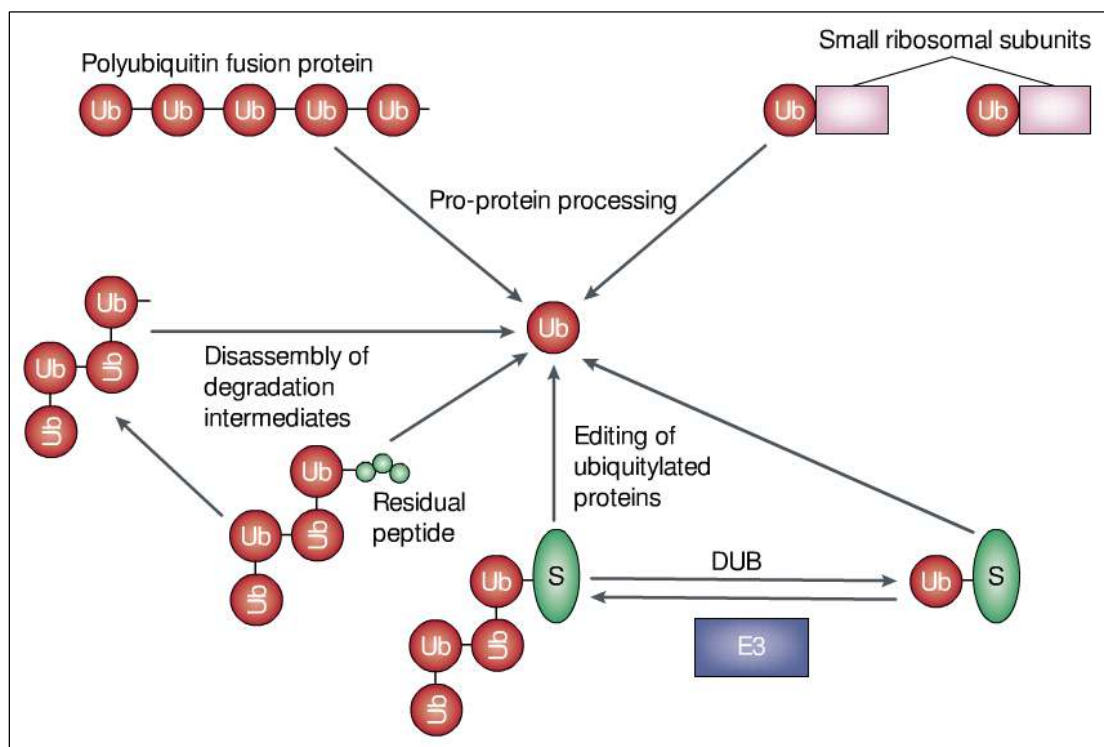


Figure 6: The many functions of deubiquitylating enzymes. Ubiquitin is synthesised as fusion proteins of ubiquitin (Ub) monomers (polyubiquitin) or with small ribosomal subunits, which are then processed by cleavage at the carboxy-terminal glycine. After the degradation of protein substrates, ubiquitin must be freed from residual peptides and disassembled. DUBs also reverse the activity of E3s, sequentially removing ubiquitin from substrates (S). (taken from Weissman⁸¹)

to cellular and environmental changes at minimal consumption of cellular energy for proteasomal degradation. Deregulation of this balanced state often results in cancer formation¹⁰⁵. Given their diverse functions, substrate recognition and target specificity of DUBs are not uniform as well. As for Usp28, a DUB can bind to its opposing ligase, thereby exerting its activity on the target¹⁰⁵, while others, such as Poh1, recognise the substrate via the polyubiquitin chains⁷⁶, and even others display a binding motif specific for the ubiquitylated substrate. Hydrolysis of ubiquitylation bonds can be processive removing one Ub after the other or direct by detaching ubiquitin polymers. In addition, certain preferences for lysine linkage-types have been reported¹⁰⁶. Furthermore, the DUB enzymes themselves can be regulated via variations in transcription and PTMs, as well as distinct cellular localisation¹⁰⁷. Thus, similarly to other members of the UPS, specificity of deubiquitylation is granted by a vast variety of regulatory modes, indicating an essential role for DUBs within the complex network of the UPS.

In summary, the UPS represents one of the most powerful, tightly regulated systems within the cell, functioning in almost every aspect of cellular mechanisms to maintain viability, integrity and genomic stability of a cell, whose full capacities still remain to be elucidated.

3.3 The mTOR pathway

A major task of every cell is to accurately couple protein synthesis, growth, and survival to nutrient, growth factor and energy availability, as well as efficiently adapt to different stress situations¹⁰⁸. At the heart of this process is the mammalian Target of Rapamycin (mTOR) signalling pathway, which senses and integrates environmental influences to modulate organismal growth and protein homeostasis¹⁰⁹. Regulated mechanisms are multifaceted and thus, aberrant mTOR signalling is implicated in an increasing number of pathological conditions, including cancer, obesity, type 2 diabetes, and neurodegeneration, as well as ageing¹¹⁰. In the following, the diverse aspects of the mTOR pathway are discussed in greater detail.

3.3.1 mTOR

Originally found in a screen for mutations that render yeast cells resistant to the antifungal macrolide Rapamycin¹¹¹, TOR was soon identified as a major metabolic regulator, which is highly conserved up to human¹¹². mTOR is an atypical serine/threonine protein kinase of ~ 280 kDa that belongs to the phosphoinositide 3-kinase-related kinase (PIKK) family¹¹³. Members of this family are all signalling proteins of large size, comprising, next to mTOR, DNA protein kinase (DNA-PKcs), Ataxia telangiectasia mutated (ATM), ATM and RAD5 [Radiation sensitive 5] related (ATR), Transformation/transcription domain-associated protein (TRRAP) and Suppressor with morphological effect on genitalia 1 (SMG1). Just like mTOR, all kinases play essential roles in the regulation of cell growth, gene expression, and genome surveillance and repair¹¹⁴. The multidomain protein mTOR consists of an N-terminal protein interaction domain of ~20 HEAT (for Huntington, Elongation Factor 3, PR65/A, TOR) repeats and a C-terminal kinase domain, flanked by activating FAT (for FRAP, ATM, TRRAP) -domains (FAT and FATC)¹¹⁵ and an inhibitory FKBP12-Rapamycin binding (FRB)-domain. Binding to FRB domain by the adaptor molecule FKBP12 and Rapamycin inhibits mTOR kinase activity¹¹⁶⁻¹¹⁷ (Figure 7).

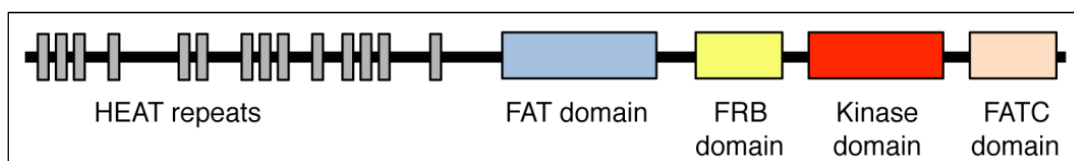


Figure 7: Domains in mTOR. Several HEAT repeats mediate protein-protein interaction, FAT and FATC dimerise to promote kinase activity of the kinase domain, and FRB mediates inhibitory binding to Rapamycin.(adapted from Laplante & Sabatini¹¹⁰)

To exert its role in metabolic fine-tuning, cellular mTOR usually sits at the core of two well-defined multimeric complexes. mTOR complex 1 and 2 (mTORC1 and mTORC2) have distinct composition and functions¹¹³, which are introduced in the following.

3.3.2 mTOR complex 1

3.3.2.1 mTORC1 composition

Three members of mTORC1 can also be found associated with mTORC2, suggesting overlapping functions: mammalian Lethal with sec-13 protein 8 (mLST8)¹¹⁸, DEP [Dishevelled, Egl-10 and Pleckstrin] domain containing mTOR-interacting protein (Deptor)¹¹⁹, and the Telomere maintenance 2 (Tel2) and Tel2 interacting protein 1 (Tti1) complex¹²⁰ (s. chapter 3.3.5), acting as scaffolds, inhibitors, and stabilising agents, respectively. In contrast, Regulatory associated protein of mammalian target of Rapamycin (Raptor)¹²¹⁻¹²², which is required for binding to downstream targets and the inhibitory proline-rich Akt substrate 40 kDa (PRAS40)¹²³ are specific to mTORC1 (Figure 8).

3.3.2.2 mTORC1 activation and regulation

Long before a different composition of both mTORCs at the protein level was experimentally clarified, mTORC1 was defined by its specific Rapamycin-sensitivity. Upon Rapamycin treatment many cellular processes are inhibited and those were designated to be governed solely by mTORC1 activity¹²⁴. To date, the mechanism of how Rapamycin binding to the FRB domain results in inhibitory effects remains unclear^{110, 125}.

The phosphorylation activity of mTORC1 is stimulated by growth factors, amino acid uptake and high energy levels (e.g. ATP), while starvation, hypoxia and other stress strongly reduce signalling¹¹⁰. Upon these stimuli, several well studied signalling molecules, e.g. growth factor stimulated ERK1/2 (extracellular-signal-regulated kinase 1/2)¹²⁶, and TNF α (Tumor necrosis factor α) responsive I κ B β (I κ B kinase β)¹²⁷ subsequently modulate activity of their downstream kinases. As a consequence, a dimeric complex called Tuberous sclerosis 1/2 (TSC1/2), which acts as a GTPase-activating protein (GAP) for the GTPase Rheb (Ras homologue enriched in brain), is phosphorylated. Since only the active GTP-bound form of Rheb can interact with mTORC1 and promote its kinase activity, TSC1/2 acts as negative regulator of the mTORC1 pathway¹²⁸.

3.3.2.3 Functions of mTORC1

A broad variety of downstream effects have been identified for mTORC1, justifying its role as master sentinel of cellular growth. For instance, in favourable situations, growth, i.e. accumulation of cell mass and content, is permitted by positive activation of energy production¹²⁹, fat synthesis¹³⁰, ribosome biogenesis¹³¹, mRNA transcription¹³² and protein translation¹⁰⁹. In contrast, upon growth factor deprivation or stress situations, aforementioned processes are restrained, while the negative regulation of both autophagy and lysosomal degradation¹³³ is relieved, allowing a rapid recycling of cytoplasmic components required for immediate metabolic adaption. The most renowned substrates of mTORC1 are p70-S6 kinase 1 (S6K1), and the eukaryotic initiation factor 4E (eIF4E) binding

protein 1 (4E-BP1), whose specific phosphorylation is assisted by Raptor mediated interaction¹³⁴. Upon phosphorylation of 4E-BP1, its inhibitory association with the cap-binding protein eIF4E is resolved, enabling the formation of the cap-dependent translation initiation complex¹³⁵. While 4E-BP1 phosphorylation drives protein biogenesis, functions of phosphorylated S6K1 are more versatile. Being a kinase itself, the AGC [related to cAMP-dependent protein kinase 1 (PKA), cGMP-dependent protein kinase (PKG), and protein kinase C (PKC)] type kinase S6K1 can phosphorylate many effector molecules which leads to an increase in mRNA biogenesis, as well as translational initiation and elongation¹¹⁰. Apart from activation of its target ribosomal protein S6, S6K1 for example also phosphorylates PDCD 4 (Programmed cell death protein 4) – a translation elongation inhibitor – at its degran, marking it for polyubiquitylation and subsequent proteasomal degradation¹³⁶. Thus, an interplay between tightly balanced activatory and repressive phosphorylation events enables metabolic regulation, driven by mTORC1 and its major target kinase S6K1.

3.3.3 mTOR complex 2

3.3.3.1 mTORC2 composition

mTORC2 forms a seven-membered multiprotein complex. Like mTORC1, mTORC2 interacts with the scaffold protein mLST8¹²⁴, inhibitory Deptor¹¹⁹, and Tel2/Tti1 stability complex¹²⁰. Specifically part of mTORC2 are Rapamycin-insensitive companion of mTOR (Rictor)^{124, 137}, the mammalian Stress-activated map kinase-interacting protein 1 (mSin1)¹³⁸, and the Protein observed with Rictor 1 and 2 (Protor1/2)¹³⁹, which are all essential for directed kinase activity (Figure 8).

3.3.3.2 mTORC2 activation and regulation

In contrast to mTORC1, the less well studied mTORC2 was initially found to be non-responsive to Rapamycin treatment; however, it was later shown that long-term treatment can also impair mTORC2 functions¹⁴⁰. So far, the only defined upstream kinase of mTORC2 is phosphoinositide 3-kinase (PI3K), which can be activated by Insulin or Insulin-like growth factors (IGF) that bind and activate the transmembrane receptor Insulin receptor substrate (IRS). mTORC2 signalling is also dependent on ribosome association, tightly coupling its kinase activity to the translational capacity of the cell¹⁰⁸.

3.3.3.3 Functions of mTORC2

mTORC2 has been assigned functions in regulation of proliferation, cell survival, and motility. Upon its stimulation, mTORC2 phosphorylates distinct AGC kinase family members including PKCa (Protein kinase Ca), SGK (Serum and glucocorticoid-inducible kinase), and Akt (also known as Protein kinase B [PKB])¹⁴¹. While PKCa has been implicated in regulating actin cytoskeleton dynamics¹¹⁰, SGK1 is thought to be involved in an ion transport and growth regulation¹⁴². Being a

well-known oncogene that regulates cellular integrity, the most prominent target of mTORC2 is Akt¹⁴³. Since the phosphorylation status of Akt determines its substrate specificity, it is noteworthy that the specific phosphorylation of Akt at S473 by mTORC2 kinase activates signalling for cell survival and proliferation¹⁴⁴, while other Akt regulated pathways are not affected¹³⁸. An exemplary apoptosis inhibiting process driven by Akt is the phosphorylation dependent sequestration of the pro-apoptotic protein BAD from mitochondria membranes¹⁴⁵. Another target of mTORC2 activated Akt is the cell cycle inhibitory p27 that is retained in the cytoplasm after phosphorylation, allowing cell cycle progression¹⁴³. Thus, by combining both anti-apoptotic and proliferative actions, mTORC2 dependent signalling via its target kinase Akt eventually promotes cell survival.

3.3.4 mTORC1 and mTORC2 – feedback inhibition

Although mTORC1 and mTORC2 have exclusive functions, metabolism and survival are tightly linked via a feedback mechanism¹¹⁰ (Figure 8). This makes sense in a setting, where the cell has to ensure a temporal control of cell cycle progression, according to the adequate production of cellular components. For instance, mTORC1 activated S6K1 can phosphorylate IRS1, which leads to its degradation, thus disabling Insulin and growth factor induced activation of mTORC2 by PI3K¹⁴⁶.

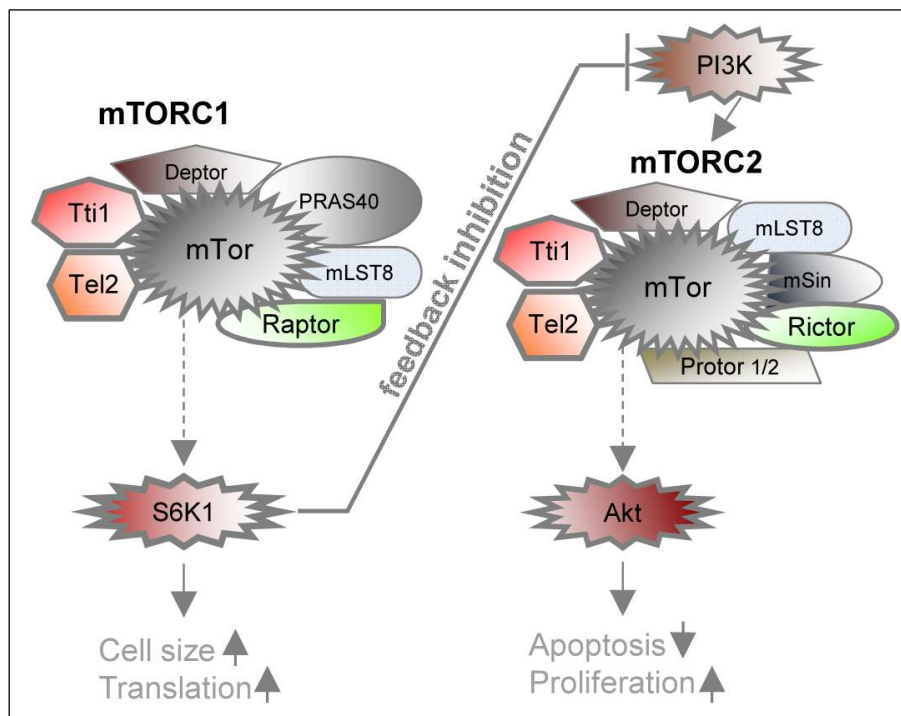


Figure 8: Schematic illustration of the mTORC1 and the mTORC2 components, their signalling cascade, their cellular function and their tight connection via a feedback mechanism. Upon stimulation mTORC1 phosphorylates its target kinase S6K1. Several substrates of S6K1 contribute to increased cell size and translation. On the other hand mTORC2 signalling leads to increased Akt kinase phosphorylation, which promotes proliferation and prevents apoptosis. Importantly, the mTORC1/S6K1 axis is tightly linked to the PI3K/mTORC2/Akt axis via feedback inhibition on PI3K activity.

Moreover, mTORC1 can directly phosphorylate IRS1¹⁴⁷ and the mTORC2 inhibitory receptor tyrosine kinase (RTK) inhibitor Growth factor receptor-bound protein 10 (Grb10) thus reducing growth factor signalling¹⁴⁸⁻¹⁴⁹. Of note, even though Akt has been reported to phosphorylate the TSC1/2 complex upstream of mTORC1, a positive feedback following mTORC2 activation has not been observed, suggesting that mTORC2 activates a pool of Akt that cannot signal upstream of mTORC1¹¹³.

3.3.5 Tti1/Tel2

Of particular interest, Tel2 and Tti1 proteins have recently been identified to interact with all known mammalian PIKKs and essentially regulate their cellular abundance¹⁵⁰. Both PTMs and transcriptional regulation have been largely excluded as regulatory means by which Tel2/Tti1 proteins control PIKK abundance¹⁵¹⁻¹⁵². Instead, it was suggested that Tel2/Tti1 mediate the assembly and maturation of PIKKs. Maturation assistance has been proposed to involve a promotion of PIKK *de novo* synthesis by Tel2/Tti1¹⁵⁰ as well as chaperone-like functions during protein biogenesis, since Tel2/Tti1 are found in association with the chaperone Hsp90¹⁵³. Furthermore, dependent on the phosphorylation status of Tel2/Tti1¹⁵⁴, those proteins are thought to enhance PIKK stability by direct binding¹⁵⁵. With regard to mTOR, Tel2 and Tti1 proteins are not only crucial for protein stability¹³⁰⁻¹³², but constitute essential components of both mTORC1 and mTORC2 complexes, which are vital for their assembly^{120, 152-154}.

In summary, mTOR kinase signalling is generally mediated through two distinct multimeric complexes, mTORC1 and mTORC2. Stability and assembly of both complexes is ensured by Tel2/Tti1. While mTORC1 mainly regulates cell growth, energy consumption, and cellular biomolecule synthesis or breakdown, mTORC2 controls motility, proliferation, and survival. Both signalling pathways are tightly linked via a feed-back mechanism, to reliably adjust responses to the given cellular growth condition.

3.4 Aim of the study

Novel clinical therapies inhibiting the proteasome have essentially advanced the effectiveness of treatment for MM patients. However, clearly defined MM-specific deregulated ubiquitylation pathways have remained largely unknown and a good prediction of responsiveness is not yet available. Searching for potential UPS-related candidates in MM, analyses of CGH array data revealed a significant amplification of the FBXO9 locus. To identify the substrates of the highly conserved orphan FBP Fbxo9, which composes the E3 ligase SCF^{Fbxo9} with yet unknown functions, in this study an unbiased screen applying tandem affinity purification (TAP) and mass spectrometric analyses thereof were conducted. In order to subsequently establish the potential interaction partners as bona fide substrates of SCF^{Fbxo9}, their ubiquitylation dependent proteasomal degradation was characterised biochemically and further investigations aimed to elucidate the biological relevance within the cellular context. By elucidating the physiological role of Fbxo9, its interactors and the involved pathways, this study wanted to provide a further rationale for mechanistic investigations in the context of pathogenesis and treatment of MM. Hence, in standard MM cell culture and patient data analyses, the importance of a non-physiological deregulation of the Fbxo9-dependent pathway should be linked to a pro-survival advantage in MM-cells. By gaining a more detailed insight into the molecular characteristics of a specific UPS-mediated pathway that is often deregulated in MM, this study eventually aimed to identify novel reliable biomarkers for better prediction of response to proteasome inhibitor treatment or to possibly provide potential new target structures for a more specific treatment of MM patients.

4 Materials and Methods

4.1 Materials

4.1.1 Chemicals

Reagent	Company
[γ - ³² P]Adenosine 5'-triphosphate (γ ATP)	HartmannAnalytics, Braunschweig
β -Mercaptoethanol	Sigma-Aldrich, Taufkirchen
3x FLAG Peptide	Sigma-Aldrich, Taufkirchen
4-(2-hydroxyethyl)-1-piperazineethanesulfonic acid (HEPES)	SERVA, Heidelberg
Acetic acid	Roth, Karlsruhe
Acetone	Roth, Karlsruhe
Acrylamide/Bis Solution 40%, 29:1	Bio-Rad, München
Adenosintriphosphate (ATP)	Sigma-Aldrich, Taufkirchen
Agarose	Roth, Karlsruhe
Albumin fraction V (BSA)	Roth, Karlsruhe
Ammonium persulfate (APS)	Roth, Karlsruhe
ANTI-FLAG M2 Affinity Gel	Sigma-Aldrich, Taufkirchen
Aqua ad injectabilia, sterile	Braun, Melsungen
ATX Ponceau S red staining solution	Sigma-Aldrich, Taufkirchen
Bacto agar	BD, Franklin Lakes, USA
Bacto trypton	BD, Franklin Lakes, USA
Bacto yeast extract	BD, Franklin Lakes, USA
Borate 20x Solution	Pierce, Rockford, USA
Bromphenol blue	Sigma-Aldrich, Taufkirchen
Calcium chloride (CaCl ₂)	Sigma-Aldrich, Taufkirchen
CHAPS	Sigma-Aldrich, Taufkirchen
Coomassie Brilliant Blue	Roth, Karlsruhe
Cycloheximide	Sigma-Aldrich, Taufkirchen
Deoxynucleotide triphosphate (dNTP) mix (10mM)	Fermentas, St. Leon-Rot
Dimethyl sulfoxide (DMSO)	Roth, Karlsruhe
Ethanol	Merck, Darmstadt
Ethidium bromide	Roth, Karlsruhe
Ethylendiamintetraacetic acid (EDTA)	Sigma-Aldrich, Taufkirchen
Freund's Incomplete Adjuvant	Sigma-Aldrich, Taufkirchen
Gelatine	Sigma-Aldrich, Taufkirchen
Gluthatione Sepharose™ 4B	GE Healthcare, Louisville, USA
Glycerol	Sigma-Aldrich, Taufkirchen
Glycine	Roth, Karlsruhe
Hydrochloric acid (HCl)	Roth, Karlsruhe
Isopropanol	Roth, Karlsruhe
Isopropyl β -D-1-thiogalactopyranoside (IPTG)	Sigma-Aldrich, Taufkirchen

L-[³⁵ S]-Cysteine	Hartmann Analytics, Braunschweig
L-[³⁵ S]-Methionine	Hartmann Analytics, Braunschweig
L-Glutathione	Sigma-Aldrich, Taufkirchen
Magnesium chloride (MgCl ₂)	Sigma-Aldrich, Taufkirchen
Methanol	Merck, Darmstadt
N,N-Bis(2-hydroxyethyl)-2-aminoethanesulfonic acid (BES) pH 7.1	Sigma-Aldrich, Taufkirchen
Nocodazole (Noc)	Sigma-Aldrich, Taufkirchen
Nonidet P40, 10% (w/v)	Roche, Penzberg
NuPAGE® MES SDS Running Buffer	Invitrogen, Karlsruhe
Paraformaldehyde (PFA)	Sigma-Aldrich, Taufkirchen
Polybrene (Hexdimethrine bromide)	Sigma-Aldrich, Taufkirchen
Potassium chloride	Fluka, Taufkirchen
Propidium iodide	Sigma-Aldrich, Taufkirchen
Protein A Sepharose	GE Healthcare, Louisville, USA
Protein G Agarose	Sigma-Aldrich, Taufkirchen
Protein G Sepharose	Invitrogen, Karlsruhe
Skim milk powder	Fluka, Taufkirchen
SlowFade® Gold antifade reagent with DAPI	Invitrogen, Karlsruhe
SOC Media	NEB, Frankfurt
Sodium acetate	Merck, Darmstadt
Sodium azide	Merck, Darmstadt
Sodium chloride (NaCl)	Roth, Karlsruhe
Sodium citrate	Sigma-Aldrich, Taufkirchen
Sodium dihydrogenphosphat	Merck, Darmstadt
Sodium dodecylsulfate (SDS)	Roth, Karlsruhe
Sodium fluoride (NaF)	Sigma-Aldrich, Taufkirchen
Sodium hydroxid (NaOH)	Roth, Karlsruhe
Sorbitol	Sigma-Aldrich, Taufkirchen
Strep-Tactin Superflow 50%	IBA, Göttingen
Strep-tag elution buffer (10x) with Desthiobiotin	IBA, Göttingen
SuperSignal® Chemiluminescence Substrat	Pierce, Rockford, USA
Tetramethylethylenediamine (TEMED)	Sigma-Aldrich, Taufkirchen
TiterMax Gold	Sigma-Aldrich, Taufkirchen
Thymidine (Thy)	Sigma-Aldrich, Taufkirchen
Trichloroacetic acid (TCA)	Sigma-Aldrich, Taufkirchen
Tris(hydroxymethyl)aminomethane (Tris)	Roth, Karlsruhe
Tris buffered saline (TBS) (10X)	Sigma-Aldrich, Taufkirchen
Triton X-100	Fluka, Taufkirchen
Trypan blue	Invitrogen, Karlsruhe
Tween 20	Fluka, Taufkirchen
Ubiquitin (Ub)	Boston Biochem, Cambridge, USA
UltraPure™ 10 x Tris/Borate/EDTA (TBE) Buffer	Invitrogen, Karlsruhe

4.1.2 Media and supplements for cell culture

Dulbecco's Modified Eagle's Medium (DMEM)	PAA, Pasching, Austria
Express Five SFM	Invitrogen, Karlsruhe
Iscove's Modified Dulbecco's Media (IMDM)	Invitrogen, Karlsruhe
Grace's Insect Medium	Invitrogen, Karlsruhe
McCoy's 5A Medium Modified	PAA, Pasching, Austria
RPMI 1640	PAA, Pasching, Austria
Sf-900 II SFM	Invitrogen, Karlsruhe
Fetal Bovine Serum (FBS) Gold	PAA, Pasching, Austria
Bovine Serum (BS)	PAA, Pasching, Austria
Opti-MEM® I, reduced serum media	Invitrogen, Karlsruhe
Phosphate buffered saline (PBS), 10X, sterile	PAA, Pasching, Austria
Penicillin/ Streptomycin (100X)	PAA, Pasching, Austria
Trypsin-EDTA (10X) solution	PAA, Pasching, Austria
Glutamine (100X)	PAA, Pasching, Austria
Interleukin 6 (IL-6)	Sigma-Aldrich, Taufkirchen
β-Mercaptoethanol	Invitrogen, Karlsruhe

4.1.3 Antibiotics

Ampicillin	Roth, Karlsruhe
Kanamycin	Fluka, Taufkirchen
Puromycin	Sigma-Aldrich, Taufkirchen

4.1.4 Transfection reagents

ExGene 500	Fermentas, St.Leon-Rot
FuGENE HD	Roche, Penzberg
HiPerFect	Quiagen, Hilden
Lipofectamine. 2000	Invitrogen, Karlsruhe
TurboFect siRNA	Fermentas, St.Leon-Rot

4.1.5 Enzymes

Antarctic Phosphatase	NEB, Frankfurt
Benzonase	Sigma-Aldrich, Taufkirchen
DNase I	Sigma-Aldrich, Taufkirchen
Ribonuclease A	Sigma-Aldrich, Taufkirchen
Pfu Ultra DNA Polymerase	Agilent, Loveland, USA
SuperScript II Reverse Transcriptase	Invitrogen, Karlsruhe
T4 DNA Ligase	Fermentas, St.Leon-Rot

Restriction enzymes

Fermentas, St.Leon-Rot

ApaI / BamHI / BglII / DpnI / EcoRI / HindIII / NheI / NotI / SalI / XbaI / XhoI

All enzymes were supplied with suitable reaction buffers.

4.1.6 Inhibitors

Aprotinin	Sigma-Aldrich, Taufkirchen
Akt inhibitor IV	Calbiochem, La Jolla, USA
Glycerol 2-phosphate disodium salt hydrate (G2P)	Sigma-Aldrich, Taufkirchen
Leupeptin	Sigma-Aldrich, Taufkirchen
Ocadaic acid	Sigma-Aldrich, Taufkirchen
Phenylmethylsulfonyl fluoride (PMSF)	Sigma-Aldrich, Taufkirchen
Rapamycin	Sigma-Aldrich, Taufkirchen
Sodium orthovanadate (Na ₃ VO ₄)	Sigma-Aldrich, Taufkirchen
Soybean Trypsin Inhibitor	Sigma-Aldrich, Taufkirchen
Tosyl-L-lysyl-chloromethyl ketone hydrochloride (TLCK)	Sigma-Aldrich, Taufkirchen
Tosyl-phenylalanyl-chloromethyl ketone (TPCK)	Sigma-Aldrich, Taufkirchen
TBB (4,5,6,7-tetrabromobenzotriazole)	Sigma-Aldrich, Taufkirchen
Wortmannin	Sigma-Aldrich, Taufkirchen
Proteasom Inhibitor MG-132	Boston Biochem, Cambridge, USA

4.1.7 Molecular weight standards for DNA and proteins

GeneRuler 1kb DNA Ladder	Fermentas, St.Leon-Rot
GeneRuler 100bp DNA Ladder	Fermentas, St.Leon-Rot
6X DNA Loading Dye	Fermentas, St.Leon-Rot
PageRulerPrestained Protein Ladder	Fermentas, St.Leon-Rot
PageRuler Plus Prestained Protein Ladder	Fermentas, St.Leon-Rot

4.1.8 Molecular biological Kits

Bio-Rad Protein Assay	Bio-Rad, München
Dual-Luciferase Reporter Assay System	Promega, Mannheim
GeneJET™ Gel Extraction Kit	Fermentas, St.Leon-Rot
GeneJET™ PCR Purification Kit	Fermentas, St.Leon-Rot
Inject Maleimide Activated mcKLH Kit	Pierce, Rockford, USA
LightCycler 480 SYBR Green I Master	Roche, Penzberg
QIAGEN Plasmid Maxi Kit	Qiagen, Hilden
QIAprep Spin Miniprep Kit	Qiagen, Hilden
QIAshredder homogenizer Kit	Qiagen, Hilden
QuikChange Site-Directed Mutagenesis Kit	Stratagene, Heidelberg
RNeasy Mini Kit	Qiagen, Hilden
SuperScript III Reverse Transcriptase	Invitrogen, Karlsruhe

4.1.9 Buffers

All buffers were prepared in dH₂O (aqua dest), if not stated differently.

<u>Lysis Buffer</u> :	50 mM Tris (pH 7.5)
	250 mM NaCl
	0.1% Triton X-100
	1 mM EDTA
	50 mM NaF
	+ inhibitors

<u>Lysis Buffer (MS/IP) :</u>	50 mM Tris (pH 7.5) 150 mM NaCl 0.1% NP40 1 mM EDTA 5 mM MgCl ₂ 5% Glycerol 5 nM Ocadaic Acid + inhibitors
<u>CHAPS Buffer :</u>	40 mM HEPES (pH 7.4) 0.3% CHAPS 10 mM pyrophosphate 2 mM EDTA + inhibitors
<u>NETN Buffer (10X) :</u>	20 mM Tris (pH 8,0) 100 mM NaCl 1 mM EDTA 0.5% NP40 1 mM PMSF + inhibitors
<u>Inhibitors :</u>	1 µg/ml Aprotinin 1 mM DTT 10 mM G2P 1 µg/ml Leupeptin 0.1 mM PMSF 0.1 mM Na ₃ VO ₄ 10 µg/ml Soybean Trypsin Inhibitor 5 µg/ml TLCK 5 µg/ml TPCK
<u>Denaturing Buffer (for Quenching) :</u>	100 mM Tris/HCl (pH 7,5) 1 mM EDTA 2% SDS 2mM DTT
<u>Ubiquitylation Assay Buffer :</u>	50 mM Tris (pH 7.6) 5 mM MgCl ₂ 0.6 mM DTT 2 mM ATP 1.5 ng/µl E1 10 ng/µl Ubc3 10 ng/µl Ubc5 2.5 µg/µl ubiquitin 1 µM ubiquitin aldehyde respective E3-components

<u>Kinase Assay Buffer</u> :	80 mM HEPES (pH 7.4) 10 mM MgCl ₂ 50 μM ATP 1 μCi [γ- ³² P] ATP 1 mM DTT
<u>Running Buffer (10X)</u> :	250 mM Tris (pH 7.5) 1.92 M Glycine 1% SDS
<u>Transfer Buffer (10X)</u> :	250 mM Tris (pH 7.5) 1.5 M Glycine 1% SDS for 1X: 2 vol Methanol and 7 vol dH ₂ O
<u>Stripping Buffer</u> :	62.5 mM Tris (pH 6.8) 0.867% β-Mercaptoethanol 2% SDS
<u>Washing Buffer</u> :	PBS (1X) 0.1% Tween 20
<u>Blocking Buffer (Western Blot)</u> :	PBS (1X) 0.1% Tween 20 5% Milk powder
<u>IF-Buffer</u> :	PBS (1X) 0.5% Tween 20
<u>BrdU wash buffer I</u> :	PBS (1X) 1% BSA
<u>BrdU wash buffer II</u> :	PBS (1X) 0.5% Tween 20 1% BSA
<u>DNA Denaturing Buffer</u> :	2 N HCl 0.5% Triton X-100
<u>Laemmli Buffer (5X)</u> :	300 mM Tris (pH 6.8) 50% Glycerol 10% SDS 5% β-Mercaptoethanol 0.05% Bromphenolblue
<u>Stacking Gel Buffer</u> :	0.5 M Tris (pH 6.8)
<u>Seperation Gel Buffer</u> :	1.5 M Tris (pH 8.8)
<u>Coomassie Staining</u> :	0.25% Coomassie brilliant blue 45% Methanol 10% Acetic Acid

<u>Coomassie Destain</u> :	45% Methanol 10% Acetic Acid
<u>Luria-Bertani (LB) medium</u> :	1% Bacto trypton 0.5% Bacto yeast extract 1% NaCl
<u>LB-agar plates</u> :	1% Bacto trypton 0.5% Bacto yeast extract 1% NaCl 1.5% Bacto agar

4.1.10 Antibodies

Primary rabbit antibodies

Antibody	Dilution	Company
ATM	1:1000	Cell Signaling, Danvers, USA
ATR	1:1000	Cell Signaling, Danvers, USA
Caspase 3	1:1000	Cell Signaling, Danvers, USA
cleaved Caspase 3	1:400	Cell Signaling, Danvers, USA
CK2 (α)	1:1000	Cell Signaling, Danvers, USA
Cyclin B1	1:1000	Cell Signaling, Danvers, USA
Deptor	1:1000	Millipore, Schwalbach/Ts
Fbxo9	1:1000	this study
Flag	1:1000	Sigma-Aldrich, Taufkirchen
GRB10 (K-20)	1:400	Santa Cruz Biotechnologies, Santa Cruz, USA
HA-411 (Y11)	1:500	Santa Cruz Biotechnologies, Santa Cruz, USA
mTOR	1:1000	Cell Signaling, Danvers, USA
Myc	1:1000	Millipore, Schwalbach/Ts
p70 S6 Kinase 1	1:1000	Cell Signaling, Danvers, USA
Phospho Akt (S473)	1:1000	Cell Signaling, Danvers, USA
Phospho Chk2 (S19)	1:1000	Cell Signaling, Danvers, USA
Phospho Histone H3	1:4000	Millipore, Schwalbach/Ts
Phospho p70 S6 Kinase 1(T389)	1:1000	Cell Signaling, Danvers, USA
Phospho S6 (S235/236)	1:1000	Cell Signaling, Danvers, USA
Phospho Tel2 (S485)	1:1000	this study (Innovagen, Sweden)
Phospho Tti1 (S828)	1:1000	this study (Innovagen, Sweden)
Raptor (for IP)	0,5 μ g/ μ l	Bethyl Laboratories, Montgomery, USA
Raptor	1:1000	Cell Signaling, Danvers, USA
Rictor (for IP)	0,5 μ g/ μ l	Bethyl Laboratories, Montgomery, USA
Rictor	1:1000	Cell Signaling, Danvers, USA
SMG1	1:1000	Bethyl Laboratories, Montgomery, USA
Tel2	1:1000	Proteintech Group, Chicago, USA
TRRAP (D2966)	1:1000	Cell Signaling, Danvers, USA
Tti1	1:1000	kind gift of T.Kaizuka ¹⁵⁶

Table 1: List of primary rabbit antibodies

Primary mouse antibodies

Antibody	Dilution	Company
α - Tubulin	1:5000	Sigma-Aldrich, Taufkirchen
β -Actin (monoclonal)	1:10000	Sigma-Aldrich, Taufkirchen
Cul 1	1:500	Invitrogen, Karlsruhe
Cyclin B1	1:1000	Santa Cruz Biotechnologies, Santa Cruz, USA
Cyclin D1	1:1000	Invitrogen, Karlsruhe
Cyclin E	1:100	kind gift of Dr. M.Pagano
DNA-PKcs (cocktail)	1:1000	Thermo Scientific, Karlsruhe
Flag M2 (monoclonal)	1:3000	Sigma-Aldrich, Taufkirchen
HA.11 (monoclonal)	1:5000	Covance, Princeton, USA
Myc	1:1000	Santa Cruz Biotechnologies, Santa Cruz, USA
p27	1:200	BD, Franklin Lakes, USA
Plk1	1:500	Invitrogen, Karlsruhe
Ub (Fl-76)	1:1000	Santa Cruz Biotechnologies, Santa Cruz, USA
Ubiquitin (Mono/Poly)	1:500	Biomol, Hamburg

Table 2: List of primary mouse antibodiesSecondary antibodies

Antibody	Dilution	Company
Alexa Fluor anti mouse 488	1:1000	Invitrogen, Karlsruhe
Alexa Fluor anti mouse 594	1:1000	Invitrogen, Karlsruhe
Alexa Fluor anti rabbit 488	1:1000	Invitrogen, Karlsruhe
Alexa Fluor anti rabbit 594	1:1000	Invitrogen, Karlsruhe
Avidin, Texas Red conjugate	1:1000	Invitrogen, Karlsruhe
ECL anti mouse IgG horseradish peroxidase linked	1:5000	GE Healthcare, München
ECL anti rabbit IgG horseradish peroxidase linked	1:5000	GE Healthcare, München
ECL anti protein A horseradish peroxidase linked	1:5000	GE Healthcare, München
Texas Red anti mouse	1:1000	Invitrogen, Karlsruhe
Texas Red anti rabbit	1:1000	Invitrogen, Karlsruhe

Table 3: List of secondary antibodies**4.1.11 Plasmids**

All plasmids were DNA sequence verified by sequencing with MWG Eurofins, Ebersberg.

N-SF-TAP-pcDNA3.0	Dr. M.Ueffing ¹⁵⁷
N-SF-TAP-pcDNA3.0_FBXO9 (iso3)	this study, cloned by Dr. V.Fernández-Sáiz
N-SF-TAP-pcDNA3.0_TEL2	this study, cloned by B.-S.Targosz
N-SF-TAP-pcDNA3.0_TEL2(S(485/487)A)	this study, cloned by Dr. V.Fernández-Sáiz
N-SF-TAP-pcDNA3.0_TEL2(S485A)	this study, cloned by B.-S.Targosz
p3XFLAG-CMV-10_TTI1	Dr. T.Kaizuka ¹⁵⁶
p3XFLAG-CMV-10_TTI1(S828A)	this study, cloned by B.-S.Targosz
pcDNA_MLV_GAG/POL	Dr. A.Krackardt

pcDNA3.1_FBXO9 (no Tag)	this study, cloned by Dr. V.Fernández-Sáiz
pcDNA3.1_Flag-CK2(α)	this study, cloned by B.-S.Targosz
pcDNA3.1_FLAG-FBXO11	Dr. F.Bassermann
pcDNA3.1_FLAG-FBXO18	Dr. F.Bassermann
pcDNA3.1_FLAG-FBXO3	Dr. F.Bassermann
pcDNA3.1_FLAG-FBXO4	Dr. F.Bassermann
pcDNA3.1_FLAG-FBXO9 (1)	Dr. F.Bassermann
pcDNA3.1_HA-FBXO9 (1)	Dr. M.Pagano
pcDNA3.1_HA-FBXO9 (3)	Dr. F.Bassermann
pcDNA3.1_HA-TEL2	this study, cloned by Dr. V.Fernández-Sáiz
pcDNA3.1_HA-TEL2(1-175)	this study, cloned by B.-S.Targosz
pcDNA3.1_HA-TEL2(1-350)	this study, cloned by B.-S.Targosz
pcDNA3.1_HA-TEL2(1-650)	this study, cloned by B.-S.Targosz
pcDNA3.1_HA-TEL2(175-350)	this study, cloned by B.-S.Targosz
pcDNA3.1_HA-TEL2(350-end)	this study, cloned by B.-S.Targosz
pcDNA3.1_HA-TEL2(650-837)	this study, cloned by B.-S.Targosz
pcDNA3.1_HA-TEL2(S485A)	this study, cloned by B.-S.Targosz
pcDNA3.1_HA-TEL2(S(485/487)A)	this study, cloned by Dr. V.Fernández-Sáiz
pcDNA3.1_HA-TEL2(S485D)	this study, cloned by B.-S.Targosz
pcDNA3.1_HA-TEL2(S491A)	this study, cloned by Dr. V.Fernández-Sáiz
pcDNA3.1_HA-TTI1	this study, cloned by Dr. V.Fernández-Sáiz
pcDNA3.1_HA-TTI1(1-466)	this study, cloned by B.-S.Targosz
pcDNA3.1_HA-TTI1(1-647)	this study, cloned by B.-S.Targosz
pcDNA3.1_HA-TTI1(466-773)	this study, cloned by B.-S.Targosz
pcDNA3.1_HA-TTI1(773-end)	this study, cloned by B.-S.Targosz
pcDNA3.1_HA-TTI1(S828A)	this study, cloned by B.-S.Targosz
pCMV_SL I	Dr. M.Pagano ¹³⁶
pCMV-HA-Ubiquitin	Dr. F.Bassermann
peGFP-C3	Clontech, Saint-Germain-en-Laye, France
peGFP-C3_FBXO9	this study, cloned by B.-S.Targosz
pGEX-4T2	Amersham Biosciences, München
pGEX-4T2_FBXO9	this study, cloned by Dr. V.Fernández-Sáiz
pLPC_N-FLAG	Addgene, Cambridge, USA
pLPC_N-FLAG_FBXO9 (1)	this study, cloned by Dr. V.Fernández-Sáiz
pLPC_N-FLAG_FBXO9 (3)	this study, cloned by B.-S.Targosz
pLPC_N-FLAG_hTEL2	Dr. T.de Lange ¹⁵⁰
pLPC_N-FLAG-TEL2(S(485/487)A)	this study, cloned by B.-S.Targosz
pLPC_N-FLAG-TEL2(S485A)	this study, cloned by B.-S.Targosz
pLPC_N-FLAG-TTI1	this study, cloned by B.-S.Targosz
pLPC_N-FLAG-TTI1(S828A)	this study, cloned by B.-S.Targosz
pRK5_MYC-RAPTOR	Addgene, Cambridge, USA
pRK5_MYC-RICTOR	Addgene, Cambridge, USA
pRL-nulll	Promega, Mannheim

pXJ40 (MYC Ctrl)	Dr. V.Fernández-Sáiz
VSV-G	Clontech, Saint-Germain-en-Laye, France

Table 4: List of plasmids.

4.1.12 Oligonucleotides

All primers were synthesised with MWG Eurofins, Ebersberg.

4.1.12.1 Primer for Cloning

CK2_EcoRI_fw	5'-CCGGAATTCTCGGGACCCGTGCCAAGC-3'
CK2_NotI_rv	5'-GGTGGCGCCGTTACTGCTGAGCGCCAGC-3'
FBXO9_BamHI_Fw_Kozak	5'-CCCGGATCCGCCACCATGCCTGACATTATTTGGGTTTTTC-3'
FBXO9_BamHI_Kozak_HA_Fw	5'-CCGGGATCCGCCACCATGTACCC CTACGACGTGCCCGACTACGCC-3'
FBXO9_BamHI_Rv	5'-CGGGGATCCCTACAGAGGCCTTTCTGAG-3'
FBXO9_EcoRI_Fw	5'-CCGGAATTCTTCCGAGCTCAGTGGATG-3'
FBXO9_EcoRI_Rv	5'-CCCGAATTCCTACAGAGGCCTTTCTGAGAAAGCTG-3'
FBXO9_Fw_EcoRI	5'-CCGGAATTCTATTCCGAGCTCAGTGGATG-3'
FBXO9_Fw_BamHI	5'-CCGGGATCCTTCCGAGCTCAGTGGATG-3'
FBXO9_HindII_FLAG_Fw	5'-CGCAAGCTTGCCACCATGGACTACAAGGACGACG-3'
FBXO9_Rv_140_SalI	5'-GGCGTCGACCTAACTGCTCTCAAGCTC-3'
FBXO9_Rv_250_SalI	5'-GGCGTCGACCTACACTTGGTGCCAGGC-3'
FBXO9_Rv_HindIII	5'-CGGAAGCTTCTACAGAGGCCTTTCTGAG-3'
FBXO9_Rv_SalI	5'-CGGGTCGACCTACAGAGGCCTTTCTGAG-3'
FBXO9_SalI_Fw_Kozak	5'-CCCGTCGACGCCACCATGCCTGACATTATTTGGGTTTTTC-3'
TEL2_506_Fw_BglII	5'-CCGAGATCTCTGAAGAGCAGCAAGGCTC-3'
TEL2_612_Rv_SalI	5'-GGCGTCGACCTAGATGTCCATGCGCTGCC-3'
TEL2_650_SalI_Rv	5'-GTTGTCGACCTAGACGGCTGCCTCTGGCAG-3'
TEL2_Fw_(S485A/S487A)	5'-CACAGCTGGCGGGCGCTGACGCGGACCTGGACAGCGATG-3'
TEL2_S(485/7)D_Rv	5'-CATCGCTGTCCAGGTCGTCGTCGCCCGCCAGCTGTG-3'
TEL2_S(485/7)D_Fw	5'-CACAGCTGGCGGGCGACGACGACGACCTGGACAGCGATG-3'
TEL2_Fw_176_NheI	5'-CCGGCTAGCGCCACCATGTACCCCTACGACGTG CCCAGACTACGCCCGGAGTTCTTCCCCCAGAAC-3'
TEL2_Fw_292_Kozak_HA_NheI	5'-CCGGCTAGCGCCACCATGTACCCCTACGACGTG CCCAGACTACGCCGTGAAGAACAAGAAGGCCAG-3'
TEL2_Fw_350_NheI	5'-CCGGCTAGCGCCACCATGTACCCCTACGACG TGCCCAGACTACGCCCACTCCCCTGCCGAG-3'
TEL2_Fw_351_BglII	5'-CCGAGATCTCACACTCCCCTGCCGAGC-3'
TEL2_Fw_604_Kozak_HA_NheI	5'-CGGGTCGACCTAGAGGGCATAGAAGCTG-3'
TEL2_Fw_HA_NheI	5'-CCGGCTAGCTACCCCTACGACGTG CCGACTACGCCGAGCCAGCACCCCTC-3'
TEL2_Fw_NheI	5'-CCGGCTAGCGAGCCAGCACCCCTCAGAGGTTTC-3'
TEL2_Fw_NheI_Kozak_HA	5'-CCGGCTAGCGCCACCATGTACCCCTACGACGT GCCGACTACGCCGAGCCAGCACCCCTCAGAG-3'
TEL2_Rv_S485A/S487A	5'-CATCGCTGTCCAGGTCGCGTCAGCGCCCGCCAGCTGTG-3'
TEL2_Rv_150_SalI	5'-GGCGTCGACCTAGATGAAGCCGGGCTG-3'
TEL2_Rv_175_SalI	5'-GTTGTCGACCTACAAGTTCTCCTGCTGC-3'
TEL2_Rv_350_SalI	5'-GGCGTCGACCTAGCGGATGGCACTGCTG-3'
TEL2_Rv_506_SalI	5'-CCGGTCGACCTACAGCTCTCTGTCCCCCG-3'

TEL2_Rv_603_Sall	5'-CCGGCTAGCGCCACCATGTACCCCTACGACGTG CCCGACTACGCCCTCCGGCAGCGCATGGACATCC-3'
TEL2_Rv_650_Sall	5'-GGCGTCGACCTAGACGGCTGCCTCTGG-3'
TEL2_Rv_Sall	5'-GGCGTCGACCTAGGGAGACGCGGGTGG-3'
TEL2_Rv_XbaI	5'-CCGTCTAGATCAGGGAGACGCGGGTGGGAG-3'
TEL2_S347A_Fw	5'-GTGGTGACTTTCTTCGCGCCCGTTCTGCAAAGATG-3'
TEL2_S347A_Rv	5'-CATCTTTGCAGAACCGGGCGGAAGAAAGTCACCAC-3'
TEL2_S398_Fw	5'-GCGGGCGTGAAGTGCCGCTGGAC GCTGCCCTGCCCCCGTGCGACGC-3'
TEL2_S398_Rv	5'-GCGTCGCACGGGGGGCAGGGCAG CGTCCAGGCGGCACTTCACGCCCGC-3'
TEL2_S485A_Fw	5'-CACAGCTGGCGGGCGCTGACTCGGACCTGGACAGCGATG-3'
TEL2_S485A_Rv	5'-CATCGCTGTCCAGGTCCGAGTCAGCGCCCGCCAGCTGTG-3'
TEL2_S694A_Fw	5'-CCCAGCAGATTCAACGCCGTGGCCGGCCACTTCTTC-3'
TEL2_S694A_Rv	5'-GAAGAAGTGGCCGGCCACGGCGTTGAATCTGCTGGG-3'
TEL2_Sall_Rv_30pb	5'-GTTGTCGACCTAGGGAGACGCGGGTGGGAG-3'
TTI1_1-466_BamHI_Rv	5'-GCAGGATCCCTAAGGCTGTGTGGCTGAGG-3'
TTI1_1-647_Rv_XhoI	5'-GGCCTCGAGCTACAAACAGAAGTCTTTTCC-3'
TTI1_466-773_BamHI_Rv	5'-GCAGGATCCCTAGTCTGGGAACCACTGGGC-3'
TTI1_466-773_NheI_HA_Fw	5'-CCAGCTAGCGCCACCATGTACCCCTACGACGTGC CCGACTACGCCTGGAACCGCATCCAGAGG-3'
TTI1_773-end_NheI_HA_Fw	5'-CCAGCTAGCGCCACCATGTACCCCTACGACGTGC CCGACTACGCCACAGGTAATCTTGGGCACC-3'
TTI1_BamHI_Rv	5'-CCTGGATCCTCACTGCAGCTCCTTGAGC-3'
TTI1_Fv_BamHI	5'-CCGGGATCCGCAGTTTTTGATACTCCTG-3'
TTI1_Fw_774_BamHI	5'-CCGGGATCCACAGGTAATCTTGGGCACC-3'
TTI1_Fw_889_BamHI	5'-CCGGGATCCCTGGATCTGTGTGTGGTTG-3'
TTI1_Fw_956_BamHI	5'-CCGGGATCCGTCTTACAGGGCCTGGGCC-3'
TTI1_NheI_HA_Fw	5'-CCAGCTAGCGCCACCATGTACCCCTACGACGTGC CCGACTACGCCGAGTTTTTGATACTCCTGAGG-3'
TTI1_Rv_773_XhoI	5'-GGCCTCGAGCTAGTCTGGGAACCACTGG-3'
TTI1_Rv_888_XhoI	5'-GGCCTCGAGCTACACATCCAAGACCTTC-3'
TTI1_Rv_955_XhoI	5'-GGCCTCGAGCTAAGCCAGCTGCAACTTG-3'
TTI1_Rv_XhoI	5'-GGCCTCGAGCTACTGCAGCTCCTTGAGC-3'
TTI1_S1016_Fw	5'-CTGCTTGATTACCTCGCTGTCAAACAGCCCGTG-3'
TTI1_S1016_Rv	5'-CACGGGCTGTTTGACAGCGAGGTAATCAAGCAG-3'
TTI1_S459A_Fw	5'-GATGATCTGAATGCTGCTCAAAGACCTCAGCC-3'
TTI1_S459A_Rv	5'-GGCTGAGGTCTTTGGAGCAGCATTTCAGATCATC-3'
TTI1_S828A_Fw	5'-GCAGATGGAAATGTTCGGGATTTTGATAATGAAG-3'
TTI1_S828A_Rv	5'-CTTCATTATCAAATCCGCGACATTTCCATCTGC-3'
TTI1_S946A_Fw	5'-GACGTGGGGCAGCAGCGCTGCCATCCGCCCACTC-3'
TTI1_S946A_Rv	5'-GAGTGTGGCGGATGGCAGCGCTGCTGCCCCACGTC-3'
TTI1_S959A_Fw	5'-CCAAAGCTGGCTGGCGCCCTAGTCACCCAGGCC-3'
TTI1_S959A_Rv	5'-GGCCTGGGTGACTAGGGCGCCAGCCAGCTTTGG-3'
TTI1_S967A_Fw	5'-CACCCAGGCCCCCATCGCTGCCAGGGCTGGACCAG-3'
TTI1_S967A_Rv	5'-CTGGTCCAGCCCTGGCAGCGATGGGGCCTGGGTG-3'

Table 5: List of cloning primer sequences

4.1.12.2 Primer for Sequencing

check_pGEX_Rv	5'-CCGGGAGCTGCATGTGTCAGAGG-3'
check_pGEX_Fw	5'-GGGCTGGCAAGCCACGTTTGGTG-3'
check_pLPC_Fw	5'-TAGGCGTGTACGGTGGGA-3'
Check_pLPC_Rv	5'-CTTGCCAAACCTACAGGT-3'
seq_peGFP_Fw	5'-GCAGAGCTGGTTTAGTGAAC-3'
seq_peGFP_Rv	5'-CGTCGCCGTCCAGCTCGACCAG-3'
FBXO9_seq2	5'-CGACCTTGCAGAGCAGCAAGAGG-3'
FBXO9_seq3	5'-GAGACCCCTGAAATATGGCGTCTGG-3'
FBXO9_seq4	5'-GAACTAGGAATACCAGGACTGATGC-3'
seq_TEL2_1	5'-GAGCCAGCACCCCTCAGAGG-3'
seq_TEL2_2	5'-GGCGTGTGGTACCCCGGCTGG-3'
seq_TEL2_3	5'-CAGAGAGCTGAAGAGCAGC-3'
seq_TEL2_4	5'-CAGAAGCAAGACCCAGC-3'
check_TTI1_1	5'-GCAGAGCTGATGGTTTACAG-3'
check_TTI1_2	5'-GGGAGAGGAGCTGATGATGG-3'
check_TTI1_3	5'-GGAGCCACCACTGCCATTGC-3'

Table 6: List of sequencing oligos

4.1.12.3 Primer for qPCR

FBXO9_qPCRII_Fw	5'-GGGCAACTGGTGTGTTTATATGCC-3'
FBXO9_qPCRII_Rv	5'-TGTGCCTGCAGATCTGTTTCAGC-3'
mTOR_qPCR_Fw	5'-CTGGGACTCAAATGTGTGCAGTTC-3'
mTOR_qPCR_Rv	5'-GAACAATAGGGTGAATGATCCGGG-3'
qPCR_ARPPA_Fw	5'-GCACTGGAAGTCCAACACTTTC-3'
qPCR_ARPPA_Rv	5'-TGAGGTCCCTCCTTGGTGAACAC-3'
qPCR_GAPDH_Fw	5'-GAAGGTGAAGGTCGGAGTC-3'
qPCR_GAPDH_Rv	5'-GAAGATGGTGTGATGGGATTTC-3'
qPCR_Integrin_Fw	5'-TGGAGCGCTGCCAGTCACCATT-3'
qPCR_Integrin_Rv	5'-CGTCTGAAGTGAACACCAGCAGC-3'
TEL2_qPCR_Fw	5'-ATC GTG GCA GAG GTC GTT AGT G -3'
TEL2_qPCR_Rv	5'-GCTCAGTTCATCCTCTTCGTACTG -3'
TTI1_qPCR_Fw	5'-TGC TCT GAT GGC AGC ATT AGC C-3'
TTI1_qPCR_Rv	5'-TGG AGG TGC CCA AGA TTA CCT G-3'

Table 7: List of qPCR probe sequences

4.1.12.4 siRNA Oligonucleotides

All siRNA duplexes were purchased from Dharmacon, Lafayette, USA.

CK2 #1	5'-AACAUUGUCUGUACAGGUU-3'
CK2 #2	5'-CGUGGUCGCUUACAUCACU-3'
CK2 #3	5'-GGAGUGUGUCUUAGUUAC-3'

CK2 #4	5'-GCAUUUAGGUGGAGACUUC-3'
Fbxo9 #1	5'-GGUGUAAGCUCUAGCAAUU-3'
Fbxo9 #2	5'-GUAUUAAACUUGUCCGUA-3'
Fbxo9 #3	5'-GAGCUCAGUGGAUGUUUGA-3'
Fbxo9 #4	5'-GCAACUUGUACCUGAUUA-3'
Tel2 #1	5'-GAGCGGAUCAGAAGCAAGA-3'
Tel2 #2	5'-UGAUGUGCCUGGCUGUUA-3'
Tel2 #3	5'-GUACGAAGAGGAUGAACUG-3'
Tel2 #4	5'-GAAGACCUGUGUGGGGA-3'
Tti1 #1	5'-GCACUGACCAGGCUUAUCA-3'
Tti1 #2	5'-AGGAUUUGCUGUAUCUUUA-3'
Tti1 #3	5'-GUGAAUGGGAUCUCUUUA-3'
Tti1 #4	5'-GAACACACCUGCCAAGUUA-3'

Table 8: List of siRNA target strand sequences

4.1.13 Lentiviral particles

For shRNA mediated silencing of Fbxo9 SMARTvector 2.0 lentiviral shRNA particles by Dharmacon, Lafayette, US were used.

The target sequences for human Fbxo9 were:

Fbxo9_sh_1	5'-GTATTAAGTGTTCGTA-3'
Fbxo9_sh_2	5'-AACCACATATATTCGTC-3'
Fbxo9_sh_3	5'-TTATACTCCTCTTACGCA-3'

4.1.14 Patient samples

Samples of formalin-fixed tissues of MM patients were kindly provided by Dr. Slotta-Huspenina (Institute of Pathology, Technische Universität München, Germany) and analysed for protein and mRNA by Clemens Reiter of Technische Universität München. Dr. Christian Langer of University of Ulm provided the analysis of 180 MM patients.

4.1.15 Mice

Wildtype C57BL/6 mice were a kind gift of Ursula Baumann (Technische Universität München) and relevant experiments were performed by Ruth Eichner of Technische Universität München in accordance to the local guidelines.

4.1.16 Bacteria

BL21(DE3) Competent <i>E. coli</i>	New England Biolabs, Frankfurt
NEB 5-alpha F ['] I ^q Competent <i>E. coli</i>	New England Biolabs, Frankfurt

4.1.17 Cell lines

Cell lines	Description	Media	Source
ANBL6	human multiple myeloma cells	RPMI 1640; + 5 ng/ml IL6	kind gift of Dr. Tobias Dechow
Cos-7	African Green Monkey kidney fibroblast cells, with SV40 large T-Antigen	DMEM	ATCC, Virginia, USA
H929	human multiple myeloma cells	RPMI 1640	DSMZ, Braunschweig
HEK293T	human embryonic kidney cells, with SV40 large T-Antigen	DMEM	DSMZ, Braunschweig
HeLa	human cervix carcinoma cells	DMEM	DSMZ, Braunschweig
High Five	Insect ovarian cells from <i>Trichopulsia ni</i>	Express Five SFM	Invitrogen, Karlsruhe
IMR-90	primary human lung fibroblast	DMEM	ATCC, Virginia, USA
INA6	human multiple myeloma cells	RPMI 1640, + 5 ng/ml IL6	kind gift of Dr. Tobias Dechow
JJN3	human multiple myeloma cells	RPMI 1640	DSMZ, Braunschweig
KMS-12-BM	human multiple myeloma cells	RPMI 1640	kind gift of Dr. Tobias Dechow
LP1	human multiple myeloma cells	IMDM	DSMZ, Braunschweig
OPM2	human multiple myeloma cells	RPMI 1640	DSMZ, Braunschweig
RPMI 2668	human multiple myeloma cells	RPMI 1640	DSMZ, Braunschweig
Sf9	Insect cells from <i>Spodoptera frugiperda</i>	Grace's Insect Medium	Invitrogen, Karlsruhe
Sf21	Insect ovarian cells from <i>Spodoptera frugiperda</i>	Grace's Insect Medium	Invitrogen, Karlsruhe
T98G	human glioblastoma cells	DMEM	ATCC, Virginia, USA
U2OS	Human osteosarcoma cells	McCoy's 5A	ATCC, Virginia, USA
U266	human multiple myeloma cells	RPMI 1640	kind gift of Dr. Tobias Dechow

Table 9: List of cell lines

All media (3rd panel) were supplemented with L-Glutamine, Penicillin/Streptomycin and 10% FBS; except for HEK293T, where 10% BS instead of FBS was used.

4.1.18 Cell culture dishes

2- and 8-well glass slides

Dishes and flasks

24-well, 12-well, 6-well, T25, T75, 6 cm², 10cm², 15cm²

Nunc, Roskilde, Denmark

Biochrom, Berlin

4.1.19 Membrane

PVDF membrane (Immobilon P)

Millipore, Schwalbach/Ts

4.1.20 Machinery and equipment

Agarose electrophoresis chamber Mini-Sub Cell GT	Bio-Rad, München
Analytical balance ABJ	Kern & Sohn, Balingen-Frommern
Bacterial Shaker	Eppendorf, Hamburg
Calligrapher MiniArrayer	Bio-Rad, München
Centrifuge Multifuge 3SR+	Thermo Scientific, Waltham, USA
CO ₂ -Incubator Hera cell 150i	Thermo Scientific, Waltham, USA
Cool-Centrifuge 5417R	Eppendorf, Hamburg
Cool-Centrifuge 5430R	Eppendorf, Hamburg
FACS Calibur	BD, Franklin Lakes, USA
Fluorescence microscope	Olympus, Hamburg
FluoView FV10i	Olympus, Hamburg
Invitrogen Chamber for Ready Gels	Invitrogen, Karlsruhe
Magnetic Thermo Stirrer RCT basic	IKA, Staufen
Microscope Axiovert 40 CFL	Carl Zeiss AG, Oberkochen
Nano-Photometer	Implen, München
Neubauer hemocytometer	Marienfeld, Lauda-Königshofen
PCR-Thermocycler Primus	Peqlab, Erlangen
pH-meter pH720 InoLab	WTW, Weilheim
Power Supply PAC Basic	Bio-Rad, München
Power Supply PAC HC	Bio-Rad, München
Precision balance 572	Kern & Sohn, Balingen-Frommern
Rotating Wheel 3000	Fröbel Labortechnik, Lindau
Safety cabinet Herasafe KS	Thermo Scientific, Waltham, USA
Scanner V750 Pro	Epson, Meerbusch
SDS-gel Electrophoresis chamber Mini-Protean	Bio-Rad, München
SpeedVac	Eppendorf, Hamburg
Tabletop centrifuge 5424	Eppendorf, Hamburg
Thermomixer	Eppendorf, Hamburg
Waving platform shaker Polymax 1040	Heidolph Instruments, Kelheim
Western Blotting chamber Trans Blot Cell	Bio-Rad, München

4.1.21 Software and Databases

Till Vision: Microscope Imaging software	Till Photonics, Gräfelfing
FlowJo Flow cytometry analysis software	Tree Star, Ashland, USA
MacVector Sequence analysis software	Mac Vector, Cary, USA
Oncomine database	Compendia biosciences, Ann Arbor, USA

4.2 Methods

4.2.1 Molecular biology

4.2.1.1 Agarose Gel Electrophoresis

To visualise DNA, its electrostatic properties originating from its negatively charged phosphate backbone were exploited. Agarose was dissolved in TBE buffer, boiled and allowed to cool down to form a stable gel, through its pores the DNA can migrate according to its charge – proportional to its size – once a potential is applied. Adding DNA intercalating ethidium bromide to the gel allows for staining under UV-light.

4.2.1.2 PCR

The polymerase chain reaction (PCR) was used to amplify genes of interest. To this end 100 ng of target DNA was diluted in a reaction mix with 1 pM primer, with compatible sequences to end or beginning the DNA segment of interest, respectively, 10 mM dNTPs new strand synthesis and the elongating enzyme DNA polymerase Pfu Ultra HF (Stratagene) in suitable buffer. DNA-double helix was separated at 95°C, primers annealed at 55-65°C and elongation carried out at 72°C. Since the processivity of the polymerase is ~ 1kb/min, the time of this step was adjusted to the length of the desired product. Repeating this reaction (25-30 cycles) amplifies the amount of DNA product exponentially.

4.2.1.3 DNA Restriction

Restriction enzymes have the capability to proteolytically sever DNA at specific sites, while producing overhanging single stranded ends. Each restriction enzyme detects a specific palindromic recognition site on the DNA. Enzymatic reactions were incubated at 37°C for 2 hrs for a complete digest.

4.2.1.4 DNA Ligation

For Ligation the T4 Ligase (Fermentas) was used for 1 hr at 24°C or over night at 16°C. The enzyme ligates compatible overhanging ends of restricted DNA molecules. For optimal integration the molarities of the DNA molecules were adjusted to be equal.

4.2.1.5 Molecular cloning

To clone a desired gene into an expression vector, PCR primers (s. chapter 4.2.1.1) were designed with short overhanging ends, which encoded for a palindromic restriction site (s. chapter 4.2.1.3) that were also present or compatible to enzymes restricting in the Multiple Cloning Site (MCS) of the vector. After the PCR, the DNA fragment had to be purified by PCR Purification Kit (Fermentas),

before sequential restriction. Digested plasmid and gene amplicon were purified on a 1.2% agarose gel for 2 hrs, and the material extracted using the Gel Extraction Kit (Fermentas). Before ligation (s. chapter 4.2.1.4) the destination vector was treated with antarctic phosphatase for 30 min at 37°C, followed by a heat inactivation at 65°C for 5 min. This step reduces the capability of the plasmid to re-ligate without the insert DNA, since the T4 ligase requires free phosphate groups for restriction end joining. Ligation reactions were transformed into bacteria, positive clones selected, plasmid extracted (s. chapter 4.2.1.7) and insertion verified by sequencing.

4.2.1.6 Mutagenesis PCR

To mutate DNA sequences, the Stratagene Quik Mutagenesis Kit was used according to the manufacturer's instructions. Primers of ~40 b were designed, which carried the mutation and compatible sequences to both sites of the base(s) to be mutated. In a PCR (s. chapter 4.2.1.1) the whole plasmid with the sequence to be mutated was amplified. To remove the template plasmid, 1 hr digestion with DpnI, an enzyme digesting only bacterially methylated sites, was performed, before transformation into competent bacteria. Positive clones were assessed by sequencing of the purified plasmid (s. chapter 4.2.1.7)

4.2.1.7 DNA extraction

Plasmid DNA was amplified using NEB5 α bacteria grown to a density of OD₆₀₀ = 0.6 – 0.8. DNA was purified using QIAprep spin Miniprep Kit for small amounts and QIAGEN plasmid Maxi Kit for larger amounts. This method uses alkaloid lysis to break the cell wall of the bacteria and subsequent immobilization of DNA on an anionic column. RNA and protein are removed by raising salt concentrations. DNA is eluted with high salt buffer and precipitated with isopropanol in the cold. DNA pellet is cleared from salt with 70% Ethanol and resuspended in suitable storage buffer.

4.2.1.8 RNA extraction

RNA was extracted from tissue and patient samples using RNeasy Mini-Kit or (Qiagen) respectively, according to the manufacturer's instructions. For stability RNA in RNase-free water was stored at -80°C.

4.2.1.9 RT-PCR

To produce complementary DNA (cDNA) 1 μ g RNA was reversely transcribed using the protocol of SuperScript III Reverse Transcriptase (Invitrogen). To this end oligo-dT primer, which amplify polyA-tails of mRNA were added to the reaction for 5 min at 42°C for annealing, before amplification for 60 min at 72°C. For subsequent qPCR analysis (s. chapter 4.2.1.10) the product was diluted 1:20 in dH₂O.

4.2.1.10 Quantitative PCR

Quantitative PCR (qPCR) was performed with SYBR Green qPCR Mix (Roche). Since the dye SYBR intercalates with DNA, the analyser can measure the fluorescence intensity as an indirect amount of PCR product in correlation with the amplification cycles. Values were given as $2^{-\Delta\Delta CT}$. For normalization, expression of the genes ARRPA, GAPDH and INTEGRIN, respectively, were assessed. qPCR primers were designed using the publically available Quant Prime software¹⁵⁸.

4.2.2 Protein biochemistry

4.2.2.1 SDS-Gel Electrophoresis

To visualise proteins, they were separated acrylamide gels according to their size. To this end the protein samples were denatured with Laemmli buffer (s. chapter 4.1.9). Its main component SDS coats all proteins with negative charge, thus once potential is applied, migration of proteins proportional to their electrostatic properties. In the stacking gel, with a pH of 6.8 negatively charged glycine of the Laemmli buffer assembles all proteins at the same horizontal barrier, in the separating gel of pH 8.8 this is neutral and proteins can resolve according to their charge, correlating with size.

4.2.2.2 Western Blot Analysis / Immunoblots

Size separated protein samples were immobilized on a nitrocellulose membrane using wet blot method for 1 hr at 100 V or at least 6 hrs at 30 V. The proteins transferred were stained with Ponceau S or Coomassie Brilliant Blue for reference and destained with Washing Buffer (WB) or Coomassie destain (chapter 4.1.9), respectively. Blocking was performed with 5% milk in WB. Membranes were incubated with first antibodies (for dilutions s. chapter 4.1.10) agitating over night at 4°C or for 1.5 hrs at room temperature (RT = 24°C) in either milk (5%) or BSA (5%). Antibodies were washed off three times for 15 min with WB and incubated with the corresponding secondary antibody diluted in milk (5%) for 1 hr. After three washes, the membrane was developed on photosensitive films using chemiluminescence substrate by Pierce. The intensities of the resulting signals were evaluated using publicly available ImageJ¹⁵⁹ program.

4.2.2.3 Cell Lysis

For whole cell lysates, cell pellets were resuspended in Lysis Buffer containing salt concentrations to keep proteins stably in solution. When interactions were to preserve, lower salt concentrations were used, for extremely pure fractionation of proteins, the concentrations were raised. Detergent was added to disrupt the cell membrane, protease, kinase and phosphatase inhibitors to avoid activity, enzymatic cleavage or modification of potential target proteins within the lysate. If DNA-bound fraction was to be prepared, Benzonase was added to the MgCl₂ containing buffer. The mixture was incubated for 20-30 min on ice, before centrifugation at maximum speed for 15-20 min. The protein containing

supernatant was transferred into pre-chilled tubes and protein concentration determined using Lowry assay¹⁶⁰ based Bio-Rad DC protein assay. For SDS-PAGE lysates were denatured with Laemmli Buffer (s. chapter 4.1.9) and denatured at 95°C for 10 min. Protein lysates can be stored at -80°C.

4.2.2.4 Immunoprecipitation

Immunoprecipitation (IP) is based on the high affinity of antibodies to their respective target. These antibodies are chemically coupled to so-called beads, which allow a clear separation in a centrifugation due to their mass. In this manner target proteins and their respective co-factors or binding partners can be easily extracted from a whole cell lysate. To detach the target proteins from the bead-coupled antibodies – a process called elution – elevation of salt concentration, addition of a competitive protein in high concentrations or denaturing the proteins by heat or SDS can be applied.

Tandem Affinity Purification (TAP)

The Tandem Affinity Purification (TAP) method enhances sensitivity by applying two sequential purifications with beads directed against two different tags. Here, Flag- and Strep-Tags were used as described previously¹⁶¹ to reduce unspecific binding to beads. In a large-scale set-up for maximal protein production, the embryonic stem cell line HEK293T was grown to 2×10^9 and transfected with either empty control vector or the construct expressing the protein of interest. Cells were harvested after a sufficient time of expression under conditions indicated and snap frozen in liquid nitrogen. The 20 ml of lysate were prepared by Dr. V.Fernández-Sáiz (TUM) using MS Lysis Buffer (s. chapter 4.1.9), adding Benzonase and homogenized by two passages through a 19 Gauge syringe. In a first purification, protein was precipitated with 2 ml Strep-Tactin superflow resin (IBA) for 1.5 hrs. After four wash steps, proteins were eluted twice using 7.5 ml desthiobiotin elution buffer (IBA). The combined eluate was then subjected to a second precipitation with 400µl anti-FLAG resin (Sigma-Aldrich) for another 1.5 hrs, washed four times with BT Buffer (s. chapter 4.1.9) and treated to a further competition with 3xFLAG peptide (Sigma-Aldrich). 1.5 ml of eluate were precipitated with TCA (10%) over night at 4°C. Pelleted proteins were washed twice with ice-cold acetone and dried using a speed vac for 20 min. These samples could then be analysed by mass spectrometry (MS) with Dr. Simone Lemeer and Prof. Bernhard Küster in TU Freising. The methods used are presented in short below.

Mass spectrometry analyses (performed by Prof. Küster and Dr. Lemeer)

In short summary, peptides generated by in-gel trypsin digestion were dried down and dissolved in 0.1% formic acid (FA). LC-MS/MS was performed by coupling a nanoLC-Ultra (Eksigent) to a LTQ Orbitrap XL mass spectrometer (ThermoFisher Scientific), using a 60 min gradient from 0 to 40% solution B (0.1% FA in AcN). Peaklists were extracted from MS data files using Mascot Distiller v2.2.1 (Matrix Science) and subsequently searched against the Human IPI database version v3.58

using Carbamidomethyl (C) as fixed and Ox (M), Phospho (ST), Phospho (Y) as variable modifications. Mass tolerance of the precursor ion was set to 5 ppm (parts per million) and for fragmentations to 0.6 Da. Scaffold2, v2.1.03 was used for data interpretation. Proteins were filtered using a minimal protein identification probability of 99% and minimal peptide identification probability of 95%.

For phosphorylation analyses, proteins of interest were immunoprecipitated with anti-FLAG resin and eluted twice by competition with 3XFLAG peptide by Dr. V. Fernández-Sáiz. The eluates were then processed for phosphopeptide enrichment. Gel bands were cut out and in-gel trypsin digestion was performed. PHOS-Select (Sigma) iron coated beads were mixed with the peptide mixture and incubated for 30 min at room temperature. Phosphopeptides were directly eluted onto a stainless steel target Maldi target (Bruker Daltonik) using 20 mg/ml DHB in 50% AcN and 1% phosphoric acid. Mass spectra were acquired in positive ion reflectron mode on an ultrafleXtreme MALDI-TOF/TOF mass spectrometer equipped with a 1 kHz Smartbeam-II laser (Bruker Daltonik). Laser intensity was adjusted for optimal signal-to-noise ratio and resolution and spectra were recorded from 1000 to 3500 m/z. Tandem mass spectra were acquired in positive ion reflectron mode using the LIFT technique with an increased laser intensity (+40%). Mass spectra were analyzed using the flexAnalysis software (version 3.3) (Bruker Daltonik). Peak picking was performed manually.

GST-Purification

Recombinant expression of GST-tagged proteins in bacteria is described in chapter 4.2.7.2. For lysis frozen bacteria pellets were resuspended in NETN buffer (s. chapter 4.1.9) and treated with 100 µg/ml lysozyme to break the cell wall for 30 min on ice. Complete disruption was further ensured by ultrasound treatment avoiding foam formation, with 10 pulses at 50% amplitude. Cell debris was discarded by centrifugation and the supernatant subjected to an immunoprecipitation with glutathione-coupled beads at 4°C for 30 min. After four washes, bound proteins were eluted four times for 10 min in the cool using glutathione elution buffer. For removal of excess glutathione, the eluate was dialysed against 10 ml PBS in the cold. Eluted protein was snap frozen in – 198°C and stored at -80°C

4.2.2.5 Reverse phase protein lysate microarrays

Extract preparation of formalin fixed bone marrow biopsies and reverse phase protein lysate microarrays were performed by Clemens Reiter (TUM). In short, formalin fixed bone marrow biopsies of MM patients were with an infiltration rate >70% were selected from the archive of the Institute of Pathology, Technische Universität München, Germany. Extract preparation was essentially performed as described¹⁶². Protein arrays were generated using the Calligrapher MiniArrayer (BioRad). For every extract and every dilution (undiluted, 1:2, 1:4, 1:8, 1:16, buffer only), three replicates were applied onto a nitrocellulose-coated glass slide (Grace Bio-Labs)¹⁶³. For quantification, parallel arrays were

stained with Sypro Ruby (Molecular Probes) according to the manufacturer's instructions.

4.2.2.6 Ubiquitylation assay

***in vivo* ubiquitylation**

By overexpression of HA-tagged ubiquitin, FLAG-tagged substrate and the F-box protein in HEK293T cells (s. chapter 4.2.5.1), the ubiquitylation reaction in physiological context could be assessed. After transfection, exogenous proteins were expressed for 24 hrs prior to treatment with 10 μ M MG132 for 3-4 hrs to inhibit proteasomal degradation of marked substrate and hence preserve ubiquitylation. Cells were pelleted and resuspended in 100 μ l Lysis buffer (s. chapter 4.1.9). The supernatant was denatured to preserve only covalent peptide bonds by addition of 0.1% NP-40, 5 mM EDTA, and 1% SDS and subsequent caefaction at 95°C for 5 min. Samples were allowed to cool down at RT, but not on ice to avoid precipitation at this point. For quenching the SDS, 900 μ l 10% Triton-X in Lysis buffer (s. chapter 4.1.9) were added to a final concentration of 1% and samples immediately put back on ice. An IP for the substrate was performed as in chapter 4.2.2.4 and ubiquitylation assessed using western blot analysis (s. chapter 4.2.2.2). These experiments were essentially performed by Dr. V.Féernandez-Sáiz.

***in vitro* ubiquitylation**

To reconstitute the ubiquitin system in a controlled environment, each component of the SCF complex was purified from insect cells by Dr. V.Féernandez-Sáiz and stored in aliquots at -80°C. Equal amounts were added to the ubiquitylation assay buffer (s. chapter 4.1.9). The reaction was incubated with the substrate purified from eukaryotic cells treated with or without the intended stimulus. The ubiquitylation reaction was carried out for 30, 60, 90, and 120 min at 37°C shaking and stopped with the addition of Laemmli buffer (s. chapter 4.1.9).

4.2.2.7 Kinase Assay

To show specific phosphorylation of the substrates and their mutated phospho-degron forms, they were overexpressed in and purified from HEK293T (s. chapter 4.2.5.1). Together with the active CK2 (Millipore) they were incubated in kinase assay buffer containing labeled ATP (s. chapter 4.1.9) for 10 min at 30°C and subsequently visualised by autoradiography.

4.2.3 Antibody production

The antibody against Fbxo9 was produced with the help of Dr. Daniel Moik and Prof. Fessler (MPI Munich) together with Dr. V.Féernandez-Sáiz. The protein sequence of Fbxo9 was screened for a suitable epitope of ~15 aa, which does not contain a Cys, does not cover a highly structured region of the protein, is predicted to be soluble, and is not present in a second human protein. For structure determination coils server¹⁶⁴ was used, GenScript (Piscataway,USA) provided information for peptide

solubility and using Basic Local Alignment Search Tool (BLAST¹⁶⁵), the non-ambiguous sequence was ascertained. The peptides were designed with an additional Cys at either C- or N-terminus. The antibody of this study was generated against a peptide containing amino acids 390-404 of human Fbxo9 (Cys_CSSGHQRFNKLIIWH)

Prior to immunization, sera of twelve rabbits were tested by Dr. V.Fernández-Sáiz, if they produced unspecific western blot signals at the size of Fbxo9 (40-60 kDa), and those were excluded from the production. Peptides were coupled to highly immunogenic carrier proteins using the Imject Maleimide Activated mcKLH Kit (Pierce). Per peptide, two rabbits were immunized injecting an antigen-adjuvant emulsion. For the first boost 1 Vol of TiterMax Gold (Sigma-Aldrich) was mixed to one aliquot of coupled peptide solution at RT by fast constant mixing for one min, just before injection to the animal. All further boosts used Incomplete Freund's Adjuvant (Sigma-Aldrich). The first boost was after four weeks and the following boosts repeated every three weeks. Sera were tested for specificity on Western Blots two weeks after boosting. The animal producing Fbxo9 Antibody positive serum, was immunized a fourth time and after two weeks, the serum collected in a final bleeding.

Using the same method, phospho-specific Antibodies to pS485-Tel2 and pS828-Tti1 were produced with Innovagen (Sweden).

4.2.4 Murine liver cell extraction

Mice liver cells were essentially extracted as described before¹⁶⁶ by Ruth Eichner (TUM). Briefly, six month old male wild type C57BL/6 mice were fed or fasted for 16hrs. After sacrificing the mice, livers were weighed, perfused with an EDTA containing buffer and hepatocytes were isolated for subsequent cell lysis and western blot analyses.

4.2.5 Eukaryotic cell culture

Cells were cultured in a humidified incubator supplied with 5% CO₂. Physiological pH and temperature were set to pH 7.365 and 37°C, respectively. When necessary the media was supplemented with essential growth factors (see chapter 4.1.14). At a density of 90% cells were splitted to allow further growth. Adherent cells that are able to form a mono-layer attached on the plates, were detached using trypsin. Cell density and viability of suspension cells was assessed by counting trypan blue stained aliquots on a Neubauer hemocytometer. For long-term storage, exponentially growing cells were pelleted and resuspended in FBS with 10% DMSO. DMSO intercalates in the cell membrane and stabilizes it. The mixture was slowly frozen in isopropanol at -80°C to avoid rupture of the cell membrane by rapid freezing. When unfreezing cells, DMSO was quickly removed by centrifugation to impair its penetration to the interior of the cell.

4.2.5.1 Transfections

Calcium Phosphate Method

HEK239T were transfected using the CaPO₄- method, if not stated differently. To this end plasmid DNA was diluted in dH₂O to 2 pM and mixed with CaCl₂ to a final concentration of 250 mM. Calcium-ions form ionic bonds with the negatively charged phosphate-backbone of plasmid DNA. Addition of 1 Vol of BES (N,N-Bis-(2-hydroxyethyl)-2-aminoethansulfonic acid buffered in NaCl and Na₂HPO₄ to pH 7.1) leads to DNA-complex formations at 24°C. After incubation for 20 min complexes were slowly dropped to 70-80% confluent cell layers. Uptake of plasmid DNA through pores formed in the cell membrane was allowed for 4 hrs. Media exchange washed away the remaining complexes and re-established physiological pH in the culture. Transfection efficiency was determined as percentage of green fluorescent cells that had been co-transfected with a peGFP expression plasmid.

Lipofection

Other cell lines were transfected using Lipofectamine™ 2000, ExGen 500 *in vitro* Transfection Reagent, or FuGene HD according to the manufacturer's instructions. Briefly, the reagents can form liposome complexes with the plasmid DNA that are more easily incorporated by the lipid bilayer of cell membranes¹⁶⁷. To avoid toxicity the complexes are washed away by media exchange after 3-4hrs.

siRNA silencing

HiPerFect Transfection Reagent was used for siRNA silencing in U2OS, HeLa, and T98G. For an efficient co-transfection of plasmids and siRNA into HEK293 TurboFect™ siRNA Transfection Reagent was used according to the manufacturer's instructions. Efficient knockdown could be observed after 24-48 hrs.

4.2.5.2 Retrovirus production

HEK293T were seeded on gelatinised 6 cm² plates one day before transfection to reach a density of 90%. With Lipofectamine 2000 (Invitrogen), cells were co-transfected with 4µg of each the VSVG plasmid encoding for the virus' envelope protein, the pcDNA-MLV_GAG/POL construct that allows expression of the viral structural proteins and the viral polymerase – a reverse transcriptase –, and the vector with the desired gene cloned in-between the LTR (Long terminal repeats) sites that allow for integration to the host cell's genome. Virus containing media was harvested 48 and 72 hrs post transfection.

4.2.5.3 Viral infection

For retroviral infection, cells were seeded on 6-well plates to reach a confluency of 50-60%, since retroviruses can only integrate their genetic information into the genome of dividing cells. For lentiviral infection particles were diluted in media to 10 Titer Units (TU)/ ml. To reduce the electrostatic repulsion between cell membrane and virus surface 8 µg/ml Polybrene was added for enhanced infection efficiency¹⁶⁸. Using the double spin infection method, cells were centrifuged with the virus containing media for 1 hr at 1200 rpm. After 4 hrs incubation, media was replaced with new infectious media the centrifugation step was repeated. Cells were allowed to recover for 1-2 days in virus-free media. At this stage stable integration could be tested by GFP signal and/or puromycin selection.

4.2.5.4 Cell Cycle Profiling

Usually cells are growing asynchronously, i.e. each cell in the culture dish can be at any point of all cell cycle stages. To access the status of a cell in a specific phase, their growth has to be synchronised applying chemical compounds.

Synchronisation in G₁-S-phase transition

Addition of 2 mM Thymidine (Thy), results in an excess concentration of one of the four bases, needed for DNA replication in S-Phase. Due to the excess, the remaining dNTPs are no longer accessible to the DNA-Polymerase, and all cells have to stall in S-Phase. This block is reversible by washing away the Thy. After the first Thy block for overnight, the cell population will be uniformly at different stages of S-Phase. For an exact synchronization in the G₁-S-phase transition, this population is released from Thy for 7-10 hrs according to the replication time of the respective cell line, before addition of a second Thy block for overnight. All cells will now accumulate at the entry to S-Phase.

Synchronisation in M-phase

For synchronisation in Mitosis, cells can be treated with either 500 ng/ml Nocodazole or 1µM Taxol. Both are spindle poisons, destabilizing or stabilizing the microtubules of the spindle apparatus, respectively. While Nocodazole arrests cells in Prometaphase, Taxol will perturb Anaphase-transition.

For time course experiments cells were synchronized for 18 hrs with non-toxic Thy, released and supplemented with Nocodazole, to reduce the incubation with the poison to a minimal time of 10-12 hrs depending on the cell line investigated. Mitotic, rounded cells could be disattached from the plate by manual shake off, and released into the cell cycle by extensive wash with PBS (twice) and media (once).

4.2.5.5 Serum deprivation

Serum withdrawal leads to accumulation of cells in G₀-Phase. T98G and U2OS were serum deprived (SD) using 0.02% FBS and restimulated by serum addition (SA) of 10% FBS containing media. For the HEK293T starving with 0.1% FBS in media was sufficient. Deprivation of IMR90 was conducted with 0.2% FBS containing media. For HeLa, FBS was completely removed from media to induce apoptosis. To effectively starve cells, they were plated one day prior for a density of 60%. Then growth media was washed away twice with PBS. A final wash for 5 min with the SD media was performed to completely remove remaining FBS from cells.

4.2.5.6 Proteasome inhibition

To analyse cells for polyubiquitin mediated degradation of certain proteins, the activity of the proteasome has to be impaired. To inhibit the proteasomal function 10µM MG132 in DMSO were added to the media for 3-4 hrs.

4.2.5.7 Ribosome inhibition

By inhibition of the ribosome with Cycloheximide novel protein biosynthesis is impaired. Thus, levels of those proteins that are constantly reproduced will eventually decline. Taking cell samples over time the stability and half-life of proteins can be analysed by Western Blot (s. chapter 4.2.2.2). Cycloheximide was dissolved in 100% Ethanol and added to culture media in a final concentration of 100µg/ml.

4.2.5.8 Kinase agonism and antagonism

CK2 was specifically inhibited using 50 µM TBB (diluted in DMSO). Starved cells could be incubated for up to 9 hrs, untreated for more than 24 hrs. Activity of CK2 was stimulated with 0.5 M Sorbitol for 2 hrs.

4.2.5.9 mTOR signalling inhibition

To inhibit mTORC1 signalling, cells were treated with 50 nM Rapamycin (Rapa). To block PI3K/mTORC2/Akt signalling cells were either treated with 500 nM Wortmannin or 1.5 µM Akt inhibitor IV, which specifically impairs Akt activity. All inhibitors were dissolved in DMSO.

4.2.5.10 Protein Translation Assays

Luciferase Assay

To monitor *in vivo* protein translation, HEK293T cells were seeded in a 24-well plate to 60% confluency and transfected with either pcDNA3.1 Tti1 (WT or S828A), or siRNA oligonucleotides directed against Fbxo9 or LacZ, a 5' structured stemloop firefly luciferase reporter gene (pcDNA-SL-LUC)¹³⁶, and a pRL-null Renilla luciferase plasmid. The co-transfection of two different luciferase

encoding constructs allows for normalisation of the values to the general transfection efficiency, whereas the firefly luciferase construct experimentally measures starvation induced translation, and Renilla luciferase general translation. Cells were allowed to recover for 12 hrs in DMEM with 10% FBS and then serum starved for 48 hrs. The luciferase activity was measured using a dual-luciferase reporter assay system (Promega) according to the manufacturer's instructions.

de novo protein biosynthesis

Metabolic *in vivo* cell labelling with [³⁵S]-Met/Cys was essentially performed as described previously.¹⁶⁹ Briefly, 15 cm² plates with serum starved cells were washed three times with Met/Cys-free media and incubated with 8 ml labelling medium (Met/Cys-free DMEM, 10% dialyzed FBS, 2 mM L-glutamine) supplemented with 0.2 mCi/ml of [³⁵S]-Met/Cys mix for 2 hrs before harvesting. Thereafter IP reactions against the proteins of interest were conducted. Purified newly synthesized proteins that incorporated the radioactive amino acid can be visualised by autoradiography.

4.2.5.11 Flow cytometry (FACS Analysis)

The Fluorescence Activated Cell Sorting (FACS) analysis allows for quantitative characterization of surface markers or intracellular molecules on a single cell level and specific sorting of heterogenic populations according to desired parameters. The basic principle is that cells are specifically stained with fluorescently labelled substances or antibodies which can be excited by lasers of the appropriate wavelength. These dyes then emit photons of a certain energy that can be detected. The concentration of photons is thus proportional to the amount of dye per cell. The FACS machine can simultaneously measure different emission wavelengths for one cell. Additionally, the forward scatter (FSC), a measure of scattered laser signals, gives information about cell size, since proportionally to its size the cell will produce lighter scattering. Sideward Scattering (SSC) is produced by the cells' inner compartments. Data was analysed with FlowJo software.

Proliferation analysis

Bromodesoxyuridin (BrdU) can be incorporated into the DNA of replicating cells instead of base desoxy thymidine triphosphate (dTTP). For assessment of proliferation exponentially growing cells were pulsed for one hour with 10µM BrdU before harvesting. This was followed by a washing step with BrdU wash buffer I and fixation in 70% Ethanol as described above. After removal of Ethanol the DNA was denatured for 30 min with 500µl DNA denaturing buffer, cells pelleted and resuspended in 1M Borate to neutralize the acid. Then cells were washed with BrdU wash buffer II, resuspended in 20µl/1x10⁶ cells containing FITC labeled BrdU antibody for 30 min at 24°C and finally stained with 0.5µg/ml with the DNA intercalating agent propidium iodide (PI) to measure DNA content as a marker for cell cycle distribution in homogenous populations.

4.2.5.12 Immunofluorescence staining

To visualise the localisation of proteins within an intact cell, fluorescent dyes, fluorescent tags or specific antibodies coupled to dyes were applied onto fixed cells. Pictures were obtained using the laser-scanning confocal microscope FluoView FV10i (Olympus) for blue (excitation (Ex) = 400 nm; emission (Em) = 460 nm), green (Ex= 495 nm; Em= 530 nm) and red (Ex= 570 nm; Em= 635 nm), and processed with the accompanying Olympus Software. For quantification of protein localisation, 100 cells were analysed in three different sets.

Direct Immunofluorescence

For direct staining, cells were grown on glass cover slips (Nalgene), transfected with an expression vector coding for fluorescently labelled protein of interest, allowed time for expression and treated as indicated. Cells were fixed with ice-cold methanol for 10 min at -20°C, permeabilising the membrane at the same time. Methanol was washed away with PBS, and the cells briefly dried, before staining with DAPI, a dye that can intercalate with the DNA and allows for localisation of the nucleus. To protect from oxygen the cell layer was shielded with Slow Fade Gold (Invitrogen) and sealed with nail polish. To preserve the samples, they were stored in the cold protected from light.

Indirect Immunofluorescence

Cells were grown and fixed as above. After washing with PBS, cells were additionally permeabilised for 20 min with IF buffer (s. chapter 4.1.9). Then first antibodies against either endogenous protein or its tag, were diluted 1:500 in IF buffer, if not stated differently (s. chapter 4.1.10) and applied on the fixed cells for 1-1.5 hrs. In three wash steps first antibodies were removed before addition of the corresponding fluorescently labeled secondary antibody (1:1000 dilution) for 45-60 min in the dark. As a reference for background staining, one sample was only incubated with the secondary antibody. After thorough washing with PBS, cells were DAPI stained and shielded as described before.

4.2.6 Insect cell culture

Insect cells were cultured in respective media at 30°C in a controlled environment in collaboration with Dr. V.Fernández-Sáiz. For virus production, Sf9 were transfected with BacFectin (Invitrogen) and the cDNAs encoding the entire coding region of human Fbxo9, Fbxw7, Cul1, Roc1, and Skp1 inserted into the baculoviral expression vector pFastBac6 (Invitrogen). After five days virus containing supernatant was used to infect High Five cells that could produce high amounts of the recombinant proteins in their media for further purification.

4.2.7 Bacteria cell culture

For amplification, all bacteria were cultivated in LB Media at 37°C under constant shaking, to allow optimal oxygen distribution in the culture. If necessary, selection pressure was applied using 100µg/ml Ampicillin or 50µg/ml Kanamycin. For long-term storage an over-night culture was supplied with 30% Glycerol and kept frozen at -80°C.

4.2.7.1 Transformation

For amplification, desired plasmids were transformed in chemically competent NEB5αFI' E.coli bacteria using a heat shock for 45 sec at 42°C and subsequent incubation on ice for 2 min. For recovery, cells were supplemented with SOC Media and agitated at 37°C for 1 hr. Bacteria suspension was distributed on LB-Agar plates containing antibiotics specific to the resistance encoded on the respective plasmid. Bacteria colonies were visible after 12h incubation at 37°C.

4.2.7.2 Induction of protein expression

For expression of recombinant proteins, pGEX-4T2 vectors coding for the desired GST-fusion proteins were transformed in BL21. Positively selected colonies were amplified in LB_{AMP} media over night at 37°C. The Optical Density (OD₆₀₀) of the culture was assessed photospectrometrically and adjusted to be 0.4 - 0.6 with LB media. This value is specific for exponentially growing bacteria. Then 1 µM IPTG was added to induce expression from the LAC promoter for 2 hrs. The activity of the LAC promoter is usually blocked by the Lac repressor molecule. By binding to this repressor IPTG removes it from the promoter and allows for active transcription of the encoded gene. The bacteria were harvested by centrifugation and the pellet frozen at -80°C. In a following GST-Purification (s. chapter 4.2.2.4) recombinant proteins could be extracted.

4.2.8 Data mining

In order to investigate a potential correlation between the expression levels and response to the proteasome inhibitor Bortezomib, a previously published gene expression data set available at Gene Expression Omnibus (GEO)¹⁷⁰ (GEO accession number: GSE9782) was correlated with outcome in clinical trials of Bortezomib treatment by Prof. L.Bullinger (University of Ulm). Based on the normalized gene expression data provided in the repository, expression data was correlated with clinical data. Samples were grouped based on the median *Fbxo9* expression (probe set 238472_at). Kaplan Meier curves were plotted using GraphPad Prism 4 (GraphPad Software Inc., La Jolla, USA).

Further expression data were retrieved from the Oncomine website¹⁷¹. Histograms depicting *Fbxo9* gene expression in each sample, as well as a student's t-test giving a P value for the comparison of candidate gene expression between the groups, were obtained directly through the Oncomine 3.0 software.

5 Results

The presented data of this study was obtained as part of a large collaborative project, which was jointly conducted by the submitting author (Bianca-Sabrina Targosz, M.Sc) and Dr. Vanesa Fernández-Sáiz at the research group of PD Dr. Florian Bassermann at the Klinikum rechts der Isar (TUM) as well as other collaborators. To ensure a comprehensive presentation of the results within the scope of the project, the present work comprises also those results that were provided by researchers other than the submitting author. For clarity, those contributions are indicated in the following text as well as in the figure legends.

5.1 Fbxo9 mediates degradation of Tel2 and Tti1 proteins in response to serum withdrawal to regulate mTOR abundance and function

5.1.1 Fbxo9 interacts with Tel2 and Tti1

In an attempt to identify interactors of the orphan F-box protein (FBP) Fbxo9, an unbiased mass spectrometry (MS) based screen for co-immunoprecipitating proteins was conducted by Dr. V. Fernández-Sáiz (TUM). To this end FBXO9 gene was cloned into an expression vector that encodes an N-terminal tag consisting of a combination of Tandem-Strep-single-FLAG peptides. After transfection into human embryonic kidney (HEK) 293T cells, the resulting fusion-protein was subsequently expressed. This allowed for Tandem affinity purification (TAP), a method that enhances specificity and reduces false positive counts (s. chapter 4.2.2.4). To account for the reduced sensitivity of a TAP, a large scale purification with cell lysates of 2×10^9 cells was performed. As a control, cells were transfected with an empty vector (Ctrl) and the cell lysate subjected to the purification process in parallel. Figure 9 shows 5% of the final eluate visualised on a SDS-gel with silver staining methods. The prominent band at 53 kDa (s. molecular weight (MW) marker on the left) was detected at the expected size of the Fbxo9 protein. Compared to the control (Ctrl)

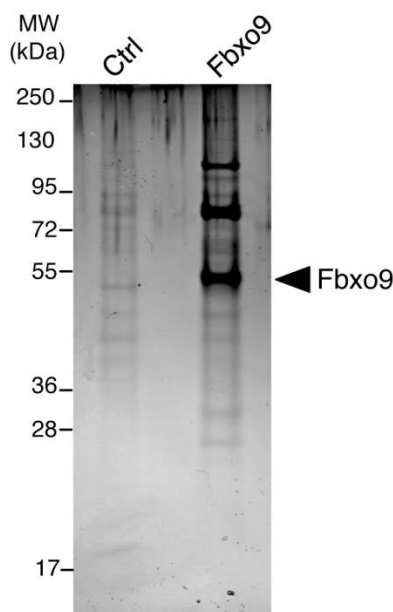


Figure 9: Silver Gel of TAP- purified Fbxo9 for mass spectrometry analysis. Tandem-Strep-single-FLAG-tagged (SF-TAP)-Fbxo9 (Fbxo9) was transiently overexpressed in HEK293T cells (2×10^9 cells) and subjected to a sequential immunopurification comprising immobilisation on Strep-Tactin beads and elution with desthiobiotin in the first step, and immobilization on anti-FLAG resin and elution with 3xFLAG-octapeptide in the second step. The FLAG eluate was separated by SDS-PAGE and analysed by mass spectrometry. As a control (Ctrl), a parallel purification was performed from HEK293T transfected with an empty vector. The depicted gel corresponds to 5% of the final FLAG-eluates visualized by silver staining. (MW: molecular weight) [Data provided by Dr. V. Fernández-Sáiz]

eluate, there are several bands with a strong signal intensity, which is only present in the Fbxo9 eluate, indicative of putative abundant interactors of Fbxo9. The weakly stained bands that are present in both lanes reflect the unspecifically co-purifying proteins. Eluates were analysed in the MS facility of the chair for Proteomics and Bioanalytics (TUM) in collaboration with Prof. B. Küster and Dr. S. Lemeer, and a list of detected peptides was provided. Unspecific background detection was defined as similar peptide counts in both the Fbxo9 and Ctrl eluate and omitted from further analyses. Interestingly, the resulting list of putative interactors of Fbxo9 denoted a high number of peptides corresponding to the proteins Skp1 and Cull1 – the main components of the SCF complexes (s. chapter 3.2.3.3). This served as an internal control that indeed interacting proteins of the FBP Fbxo9 can be co-immunoprecipitated by TAP and subsequently be detected by MS analysis. After an intensive review of the MS results, Telomere length regulation protein Tel2 homolog (IPI00016868) – in the following referred to as Tel2 – emerged as an interesting candidate with ten unique peptides identified (Table 10). Tel2 is a protein of 838 aa and the peptides detected could cover almost the entire protein of ~ 95 kDa with high confidence (Table 10).

Sequence	Mascot Ion score	Modifications	Start	Stop
(R)QGLLSAVSSVLLSLPAAR(L)	72.1		768	785
(R)EVSVELAK(V)	26.45		551	558
(R)LVEQVPDR(A)	28.05		255	262
(R)QGLLSAVSSVLLSLPAAR(L)	34.48		768	785
(R)AmEAVLTGLVEAALGPEVLSR(L)	25.89	Oxidation (+16)	263	283
(R)LLEDLMDELLEAR(S)	90.83		786	798
(R)LLEDLmDELLEAR(S)	73.31	Oxidation (+16)	786	798
(K)AVLIcLAQLGPELR(D)	63.76	Carbamidomethyl (+57)	363	377
(R)QGLLSAVSSVLLSLPAAR(L)	94.96		768	785
(R)LQQENLAEFFPQNYFR(L)	111.71		171	186
(R)AmEAVLTGLVEAALGPEVLSR(L)	90.93	Oxidation (+16)	263	283

Table 10: Sequences and modifications of the identified peptides corresponding to Telomere length regulation protein Tel2 homolog (IPI00016868) (Tel2). The letters ‘m’ or ‘c’ represent Oxidation or Carbamidomethyl, respectively. [Data provided by Dr. S. Lemeer and Prof. Dr. B. Küster]

Because Tel2 is known to regulate the abundance of PIKKs as part of a protein complex¹²⁰, the MS analysis data was further scanned for its interacting protein. Indeed, also Tel2-interacting protein 1 homolog (IPI 00011702) – from now on called Tti1 – could be matched to five unique peptides of the list of putative interactors of Fbxo9 (Table 11). Tti1 is a large protein of 1089 aa and ~128 kDa, thus only a relatively small portion of the protein was covered by the identified peptides (Table 11). This might reflect stoichiometric abundance of the protein, but could as well be explained by experimental limitations to detect all resulting peptides of Tti1 with the MS method.

Sequence	Mascot Ion score	Modifications	Start	Stop
(K)FSTLSLLLGYLK(L)	41.07		398	409
(K)ALADILSESLHSLATSLPR(L)	47.69		369	387
(K)FSTLSLLLGYLK(L)	92.03		398	409
(K)ALIQVLELDVADIK(I)	76.35		431	444
(K)QLGDLFASFLPGISTALTR(L)	71.94		201	219

Table 11: Sequences of identified peptides corresponding to Tel2-Interacting protein 1 homolog (IPI 00011702) (Tti1). [Data provided by Dr. S. Lemeer and Prof. Dr. B. Küster]

To confirm the results of the MS screen, a series of immunoprecipitations (IP) was performed by Dr. V.Fernández-Sáiz. First, to rule out that interactions of Fbxo9 with Tel2 and Tti1 are mediated via other components of the SCF, binding to five different FLAG-tagged FBPs was tested in a simultaneous experiment. Expression constructs were transfected and cells collected for analysis 24 hrs post transfection. As negative control an empty vector (EV) was used. Western blot analyses of whole cell extracts (WCE) show expression levels of the different FBPs, as well as endogenous expression of Tti1 and Tel2 proteins (Figure 10). While all FBPs could be efficiently immunoprecipitated (IP), a co-immunoprecipitation of Tel2 and Tti1 could only be observed with Flag-tagged Fbxo9.

This result suggested a specific interaction of Tel2/Tti1 with Fbxo9. To further confirm this notion reciprocal IPs with FLAG-tagged Tti1 or Tel2, respectively, were performed by Dr. V.Fernández-Sáiz. As expected for a direct interaction, in immunoblot analyses endogenous Fbxo9 was detected to co-immunoprecipitate with both overexpressed proteins and while in the control IP (EV) Fbxo9 could not be detected (Figure 11).

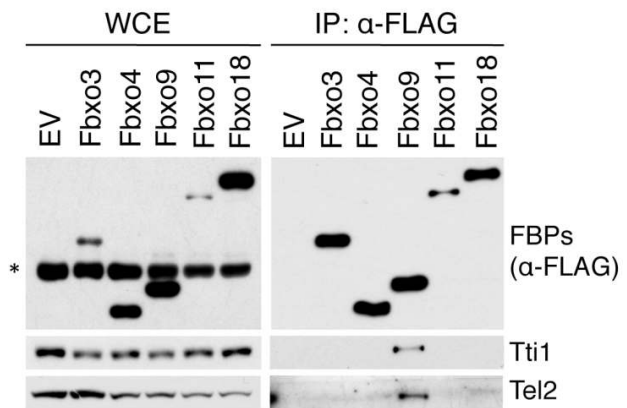


Figure 10: Fbxo9 is the only F-box protein that interacts with Tel2 and Tti1. HEK293T cells were transfected with empty vector (EV) or constructs of the indicated FLAG-tagged F-box proteins (FBPs). Whole cell extracts (WCE) were immunoprecipitated (IP) with anti-FLAG beads, and subjected to a denaturing SDS-PAGE, immobilised on a membrane by Western Blot methods and subsequently probed with antibodies to the indicated proteins. Asterisks denote a nonspecific band. [Data provided by Dr. V.Fernández-Sáiz]

Thus starting from an unbiased approach, an F-box-specific association of the orphan Fbxo9 with Tti1 and Tel2 could be demonstrated.

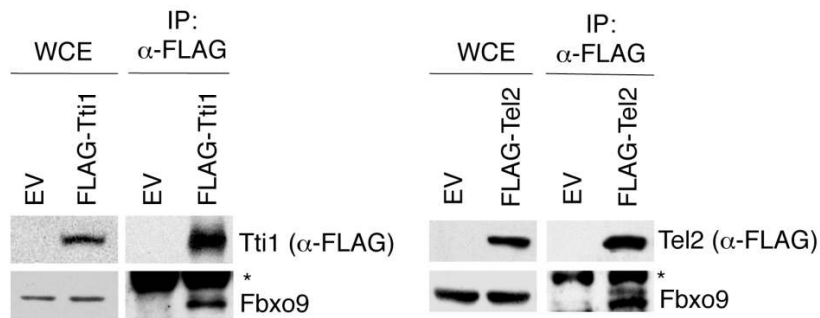


Figure 11: Reciprocal co-immunoprecipitation of Fbxo9 with Tti1 and Tel2. HEK293T cells were transfected with empty vector (EV) or FLAG-tagged Tti1 (left panel) or Tel2 (right panel) constructs, respectively. Whole cell extracts (WCE) were immunoprecipitated (IP) with anti-FLAG beads and probed with the indicated antibodies. Asterisks denote nonspecific bands. [Data provided by Dr. V.Fernández-Sáiz]

5.1.2 SCF^{Fbxo9} ubiquitylates Tel2/Tti1

The direct binding of the proteins suggests a relevant biochemical interaction, and thus it was tested by Dr. V.Fernández-Sáiz, whether Fbxo9 possesses ubiquitin ligase properties towards Tel2 and Tti1. In a reconstituted system, purified components of the E3 ligases SCF^{Fbxo9} or SCF^{Fbxw7} were incubated with ubiquitin, E1 and E2 enzymes (s. chapter 4.2.2.6) to test ubiquitylation of FLAG-tagged Tel2 or Tti1 *in vitro* (Figure 12). Polyubiquitylation can be visualised by western blot analysis as a vertical accumulation of signal depicting the multiple numbers of ubiquitin conjugates. This is only observed for Tel2 (Figure 12a) or Tti1 (Figure 12b), respectively, if the SCF complex is reconstituted with Fbxo9, but not with an alternative F-box (Fbxw7) or in the absence of an FBP (Ctrl). During the course of time the polyubiquitylation signal becomes more intense, which is indicative of a fully functional reconstituted system. It is also worth noting that at the start of the reac-

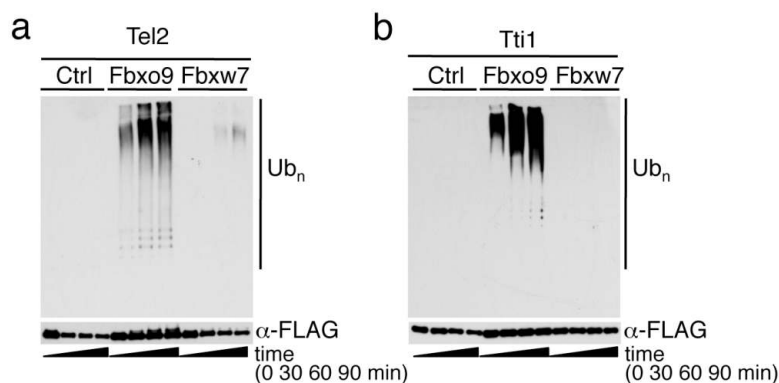


Figure 12: SCF^{Fbxo9} specifically ubiquitylates Tel2 and Tti1. *In vitro* ubiquitylation assays of Tel2 (a) and Tti1 (b) proteins. SCF^{Fbxo9} and SCF^{Fbxw7} were expressed using baculoviruses and purified from Sf21 insect cells. FLAG-tagged Tel2 and Tti1 were immunoprecipitated from HEK293T cells. Reactions were supplemented with ubiquitin, E1, and E2, and the respective E3 incubated at 37°C as specified, and subjected to immunoblotting with the indicated antibodies. As control (Ctrl) no E3 was added. The brackets on the right side mark polyubiquitylated (Ub_n) Tel2 or Tti1, respectively. [Data provided by Dr. V.Fernández-Sáiz]

tion (0 min) neither FLAG-Tel2 nor FLAG-Tti1 purified from human cells are detected when tested with an ubiquitin specific antibody. This excludes the possibility that the signal observed could result from a prior ubiquitylation event during cell culturing.

Even though ubiquitylation of Tel2 and Tti1 was selectively observed for the active SCF^{Fbxo9} *in vitro*, it remained to ensure that ubiquitylation is not due to the utilisation the artificial system. Thus to identify the relevance of the ubiquitylation reaction in *in vivo*, HEK293T cells were transfected with expression vectors coding for HA-tagged Ubiquitin (Ub), Fbxo9 and FLAG-tagged Tel2 or Tti1, respectively. Addition of the proteasome inhibitor MG132 prior to analyses blocked the degradation by the UPS to allow detection of cellular Ub conjugates. The ubiquitylation substrates Tel2 and Tti1 were then immunoprecipitated under denaturing conditions by Dr. V.Férrandez-Sáiz to detect only covalently bound Ub moieties (s. chapter 4.2.2.6). Western blot analyses showed a strong accumulation of ubiquitylated Tel2 (Figure 13a) as detected by an HA-specific antibody under conditions when Fbxo9 expression was enforced (lane 3). Of note in lane 2 a weak vertical signal accumulation could be shown, indicating that Tel2 can also be polyubiquitylated by the endogenous E3 ligase, since Fbxo9 was not overexpressed. However, this signal disappears in controls without Ha-tagged Ub or Tel2 (lane 1+4). Similarly, for purified Tti1 an enhanced intensity of the polyubiquitin signal can be detected once Fbxo9 is overexpressed (Figure 13b/lane 4). Again, a weak polyubiquitylation signal can be detected without addition of the exogenous Fbxo9 (lane 2).

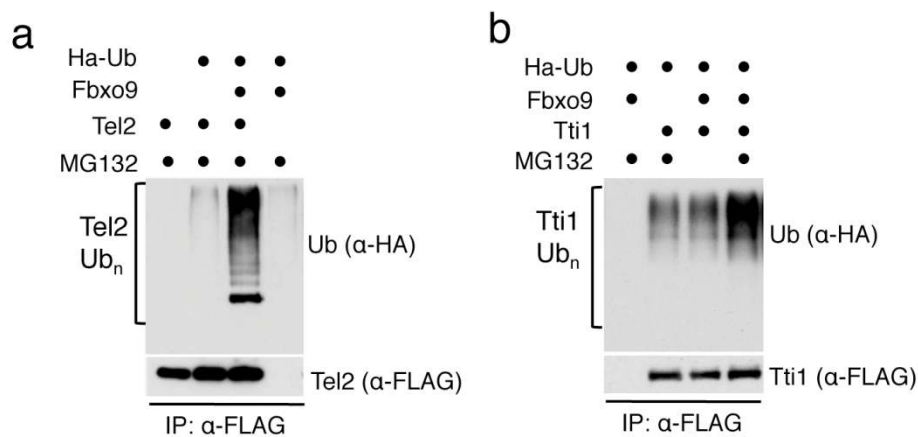


Figure 13: SCF^{Fbxo9} specifically ubiquitylates Tel2 and Tti1. *In vivo* ubiquitylation assays of Tel2 (a) and Tti1 (b) proteins. HEK293T cells were transfected with plasmids expressing FLAG-tagged Tel2 or Tti1, HA-ubiquitin and Fbxo9 as indicated. Following treatment with MG132, extracts were prepared and subjected to anti-FLAG-immunoprecipitations using denaturing conditions. The brackets mark polyubiquitylated Tel2 or Tti1 (Ub_n). [Data provided by Dr. V.Férrandez-Sáiz]

Together, the above ubiquitylation experiments could identify Tel2 and Tti1 as specific substrates of the E3 ligase SCF^{Fbxo9}.

5.1.3 Tel2/Tti1 protein levels decrease upon serum withdrawal

Because the observed polyubiquitylation possibly functions as a degradation signal, stability of Tel2 and Tti1 proteins was further examined. Considering, the well-established role of UPS in cell cycle regulation, a first approach was to test protein expression during the cell cycle. However, as shown in Figure 14 the levels of Tel2 and Tti1 were mainly unchanged throughout the cell cycle. Synchronised progression through the cell cycle is depicted by strong signals of the mitotic markers phosphorylated Histone H₃ (p-HH3) and Polo-like-kinase 1 (Plk1) as cells enter mitosis, as well as by increasing detection of cyclin E – an early S-Phase protein (Figure 14a, b). The cytoskeletal protein α -tubulin and the stably abundant Skp1 were used as controls to ensure that an equal amount of protein lysate was analysed in the immunoblot.

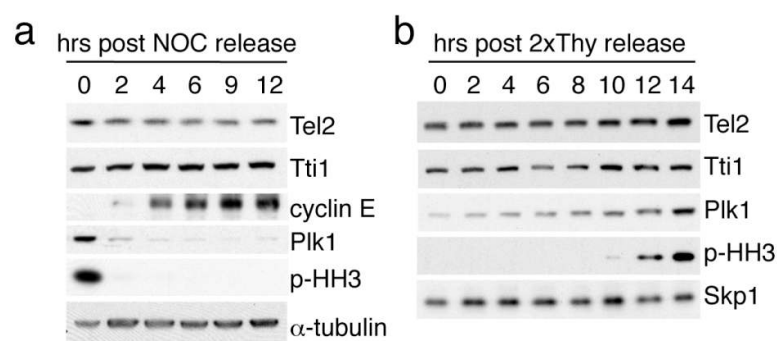


Figure 14: Cell cycle profile of Tel2 and Tti1. (a) Cell cycle release from M-Phase to S-Phase entry. HeLa cells were pre-synchronised with 2 mM Thymidine (Thy) and released into Nocodazole (NOC) ($c = 500$ ng/ml) containing media for 16 hrs. Mitotic cells were released from their block to uniformly progress into S-Phase. Samples were harvested at times indicated and probed for the indicated antibodies. (b) Cell cycle release from S-Phase to M-Phase entry. HeLa cells were synchronised by a double Thy block (2xThy) and released to progress to M-Phase. Collected samples of the time course were subjected to immunoblotting with indicated antibodies.

As protein levels of Tel2/Tti1 were constant during the cell cycle, other biological contexts that would specifically cause Tel2/Tti1 degradation were tested. Because Tel2 and Tti1 proteins regulate the abundance of all mammalian PIKKs (ATM, ATR, DNA-PKcs, SMG-1, TRRAP, and mTOR) (s. chapter 3.3.5), Tel2/Tti1 expression was monitored in response to a series of PIKK activating/inactivating stimuli. These experiments identified a decrease in Tel2/Tti1 expression levels in response to growth factor withdrawal (SD), while after growth factor stimulation (SA), levels increased (Figure 15a). Notably, the destabilization of Tel2/Tti1 paralleled decreased expression of the different PIKKs, particularly mTOR (Figure 15a), a known regulator for response to nutrient deprivation (s. chapter 3.3.1). Evidently, the phosphorylation of the downstream targets of mTOR kinase Akt, S6K1, and S6, could not be detected after serum deprivation (SD), but detection was quickly restored upon serum addition (SA) (Figure 15a). Since T98G cells are revertants from T98 glioblastoma cells, which acquired the property to accumulate in the cell cycle phase G₀/G₁ in low

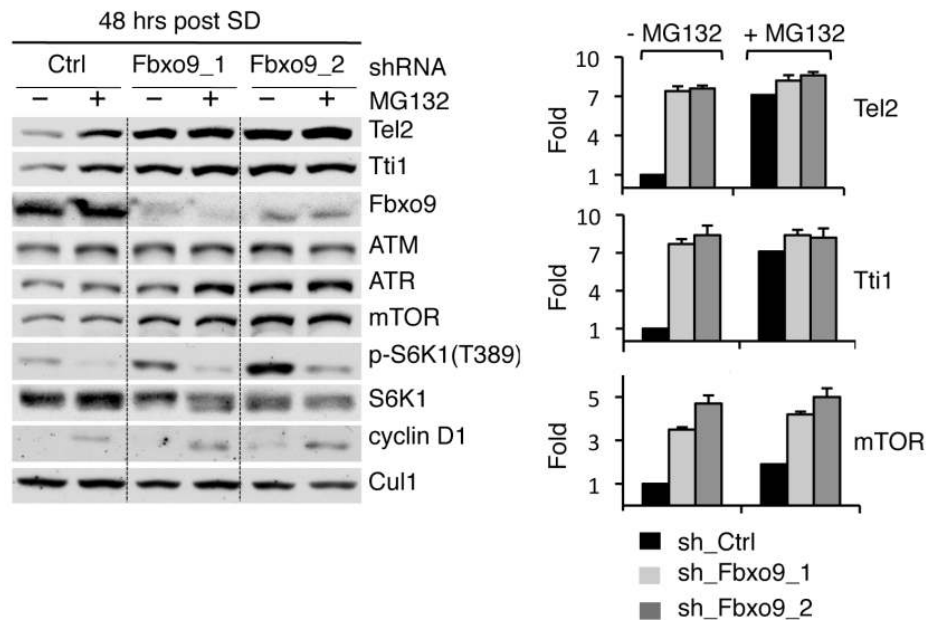


Figure 16: Tel2/Tti1 degradation is mediated by the ubiquitin proteasome system in an Fbxo9-dependent manner. T98G cells were infected with short hairpin (shRNA) constructs directed against a non-relevant mRNA (Ctrl) or against two distinct sequences of *Fbxo9* mRNA. Cells were deprived of serum (SD: 0.02% FBS) for 48 hrs and during the last 4 hrs before harvesting, cells were treated with 10 μ M MG132 where indicated. Protein extracts were analysed by immunoblotting with antibodies to the indicated proteins. The right panel shows quantification of respective protein band intensities averaged over three independent experiments. The control sample (– MG132) was set as 1 (n = 3; \pm sd).

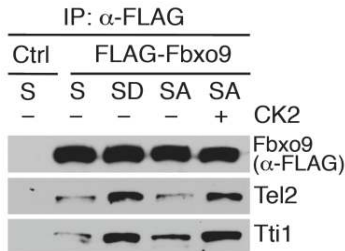


Figure 17: Fbxo9 binding to Tel2/Tti1 upon SD. U2OS cells, infected with a retrovirus expressing FLAG-tagged Fbxo9 or control virus and transfected with a CK2 expression plasmid where indicated, were either grown in normal serum (S: 10% FBS) or deprived of serum for 48 hrs (SD: 0.1% FBS) and then activated with serum for 2 hrs (SA: 10% FBS). Thereafter, cell lysates were prepared, subjected to immunoprecipitations (IP) with anti-FLAG beads and immunoblotted with antibodies to the indicated proteins.

If the SCF^{Fbxo9} marks Tel2/Tti1 for degradation especially upon serum withdrawal, it is conceivable that their interaction would also be enforced under such conditions. To test this hypothesis IPs of overexpressed Flag-tagged Fbxo9 at different conditions were probed for binding to Tel2 and Tti1 proteins. Indeed, after SD the detection of bound Tel2 and Tti1 was most pronounced, while levels of precipitated Fbxo9 were similar in all conditions tested (Figure 17/lanes 2-4). A mock transfected control (Ctrl) was used to show specificity of the signals (Figure 17/lane 1).

To further strengthen this hypothesis, indirect immunofluorescence (IF) staining analyses (s. chapter 4.2.5.12) were performed to investigate co-localisation of Fbxo9 and Tel2 or Tti1. The microscopy studies revealed a co-localization of Tel2 and Tti1 with Fbxo9 (Figure 18) as depicted by the

yellow colour in the merged image. While Tti1 (shown in green) is generally cytoplasmic (Figure 18a), Tel2 (shown in green) localises to the nucleus and cytoplasm under normal conditions, whereas it fully co-localises with cytoplasmic Fbxo9 (shown in red) in serum deprived cells (Figure 18b). The DNA was counterstained with DAPI (shown in blue) to visualise the nucleus. Thus, Tel2 and Tti1 associate with Fbxo9 particularly under conditions of serum deprivation.

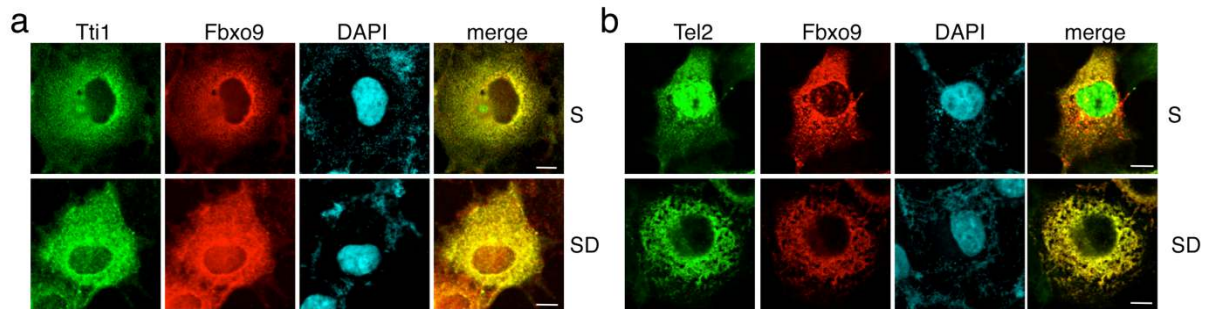


Figure 18: Co-localisation of Fbxo9 and Tel2/Tti1 under S and SD. Cos7 cells were transiently transfected with plasmids encoding HA-tagged Fbxo9 and either FLAG-tagged Tti1 (a) or Tel2 (b). Cells were then cultured in normal serum (S: 10% FBS) or deprived of serum for 5 hrs (SD: 0.02% FBS). Thereafter, cells were fixed with methanol and incubated with anti-FLAG antibody (green) and anti-HA antibody (red). DNA was counterstained with DAPI (blue). Scale bars represent 10 μ m.

5.1.4 Fbxo9 loss impairs proteasomal degradation of Tel2/Tti1 under serum deprivation

To further test whether Fbxo9 may regulate the stability of Tel2/Tti1 during serum deprivation, two different short hairpin RNA (shRNA) constructs to silence the expression of Fbxo9 were retrovirally introduced into T98G cells. Depletion of Fbxo9 using either shRNA inhibited the strongly decreased signal of Tel2 and Tti1 after serum withdrawal (Figure 19) compared to the control experiment (Ctrl). Importantly, stabilisation of Tel2 and Tti1 was associated with detection of increased expression levels of different PIKKs (Figure 19a). This effect was most prominent for mTOR, in line with its most marked loss of abundance in response to serum withdrawal (Figure 15). Importantly, stabilization of Tel2/Tti1 and mTOR resulted in sustained phosphorylation of the mTORC1 substrate S6K1, while phosphorylation of Akt, an mTORC2 substrate, was further restrained. As expected, general levels of S6K1 and Akt were not affected by starvation, as well as the levels of mTORC1 and mTORC2 components Raptor or Rictor, respectively, suggesting an opposing deregulatory effect on mTORC1/2 signalling. Of note, also phosphorylation of Chk2 – a target of ATM – was strongly attenuated in Fbxo9 depleted cells, indicative of an additional involvement for DNA damage response (DDR) mechanism. However, efficient starvation could be monitored by increase of p27 levels, a marker accumulating in G₀-Phase. These results were reproducible and respective western blot signal quantifications averaged over three independent experiments show an

overall threefold increase of signals for Tel2, Tti1, mTOR and p-S6K1, and similar dimensions of decrease for p-Akt (Figure 19b). Furthermore, in cells depleted of Fbxo9, treatment with the MG132 had no additional effect on the stability of Tel2/Tti1 and the PIKKs, demonstrating that proteasomal degradation of Tel2/Tti1 is strictly dependent on Fbxo9 (Figure 16/lanes 3-6).

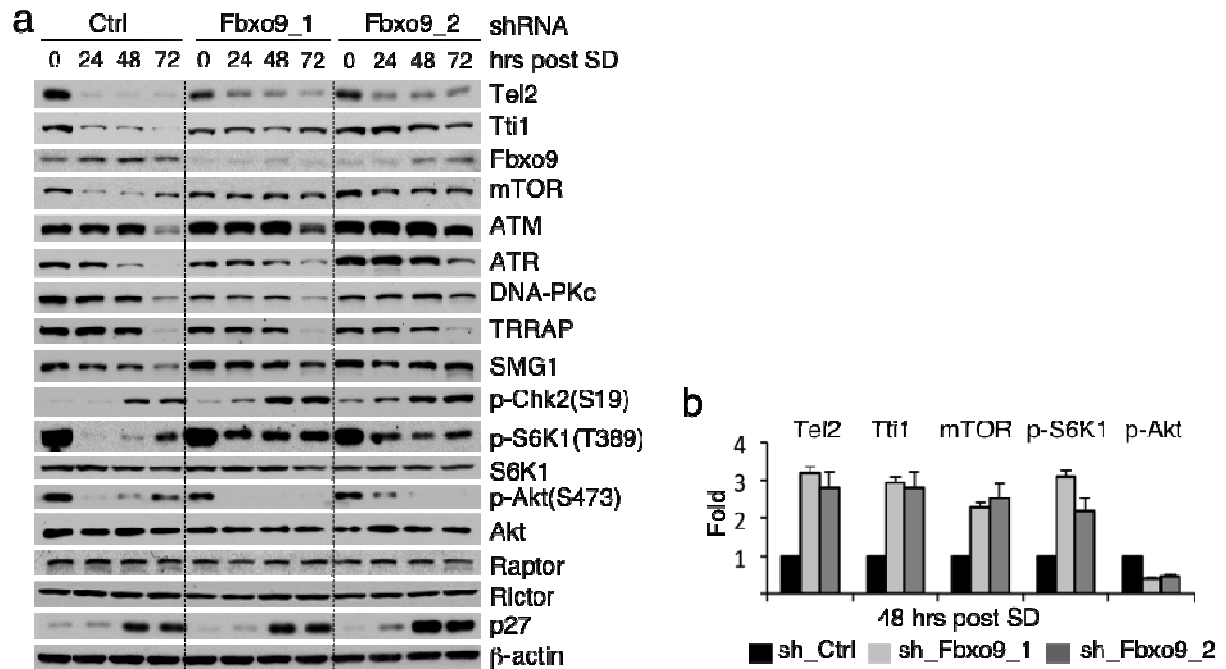


Figure 19: Fbxo9 depletion in serum starvation. (a) T98G cells were depleted of Fbxo9 with two individual shRNA constructs. Those cells were serum deprived (SD: 0.02% FBS) for indicated times, and subjected to immunoblot analyses for the indicated antibodies. (b) Quantification of proteins shown in (a) averaged with two additional, independent experiments. The value given for the amount of protein present in the control sample (sh_Ctrl) was set as 1 ($n = 3; \pm$ sd).

To validate the observed results on differential regulation of mTORC1 or mTORC2 signalling as a general cellular mechanism governed by Fbxo9, similar studies were conducted in primary human IMR90 fibroblasts. Notably, cells treated for nutrient deprivation under depletion of Fbxo9 by either small interfering RNA (siRNA) (left panel) or shRNA (right panel) reproduced above results in T98G cells (Figure 20). After serum withdrawal, depletion of Fbxo9 impaired signal reduction of Tel2 and Tti1, stabilised mTOR levels, sustained phosphorylation of S6K1 or its target S6, but diminished phosphorylation of Akt, whereas levels of the two kinases were unaffected. These results strongly suggest that Fbxo9 degradation of Tel2/Tti1 in response to starvation represents an universal mechanism to differentially regulate mTORC1 and mTORC2 signalling pathways.

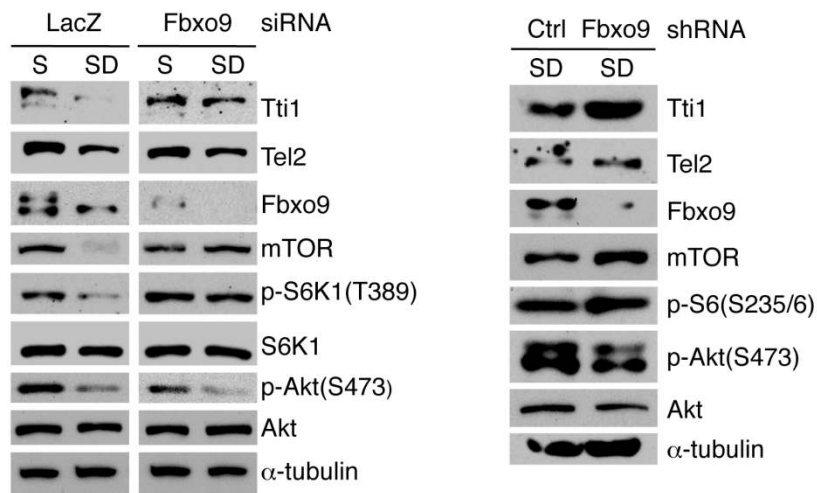


Figure 20: Fbxo9 promotes degradation of Tel2/Tti1 in response to serum withdrawal in primary IMR90 cells. IMR90 cells were treated with siRNAs directed against Fbxo9 or LacZ (left panel) or infected twice with shRNA constructs directed against *Fbxo9* or against a non-relevant mRNA (Ctrl) (right panel). Cells were grown in normal medium (S: 10% FBS) or deprived of serum (SD: 0.2% FBS) for 48 hours. Protein extracts were then prepared and probed with antibodies as specified.

5.1.5 The function of Tel2/Tti1 in serum deprivation is modulated by loss of Fbxo9

As depletion of Fbxo9 resulted in non-physiological accumulation of Tel2 and Tti1 proteins, the next investigations analysed effects of overexpressed Tel2 or Tti1 upon serum withdrawal in parallel. Tel2 was reported in the literature to affect *de novo* synthesis of ATM and mTOR¹⁵⁰, thus in an *in vivo* labelling experiment protein synthesis of these two kinases was monitored as a read-out for Tel2/Tti1 function (Figure 21). Under deprived conditions the amount of newly synthesised protein is usually low, as shown for the control cells (sh Ctrl/lanes 1+6), but upon knockdown of Fbxo9 an increase in *de novo* synthesised mTOR and ATM could be detected by autoradiography (lanes 2+7). This effect could be recapitulated to some degree by overexpression of either Tel2 or Tti1 (lanes 3, 4, 8+9). The

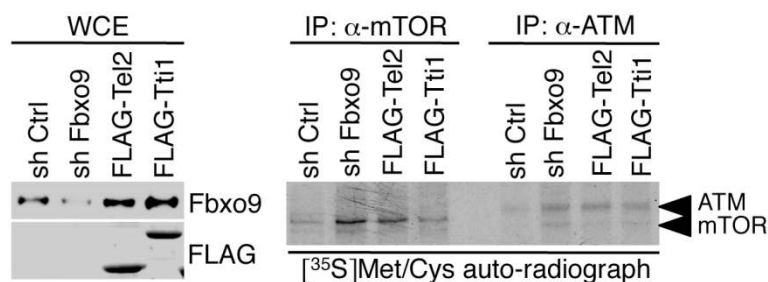


Figure 21: *De novo* synthesis of mTOR and ATM is mediated by Fbxo9. U2OS cells were retrovirally infected with either shRNA to Fbxo9 or expression constructs coding for Tel2 or Tti1 as indicated and serum starved (SD: 0.02% FBS), pulse labelled with [³⁵S]Met/Cys for 2 hrs, and subsequently subjected to immunoprecipitations (IP) with antibodies to either mTOR or ATM. *De novo* protein synthesis was visualised by autoradiography. Whole cell extracts (WCE) were immunoblotted with antibodies to the indicated proteins.

efficient knockdown and overexpression, respectively, are depicted with immunoblotting (WCE). Of note, the effect was more pronounced for mTOR, which makes sense considering its essential role during starvation (s. chapter 3.3.1)

5.1.6 Tti1/Tel2 degradation and its impact on mTOR functions upon serum withdrawal

As differential changes of mTORC1 and mTORC2 phosphorylation substrates were repeatedly found in above experiments, further investigations focussed on the elucidation of the integrity of mTOR signalling after Fbxo9 loss. To this end cell growth and mRNA translation were tested as readouts of a functional mTORC1 pathway (s. chapter 3.3.2.3), while proliferation and survival were assigned to be specific for mTORC2 signalling (s. chapter 3.3.3.3). In flow cytometric analyses, cell size was determined by forward scatter (FSC) analyses (s. chapter 4.2.5.11). Starved cells treated to downregulate Fbxo9 (blue and red) were larger than control cells (black), as shown in Figure 22.

Likewise, protein translation was enhanced upon loss of Fbxo9. In luciferase assays (s. chapter 4.2.5.10) the Cap-dependent translation of a luciferase mRNA with a stem-loop structured 5'-UTR was measured upon nutrient deprivation and demonstrated an increased translation activity in cells depleted of Fbxo9 by siRNA (Figure 23). As control (Ctrl) non-specific siRNA against LacZ was utilised. While translation is usually reduced to minimal levels in starved conditions (= 100%), deletion of Fbxo9 increased the activity more than 1.5-fold. Altered protein levels mediated by siRNA are shown in Western blot analyses. In sum, both experiments indicate increased mTORC1 signalling.

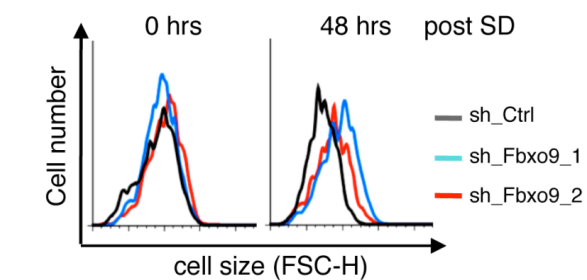
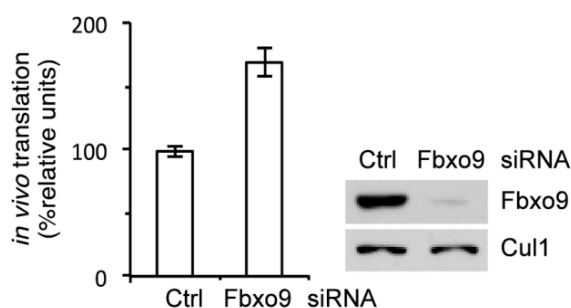


Figure 22: Cell size is increased upon loss of Fbxo9. T98G were retrovirally infected with shRNA constructs directed against a non-relevant mRNA (Ctrl) or against two distinct sequences of *Fbxo9* mRNA. Cells were deprived of serum (SD: 0.02% FBS) for 48 hrs or left untreated (0 hrs). Forward scatter analyses (FSC-H) of G₁-phase gated cells were performed to determine the size.

Figure 23: Elevated Cap-dependent translation during starvation upon depletion of Fbxo9. HEK293T cells were transfected with a pCMV-SL-LUC reporter plasmid together with a pRL-null Renilla luciferase plasmid and siRNA oligonucleotides against the non-relevant *LacZ* or *Fbxo9*. Cells were serum starved (SD: 0.1% FBS) for 48hrs, and luciferase activities were measured by a dual-luciferase assay. Data are the means of three independent experiments (in duplicate) (n=3, ±sd). Protein levels of Fbxo9 are shown in the right panel.

In stark contrast, BrdU uptake, indicative of proliferating cells, was decreased in serum starved cells upon Fbxo9 knockdown (Figure 24). In a 2D cell cycle analysis (s. chapter 4.2.5.11) by flow cytometry, distribution over the different cell cycle phases was assessed. While the cell cycle profile is almost identical in untreated conditions (panels 1+2), with few cells detected in sub-G₁, and the lion share of cells being in S-Phase, significant differences were observed in serum starved states (panels 3+4). As cells need to adapt to shortness of nutrients, proliferation is normally reduced, as evidenced by a reduction of replicating cells in S-Phase (from 40.9% to 26.7%) and accumulation of cells in G₁ (from 31.8% to 44.5%) (compare panels 1+3) in the control cell lines. For cell lines lacking Fbxo9, the proliferative capacity is further reduced (numbers shown in bold) compared to their respective controls (panels 3+4). Also quite strikingly, the fraction of cells in sub-G₁ rises from 12.1% to 32.1% for Fbxo9 depleted cells, indicative of increased cell death.

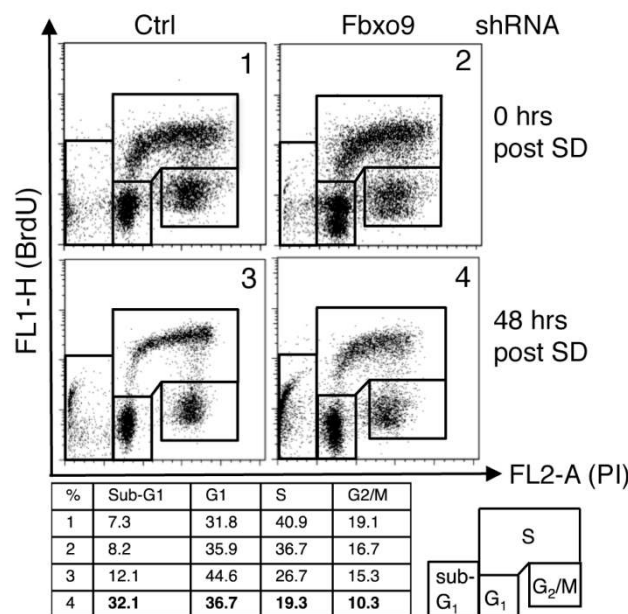


Figure 24: Proliferation is reduced upon Fbxo9 loss. 2D cell cycle analysis (BrdU/PI) of T98G infected with Ctrl or shRNA for Fbxo9 were performed for untreated or serum deprived (SD: 0.02% FBS) conditions at times indicated. Distribution of the cell population over the four different cell cycle phases sub-G₁, G₁, S and G₂/M are shown in the table below.

To gain further insights on cell death stimulation, starvation sensitive HeLa cells were deprived of serum for subsequent induction of apoptosis. As for T98G cells, deletion of Fbxo9 abolished serum withdrawal induced destabilisation of Tel2/Tti1 and mTOR, and induced oppositional deregulated phosphorylation states of S6K1 and Akt, respectively, indicative of an expedient cell line to study mTOR pathways (Figure 25). Immunoblot analyses for cleaved forms of the apoptotic markers PARP and caspase 3, revealed a specific increase of signal after SD, which was much more pronounced in Fbxo9 depleted cells (lanes 2+4), indicative for enhanced apoptosis induction.

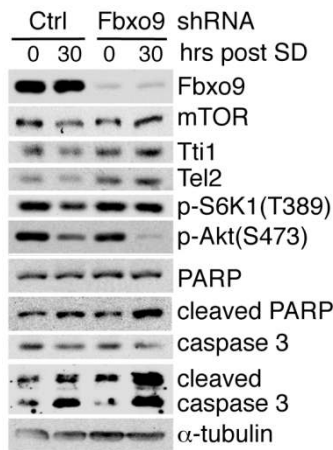


Figure 25: Apoptosis induction is enhanced by Fbxo9 depletion. HeLa cells expressing either Ctrl or Fbxo9 shRNA were serum deprived 30 hrs (SD: 0% FBS) to induce apoptosis. Cell extracts were analysed with antibodies to the indicated proteins.

Taken together, loss in mTORC2 signalling during starvation can be enhanced in an Fbxo9-dependent fashion.

To finally exclude that possibly other Fbxo9 responsive factors are involved in the deregulation of mTOR signalling, a complementation approach was designed. If stabilisation of Tel2/Tti1 was indeed the main action accompanying Fbxo9 loss, depletion of Tel2 or Tti1 proteins should readily reverse the observed phenotypes. Recapitulating former results (s. Figure 22) cell size was increased in Fbxo9 depleted cells (shown in red) compared to control cells (shown in black) (Figure 26). However additional siRNA mediated knockdown of Tti1 in Fbxo9 depleted cells yielded a similar cell size as compared to control cells. Importantly, in line with the reported complex formation of Tel2/Tti1¹⁵², upon Tti1 siRNA treatment, signals for Tel2 are decreasing in parallel to those of Tti1, demonstrating a mutual dependency of Tel2 and Tti1 protein levels (Figure 26/right panels).

Furthermore, in the cell lines treated with Fbxo9 shRNA, the mTOR bands showed the starvation-specific increase only in the presence of endogenous Tti1 (lane 2+4). Similarly, phosphorylation levels of S6K1 and Akt, respectively, were also restored in these cells, clearly demonstrating that Fbxo9 dependent regulation of mTOR signalling in response to nutrient deprivation is exclusively mediated by Tel2/Tti1 specific degradation.

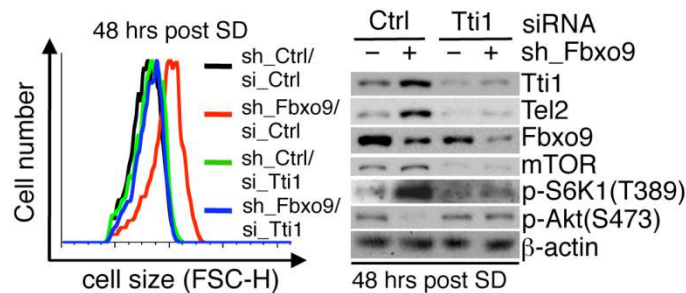


Figure 26: Tel2/Tti1 degradation via Fbxo9 specifically regulates differential mTOR signalling after serum withdrawal. T98G cells expressing either control (sh_Ctrl) or Fbxo9 shRNA were transfected with siRNA oligonucleotides either directed against a control (si_Ctrl) or Tti1 (si_Tti1) and deprived of serum for 48 hrs (SD: 0.02% FBS). Cell size was assessed using forward scatter analyses (FSC-H) as in Figure 22. Whole cell extracts were prepared and processed for immunoblotting using the specified antibodies.

5.2 Phospho-degron dependent ubiquitylation of Tel2/Tti1 via Fbxo9 regulates mTOR signalling

5.2.1 Identification of the degrons

Most SCF substrates are recognized by the FBP upon post-translational modifications (PTM), usually through phosphorylation of a specific degron motif (s. chapter 3.2.3.3)¹⁷⁴. Hence to identify the Fbxo9-specific degrons of Tel2 and Tti1, comprehensive binding experiments using deletion mutants were performed together with Dr. V.Fernández-Sáiz to specify the exact region of Fbxo9 binding to Tel2/Tti1. To this end, different truncates of both Tel2 and Tti1 proteins were generated. Those were subsequently overexpressed and tested for co-immunoprecipitation with FLAG-tagged Fbxo9 by Dr. V.Fernández-Sáiz (Figure 27). The N-terminal truncate of Tel2 (604-800) cannot be detected in the Co-IP, while the C-terminal truncate (Tel2 1-650) co-immunoprecipitated with Fbxo9, narrowing the binding region down to the first 604 aa of the protein (Figure 27a). For Tti1, binding with Fbxo9 supposedly occurs to the C-terminal part from aa 773 to 1089 of the protein, as evidenced by the absent Co-IP signal for the C-terminal truncate of Tti1 (1-647) (Figure 27b/lane 3).

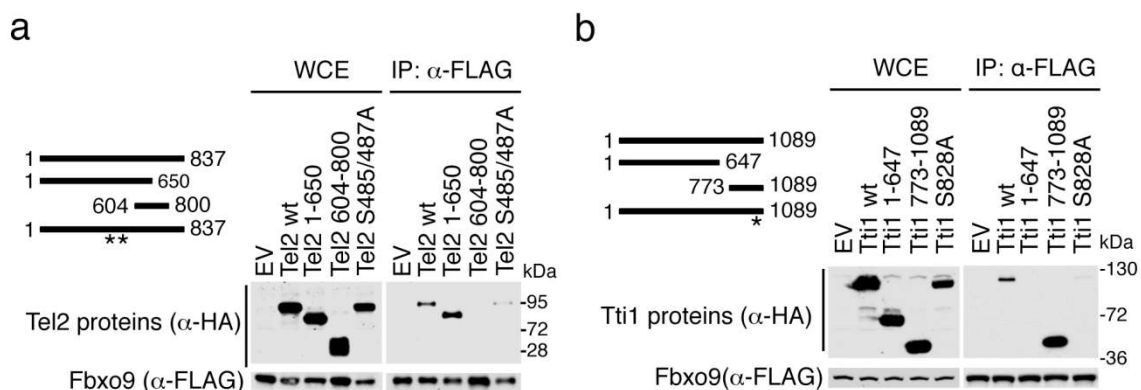
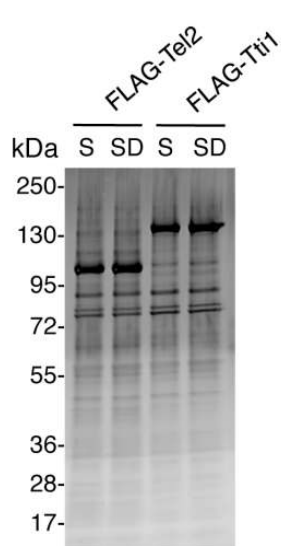


Figure 27: Binding site for Fbxo9 to Tel2 or Tti1. HEK293T cells were co-transfected with FLAG-tagged Fbxo9 and the indicated HA-tagged deletion or point mutants of Tel2 (a) and Tti1 (b) (s. graphic on the left). Whole cell extracts (WCE) were immunoprecipitated (IP) with an anti-FLAG antibody, and the indicated proteins were detected by immunoblotting. [Data provided by Dr. V.Fernández-Sáiz]

In a parallel approach phosphorylation of Tel2 and Tti1 proteins was analysed by phosphopeptide enrichment and subsequent MS in collaboration with the MS facility of the chair for Proteomics and Bioanalytics (TUM) with Prof. B. Küster and Dr. S. Lemeer (s. chapter 4.2.2.4). Assuming that Tel2/Tti1 are preferentially targeted upon SD, both proteins were overexpressed under normal and deprived conditions, purified and analysed thereafter for qualitative differences in overall phosphorylation status. Figure 28 shows the silver gel of proteins purified by Dr. V.Fernández-Sáiz. Analysis of the eluates by Dr. S. Lemeer and Prof. B. Küster identified phosphorylation of Tel2 at three serines (S, Ser): Ser⁴⁸⁵, Ser⁴⁸⁷, and Ser⁴⁹¹ (Figure 29), which are indeed comprised within the first



605 amino acids of Tel2. Further binding experiments performed by Dr. V.Fernández-Sáiz could show that mutation of Ser⁴⁸⁵ and the close Ser⁴⁸⁷ to Ala (Tel2 S485/487A) strongly impaired Co-IP detection by western blot analysis (Figure 27a/lane 5), showing relevance of the results.

Figure 28: Silver gel of purified Tel2 and Tti1 proteins for comparative phosphopeptide enrichment. FLAG-tagged Tel2 and Tti1 were transiently expressed in HEK293T cells. 24 hrs post transfection, cells were either cultured in normal serum (S: 10% FBS) or deprived of serum for 5 hrs (SD: 0.02% FBS). Thereafter, whole cell extracts were prepared and processed for IP with anti-FLAG beads and subsequent elution with 3x-FLAG-octapeptide. The eluate was then processed for MS analyses. The depicted gel corresponds to 5% of the final FLAG-eluates visualised by silver staining. [Data provided by Dr. V.Fernández-Sáiz]

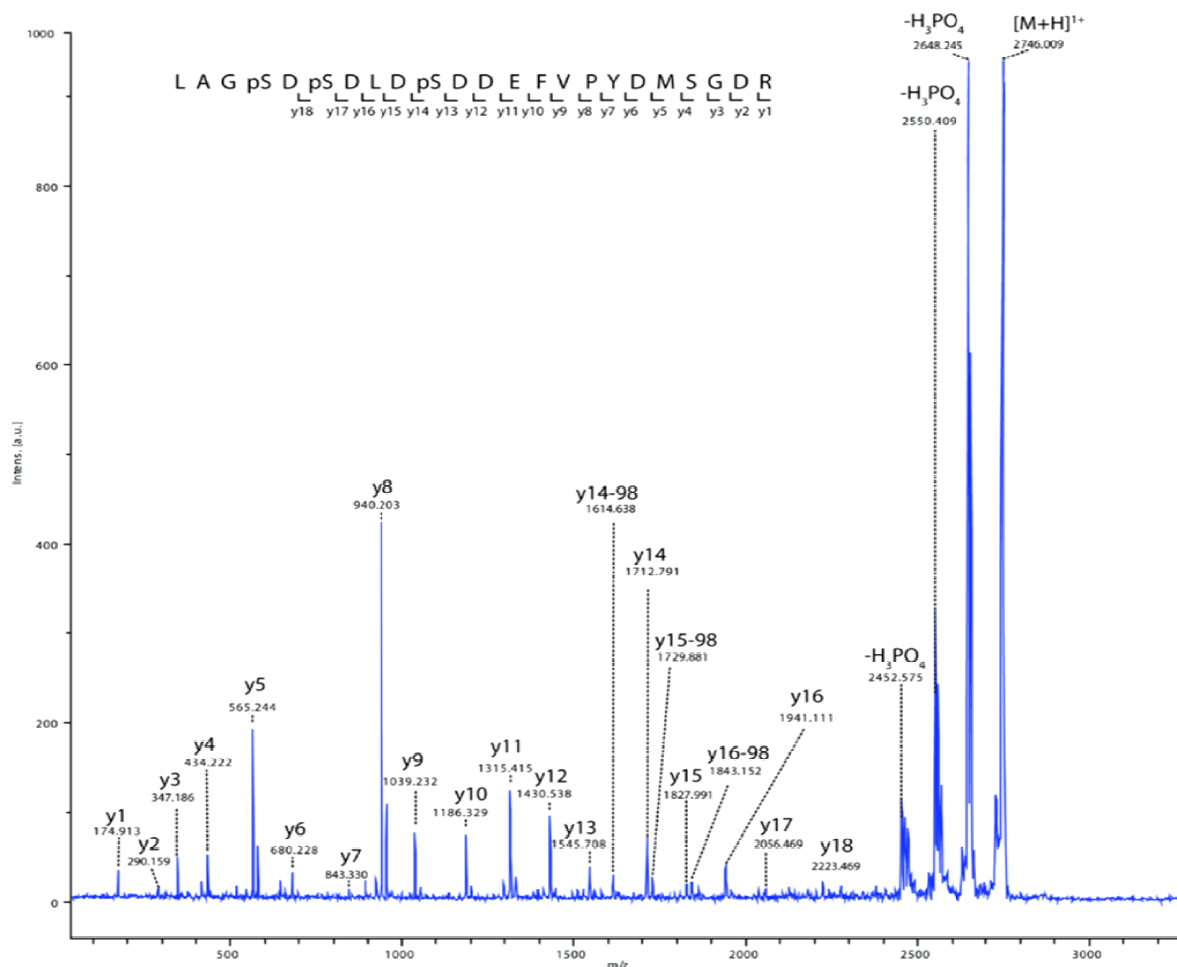


Figure 29: Phosphorylation analysis of Tel2. IMAC enrichment and subsequent MALDI-TOF mass spectrometry reveals that the peptide LAGSDSDLSDDEFVFPYDMSGDR of Tel2 is triply phosphorylated, as indicated by three major neutral losses of H₃PO₄ after fragmentation of the precursor peptide mass. Phosphorylation can readily be assigned to residues S⁴⁸⁵, S⁴⁸⁷ and S⁴⁹¹ as the indicative fragment ions, y₁₃, y₁₄ and y₁₈ are clearly present in the MS/MS spectrum. [Data provided by Dr. S. Lemeer and Prof. Dr. B. Küster]

For Tti1, Ser⁸²⁸ – a residue that indeed maps to the C-terminal part of Tti1 – was the only residue found to be phosphorylated by the analyses of Dr. S. Lemeer and Prof. B. Küster (Figure 30). Consistently, the mutation of the respective Ser⁸²⁸ to Ala (Tti1S828A) abolished Co-IP with Fbxo9 (Figure 27b/lane 5).

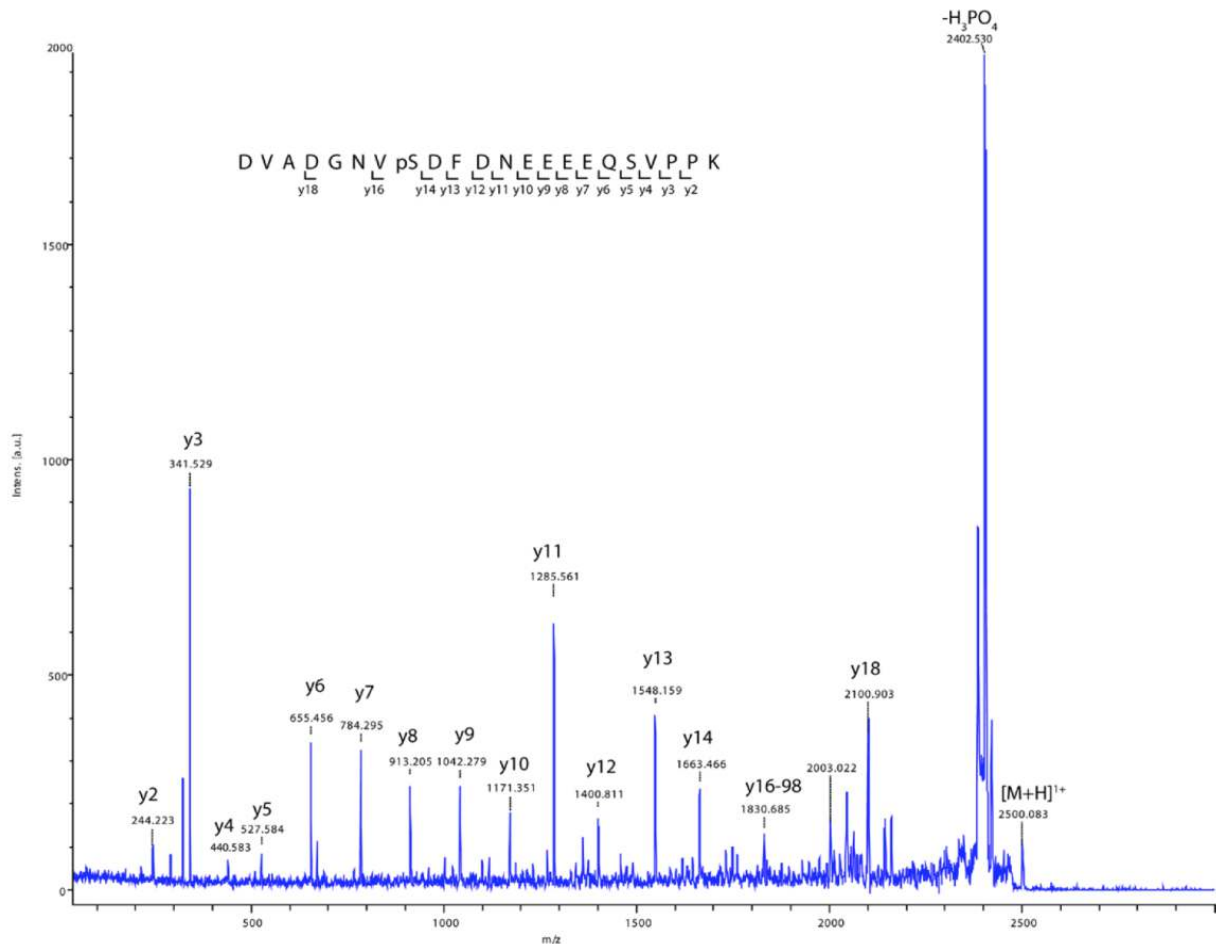


Figure 30: Phosphorylation analysis of Tti1. IMAC enrichment and subsequent MALDI-TOF mass spectrometry reveals that the peptide DVADGNVSDFDNEEEEQSVPPK of Tti1 is phosphorylated, as indicated by the major neutral loss of H₃PO₄ after fragmentation of the precursor peptide mass. Phosphorylation can be assigned to the residue S⁸²⁸ as the indicative fragment ions, y14 and y16 are present in the MS/MS spectrum. [Data provided by Dr. S. Lemeer and Prof. Dr. B. Küster]

Evolutionary analyses using CLUSTALW alignment of the identified peptides revealed that Ser⁴⁸⁵ of Tel2 and Ser⁸²⁸ of Tti1 and their surrounding amino acids are highly conserved, indicative of a functionally important motif (Figure 31). Together, the above studies could convincingly identify the evolutionary conserved motif ⁴⁸⁵pSDSDL⁴⁸⁹ of Tel2 and ⁸²⁸pSDFDN⁸³³ of Tti1 as the relevant binding sites to Fbxo9. Of note, since residues Ser⁴⁸⁷ and Ser⁴⁹¹ of Tel2 were previously described to be constantly phosphorylated¹⁵⁴, this study has focused on the newly identified Ser⁴⁸⁵ for further mutational analyses.

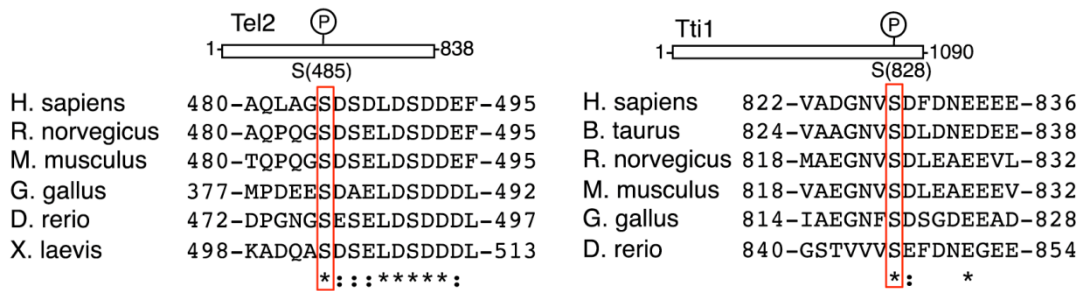


Figure 31: Degrons in Tel2/Tti1 are evolutionary conserved. CLUSTALW alignments of the candidate phospho-degrons in Tel2 and Tti1 depict conservedness. Identical residues (*), conservative residue differences (:). [Data provided by Dr. V.Fernandez-Sáiz]

5.2.2 Biological relevance of Fbxo9-specific phospho-degrons in Tel2/Tti1 in the context of serum deprivation

To additionally test the relevance of the newly identified degrons in a cellular setting, mutant and wildtype (WT) forms of both Tel2 and Tti1 proteins were transiently overexpressed in HEK293T and probed for abundance following SD. Recapitulating former results (s. chapter 5.1.3), western blot analyses showed a decreasing signal for the WT proteins upon prolonged SD (Figure 32/ lanes 1-3). In contrast, the degron-mutants Tti1(S828A) and Tel2(S485A) retained stability after nutrient withdrawal (lanes 4-6), indicating that degradation of Tel2 and Tti1 proteins upon SD is dependent on their intact phospho-degrons, further underscoring the specificity of SCF^{Fbxo9} as the relevant ligase in this context.

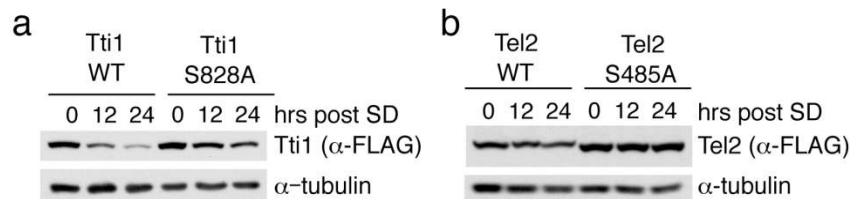


Figure 32: Stability of (a) Tti1 WT and Tti1(S828A) mutant and (b) Tel2 WT and Tel2(S485A) mutant upon SD. HEK293T cells were transiently transfected with constructs expressing wild type or degron-mutated forms of Tel2 and Tti1, which are deficient in Fbxo9 binding. Cells were subsequently deprived of serum (SD: 0.1% FBS) for the indicated times, and processed for immunoblotting with the specified antibodies.

Based on these observations, stable cell lines expressing either FLAG-tagged Tti1 WT or Tti1(S828A) were established to monitor response to nutrient deprivation. As expected, the Tti1 degron-mutant gained stability after growth factor withdrawal, as visualised in immunoblot analysis (Figure 33a). This notion was accompanied by increasing levels of mTOR, phosphorylation of mTORC1 target S6K1, and further restraint of Akt (mTORC2 substrate) phosphorylation (Figure 33b). Importantly, also Tel2 signals are detected at higher levels, again showing that protein levels of Tel2 and Tti1 are mutually dependent. Of note, the observed effects on mTOR pathway were less pronounced in alike experiments with cells expressing Tel2(S485A) (data not shown), presumably as a

result of additional interference with phosphorylation-dependent activity of Tel2 on R2TP and HSP90 during PIKK assembly¹⁵⁴.

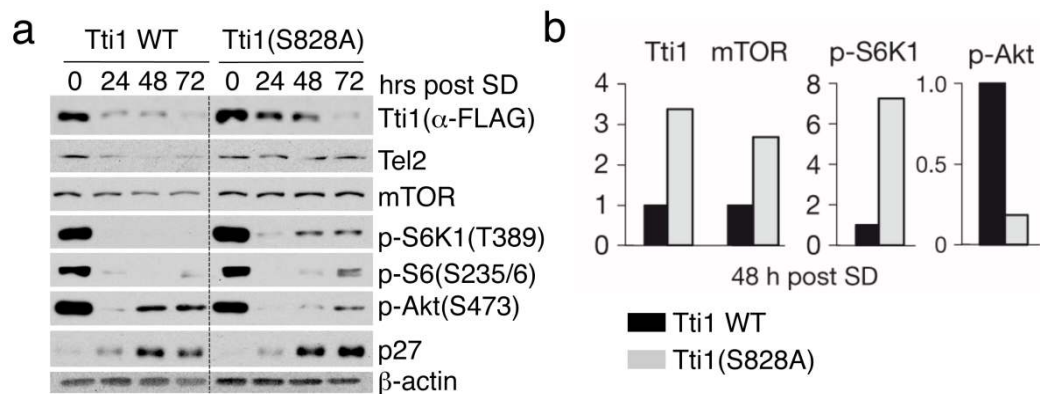


Figure 33: Effects of the non-degradable degron mutant of Tti1. (a) T98G cells were retrovirally infected with constructs for Tti1 WT or Tti1(S828A), deprived of serum (SD: 0.02% FBS), and collected at the indicated time points. Immunoblotting was performed with antibodies to the specified proteins. (b) The graphs show the quantification of Tti1, mTOR, phospho-S6K1, and phospho-Akt levels detected in (a) 48 hrs after SD averaged with an additional, independent experiment (n = 2).

To further assess, if the stable Tti1 degron-mutant can similarly compromise mTOR signalling as does Fbxo9 loss (s. chapter 5.1.6), the impact on mTORC1 and mTORC2 specific readout was investigated (Figure 34). Indeed, both an increase in cell size (Figure 34a), and a more than 2-fold elevated Cap-dependent translation activity (Figure 34b) during growth factor withdrawal could be detected for Tti1(S828), indicative of increased mTORC1 signalling. Behaviour of wildtype (WT) Tti1 was used for comparison. Conversely, mTORC2 pathway-dependent proliferation during starvation was further decreased in Tti1 degron-mutant expressing cells, as monitored in a 2D cell cycle analysis (Figure 34c). BrdU positive S-Phase cells, indicative of replicating cells, were reduced to 6.8% compared to wildtype control (16.4%). Likewise, the sub-G₁ fraction raised from 16.1% to 28.3% for Tti1(S828A) overexpressing cells (Figure 34c), which is in accordance with the increased induction of apoptosis detected in Figure 34d.

Overall, the results reproduce the observed effects for depletion of Fbxo9, suggesting that phospho-degron dependent degradation of Tel2/Tti1 by Fbxo9 essentially regulates mTOR signalling response to serum withdrawal.

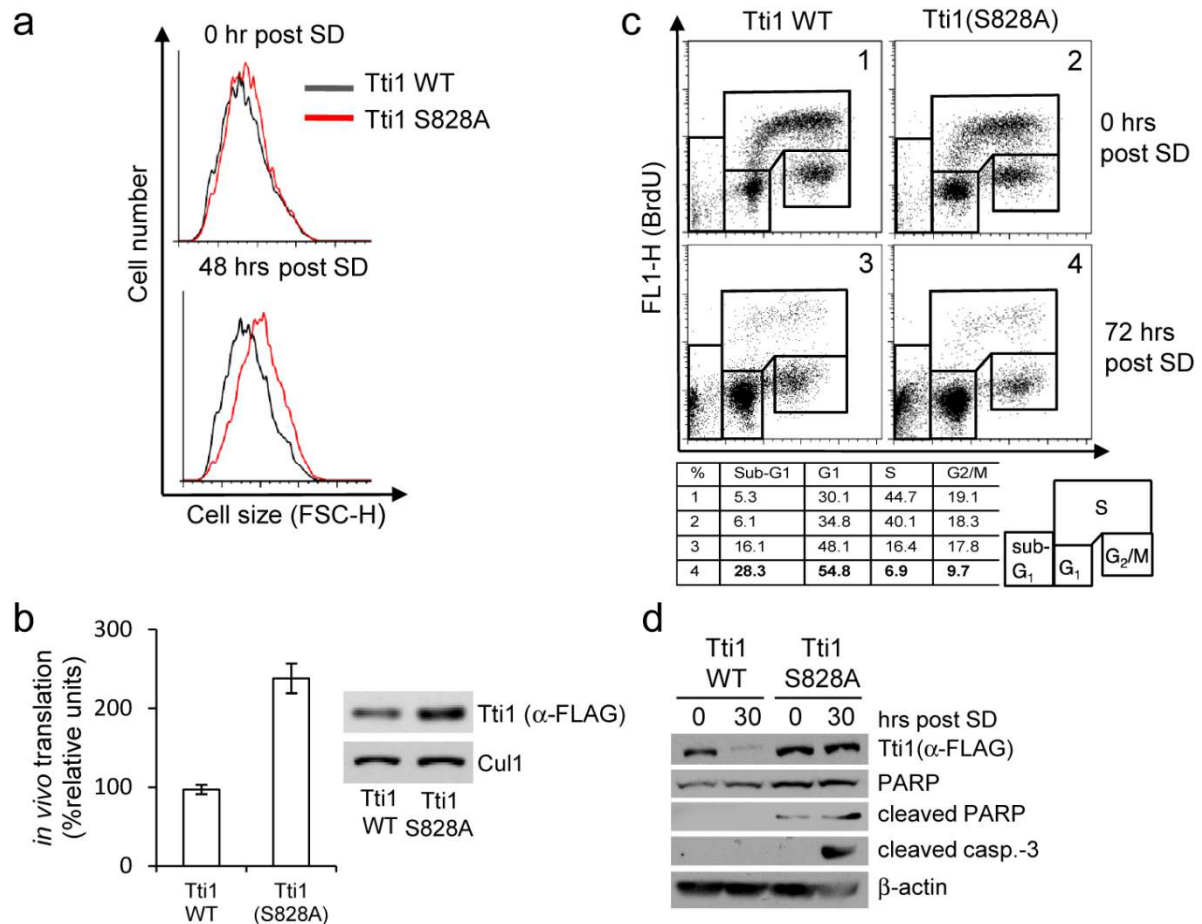


Figure 34: Expression of a non-degradable Tti1 mutant differentially affects mTORC1 and mTORC2 signalling. (a) Cell size of T98G stably expressing FLAG-tagged Tti1 WT or Tti1(S828A) was determined by flow cytometry. Forward scatter analyses (FSC-H) of G₁-phase gated cells are shown for cells either deprived of serum (SD: 0.02% FBS) for 48 hrs or left untreated (0 hr). (b) Translation assay was performed with HEK293T cells that were transfected with a pCMV-SL-LUC reporter plasmid together with a pRL-null Renilla luciferase plasmid and an expression plasmid coding for either FLAG-tagged Tti1 WT or Tti1(S828A). Cells were serum starved (SD: 0.1% FBS) for 48 hrs, and luciferase activities were measured by a dual-luciferase assay. Data are presented as the means of three independent experiments (in duplicate) (n=3, ±sd). Protein levels of Tti1 forms are shown on the right panel. (c) T98G stably expressing FLAG-tagged Tti1 WT or Tti1(S828A) were left untreated (0 hrs) or serum deprived (SD: 0.02% FBS) for 72 hrs. Proliferation was assessed by 2D cell cycle analysis (BrdU/PI). Cell cycle distribution is shown in the table below. (d) HeLa cells stably expressing FLAG-tagged Tti1 WT or Tti1(S828A) were deprived of serum for 30 hrs (SD: 0% FBS) to induce apoptosis. Cell extracts were probed with the specified antibodies.

5.2.3 Ubiquitylation is dependent on phospho-degrons of Tel2/Tti1

If the degron site in Tel2/Tti1 was important for binding and starvation response, it should also be for ubiquitylation by SCF^{Fbxo9}. Therefore an *in vitro* ubiquitylation experiment was conducted by Dr. V.Fernández-Sáiz, using either wildtype (WT) or degron mutant forms of Tel2 and Tti1, respectively, and the reconstituted E3 ligase. Figure 35 shows a marked vertical accumulation of sig-

5.3 CK2 associates with Tel2 and Tti1 upon growth factor withdrawal to mediate degron-specific phosphorylation and Fbxo9-dependent degradation

5.3.1 Identification of CK2 as kinase for Fbxo9-specific degrons in Tel2/Tti1

After characterisation of the important features the phospho-degron sites of Tel2/Tti1, the next step was to identify the involved kinase, its activation and impact on nutrient starvation. As such, sequence alignments revealed that both degron motifs of Tel2 and Tti1 represent canonical phosphorylation sites for Casein kinase 2 (CK2) (SxxD/E). Consistently, in an *in vitro* kinase assay CK2 phosphorylates both Tel2 and Tti1 proteins (Figure 37). Phosphorylation of wildtype (WT) proteins was depicted by autoradiography signals (lanes 2/left graphic; lane 2 and 4/right graphic). Neither control sample (\emptyset), with no protein included, nor purified degron-mutant forms of Tel2 and Tti1 displayed phosphorylation specific signals, demonstrating that Ser⁴⁸⁵ in Tel2 and Ser⁸²⁸ in Tti1, respectively, are indispensable for CK2 dependent phosphorylation. Of note, omitting CK2 from the reaction yielded no signal, excluding a residual kinase activity that might have been carried over with the purified Tel2/Tti1 proteins. Thus CK2 can indeed specifically phosphorylate Tel2 and Tti1 at their identified degrons.

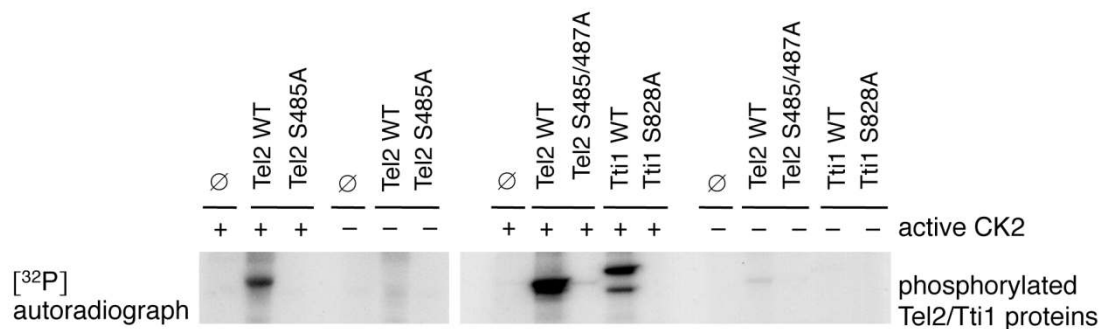


Figure 37: CK2 phosphorylates Tel2 and Tti1 degrons *in vitro*. Equal amounts of the indicated purified protein forms of Tel2 and Tti1 were transferred to an *in vitro* kinase reaction to test for phosphorylation by purified active CK2 in the presence of [³²P]-ATP. An empty vector control (\emptyset) was used. Phosphorylated proteins were visualised by autoradiography.

After the identification of the degron-specific kinase, the next experiments aimed at elucidating the interplay of CK2 and Fbxo9. Since binding of Tel2/Tti1 to Fbxo9 is dependent their phospho-degrons, enforced phosphorylation by CK2 should promote this interaction. Thus, binding capacity of purified Tel2 and Tti1 WT or mutant proteins pre-treated with active CK2 was tested in *in vitro* pull-down assays with GST-tagged Fbxo9. As controls, the prior phosphorylation step was omitted or empty-GST was used for pull-downs. Results show that even though lower amounts of phosphorylated Tti1 and Tel2 proteins were added to the reaction, only the CK2 phosphorylated wildtype forms of

Tel2 and Tti1 could be detected to bind to Fbxo9 *in vitro* (Figure 38). The amount of GST-tagged Fbxo9 and empty-GST coupled to beads was equal in all set-ups, as visualised by quantitative Ponceau S staining (lower panels). Thus, binding of Tel2/Tti1 to Fbxo9 is dependent on CK2 mediated degron phosphorylation.

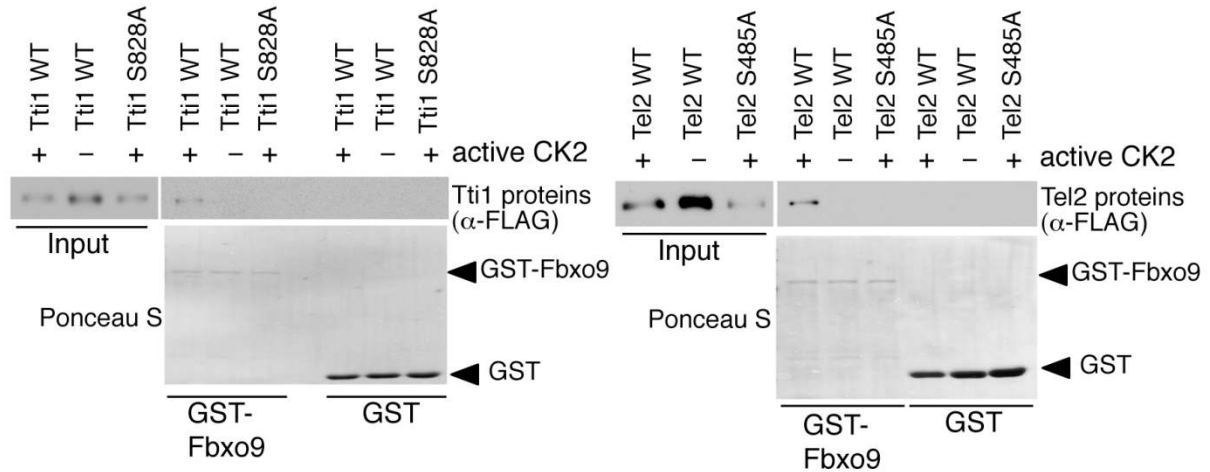


Figure 38: CK2 phosphorylation of Tel2/Tti1 mediates binding to Fbxo9 *in vitro*. The indicated forms of purified Tel2 (right panel) and Tti1 (left panel) were phosphorylated by CK2 *in vitro* as indicated (Input), and tested for their binding to GST-tagged Fbxo9 bound to GST-beads using an *in vitro* pull-down assay. Empty-GST beads were used as control. Equal amount of GST or GST-tagged proteins were visualised by Ponceau S staining.

Since these experiments confirmed that CK2 enhances substrate interaction with Fbxo9, it was reasonable to assume that the kinase might also enhance the enzymatic reaction of SCF^{Fbxo9} with Tel2

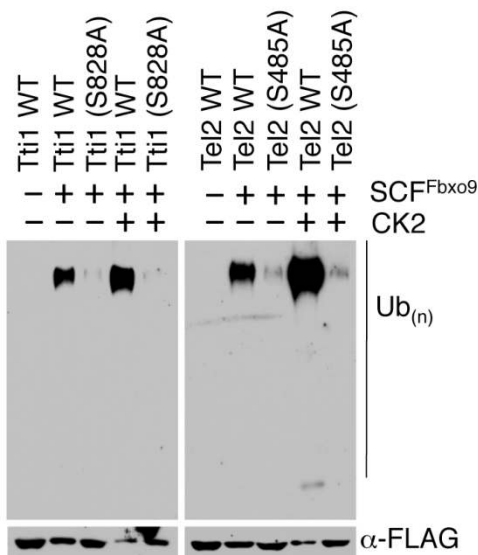


Figure 39: CK2 activity enhances Tel2/Tti1 ubiquitylation by SCF^{Fbxo9}. *In vitro* ubiquitylation assays were performed as in Figure 35 except that purified CK2 was added where indicated. Samples were immunoblotted for the antibodies specified. Brackets on the right mark polyubiquitylated Tel2 or Tti1 (Ub_n).

and Tti1 proteins. Indeed, in an *in vitro* ubiquitylation assay using reconstituted SCF^{Fbxo9}, E1/E2 enzymes, Ub and purified FLAG-tagged Tel2 and Tti1 proteins or their mutant forms, addition of purified active CK2 could intensify the detection of polyubiquitylation (). These effects were however not observed for the degron-mutants of Tel2 and Tti1 (lane 3+5), demonstrating that only degron specific phosphorylation of Tel2/Tti1 by CK2 can enhance ubiquitylation activity of SCF^{Fbxo9}.

5.3.2 Regulation of CK2 activity towards Tel2/Tti1 under serum deprivation

Next investigations focussed on how CK2 can mediate context-specific phosphorylation of Tel2/Tti1 during growth factor withdrawal, while CK2 is considered to be constitutively active and its regulation is poorly understood¹⁷⁵. In a first attempt to resolve the issue, it was hypothesised that an stimuli-dependent PTM – here serum starvation – could alter directed CK2 kinase activity. Therefore, CK2 was purified from exponentially growing cells or cells deprived of serum to test its kinase activity towards Tel2 and Tti1 in a subsequent *in vitro* kinase assay (Figure 40). No significant changes in the intrinsic *in vitro* kinase activity of CK2 could be observed in an autoradiograph of phosphorylated substrates, indicating a different mode of regulation. As a positive control, the well-established substrate casein was added to the reaction.

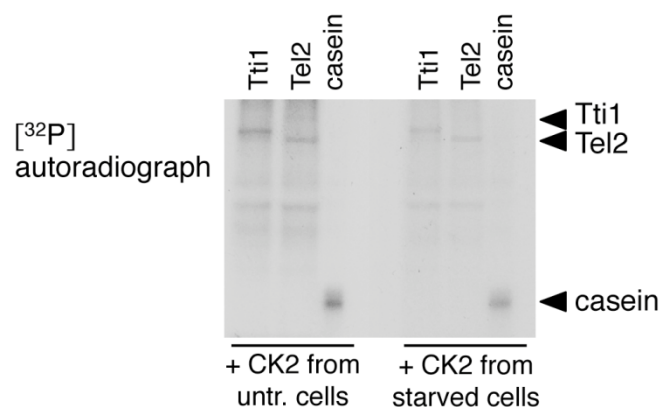


Figure 40: Intrinsic kinase activity of CK2 towards Tti1 and Tel2. FLAG-tagged CK2 α was immunoprecipitated from untreated (untr.) or serum starved HEK293T cells and subjected to an *in vitro* kinase reaction using purified Tel2, Tti1 and casein as substrates. Phosphorylated proteins were visualized by autoradiography.

Since compartmentalisation is a common theme to bring reaction partners into close proximity, the interaction of Tel2/Tti1 with CK2 was visualised by IF at different nutrient availability states. In untreated cells (S) CK2 (shown in green) was mostly localised to the nucleus (shown in blue) (Figure 41a, b). However, following serum deprivation (SD), it substantially moved to the cytoplasm to co-localise with both cytoplasmic Tel2 and Tti1 (shown in red). Fluorescence signal quantification revealed an around four-fold increase of cytoplasmic CK2 (Figure 41c) after growth factor withdrawal, indicating that Tel2/Tti1 specific phosphorylation activity is dependent on a nucleo-cytoplasmic translocation of its kinase CK2.

Consistent with the alteration of co-localisation, IPs of CK2 purified from either untreated or serum starved cells, showed different binding to Tel2/Tti1 proteins (Figure 42). After growth factor withdrawal (SD), a marked increase in Tel2/Tti1 association with CK2 could be observed. An empty vector (EV) was used as control for unspecific binding. Thus, kinase activity of CK2 directed to Tel2/Tti1 is context-specifically regulated by spatial control.

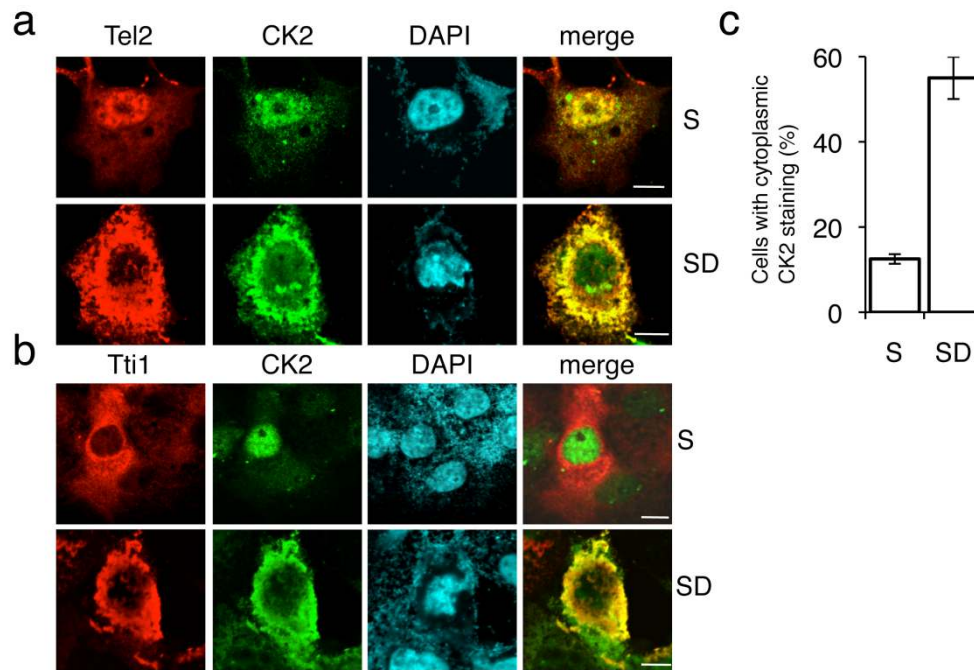


Figure 41: CK2 translocates from nucleoplasm to cytosol upon serum starvation. Cos7 cells were transiently transfected with plasmids encoding FLAG-CK2 and either HA-Tel2 (a) or HA-Tti1 (b). Cells were then cultured in normal serum (S: 10% FBS) or deprived of serum for 5 hrs (SD: 0.02% FBS). Thereafter, cells were fixed with methanol and incubated with anti-FLAG antibody (green) and anti-HA antibody (red). DNA was stained with DAPI (blue). Scale bars represent 10 μ m. (c) Quantification of cells shown in (a, b) with cytoplasmic CK2 fluorescence grown under serum containing (S) or serum deprived (SD) conditions (n = 3, \pm sd).

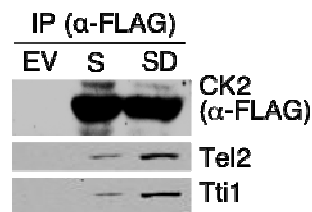


Figure 42: CK2 associates with Tel2/Tti1 upon serum deprivation. HEK293T cells were transfected with either empty vector (EV) or a FLAG-CK2 α expression plasmid. Cells were left untreated (S: 10% FBS) or serum starved (SD: 0.1% FBS) for 48 hrs as indicated, and anti-FLAG immunoprecipitations performed thereafter. Bound fractions were analysed with antibodies indicated.

5.3.3 Depletion of CK2 impacts on Tel2/Tti1 degradation upon serum withdrawal

A combinational experiment performed by Dr. V.Fernandez-Sáiz using siRNAs could further show the interdependency of Tel2 and Tti1 phosphorylation and CK2 in the biological context of growth factor withdrawal. To this end, phospho-degron specific antibodies for p-Tel2(S485) and p-Tti1(S828) were generated and applied in immunoblot analyses of cells cultured in normal (S) or serum deprived (SD) conditions (Figure 43). While signals specific for Tti1 and Tel2 decreased upon SD, their degron-specific phosphorylation status actually increased (lane 1+3), suggesting that

starvation-induced phosphorylation mediates Tel2/Tti1 signal fading. Specificity of the phospho-degron specific antibodies was confirmed by siRNA depletion of both Tel2 and Tti1 (lanes 2+4). Additionally, depletion of CK2 not only restored levels of Tel2 and Tti1 comparable to those of untreated samples, but also abrogated detection of phosphorylated Tel2 or Tti1 (lane 5), demonstrating that specific phosphorylation by CK2 is a prerequisite for proteasomal degradation Tel2 and Tti1 during deprived conditions.

Considering the importance of Fbxo9 mediated proteasomal degradation of Tel2/Tti1 in unfavourable nutrient situations, loss of the degron-specific kinase CK2 presumably has a similar impact on Tel2/Tti1 expression regulating mTOR signalling. To test this hypothesis, CK2 levels were depleted in T98G using siRNA, and cell lysates were analysed for Tel2 and Tti1 levels after SD (Figure 44a). Compared to control cells (LacZ) where signal intensities of Tel2 and Tti1 disappear in deprived conditions, Tel2/Tti1 are stabilised if CK2 levels decrease. Concomitantly with this increased abundance, mTOR levels are detected with similar intensity as in unstarved samples, and phosphorylation status increases for S6K1 or decreases for Akt, respectively. Opposite effects are observed, when CK2 kinase activity is stimulated with Sorbitol (Figure 44b), demonstrating that Fbxo9 and CK2 indeed act together to regulate the same cellular pathway.

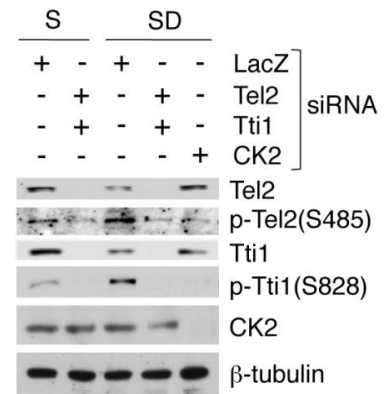


Figure 43: The phosphorylation and stability Tel2/Tti1 in SD are influenced by CK2. T98G cells were transfected with combinations of different siRNA oligonucleotides as indicated, either grown under serum containing (S: 10% FBS) or serum deprived (SD: 0.02% FBS) conditions, and subjected to immunoblot analyses with the indicated antibodies. [Data was provided by Dr. V.Fernandez-Sáiz]

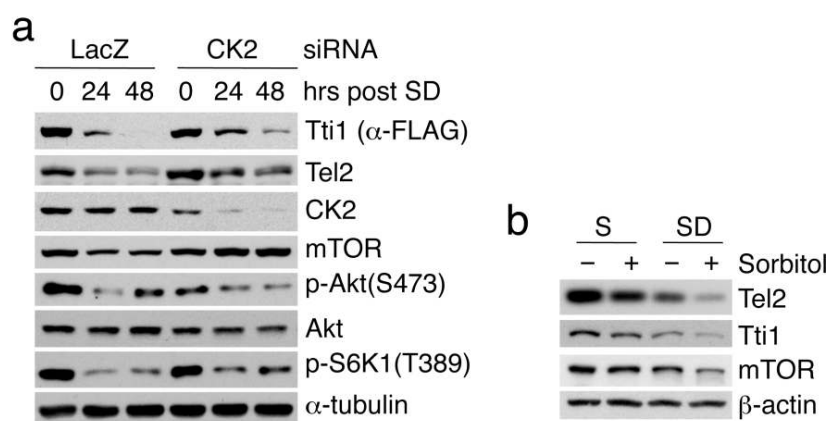


Figure 44: CK2 impacts on Tel2/Tti1 phosphorylation and stability. (a) T98G cells were treated with siRNAs directed against CK2, deprived of serum (SD: 0.02% FBS) for the indicated time points, and processed for immunoblotting. (b) T98G grown under normal (S: 10% FBS) or SD conditions were stimulated with 0.5 M Sorbitol for 2 hrs as indicated and subjected to immunoblot analyses.

5.3.4 Phospho-mimic of Tel2 degron co-localises with Fbxo9

As shown before, Tel2 does not exclusively localise to the same cellular compartment as Fbxo9 (Figure 18). To test whether phosphorylation status can influence localisation of Tel2, the Ser⁴⁸⁵ was mutated to an aspartic acid (D), an amino acid that mimics the overall negative charge of a phosphate-group. IF analyses showed a mostly cytoplasmic localisation of this phospho-mimic mutant of Tel2 (shown in red) under normal growth conditions (Figure 45a). Of note, quantification of fluorescence signal intensities showed only minor impact on localisation by serum deprivation (SD) (Figure 45b). Thus, while Tti1 is constitutively localised to the cytoplasm (s. Figure 18), CK-dependent degron phosphorylation conserves the cytoplasmic localisation of Tel2, enabling co-localisation to Fbxo9.

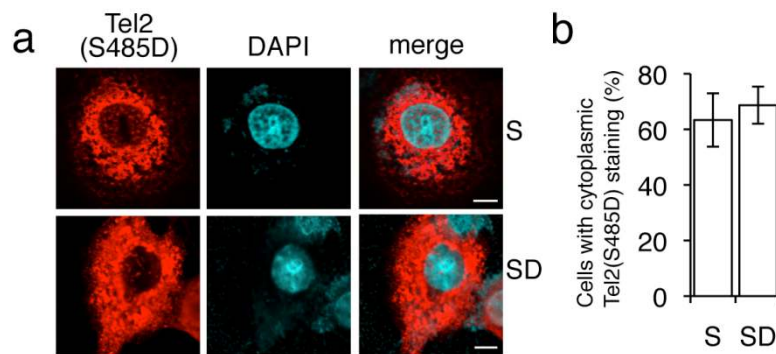


Figure 45: Localisation of phospho-mimic degron-mutant Tel2. (a) Cos7 cells were transiently transfected with a plasmid encoding HA-Tel2(S485D) and subsequently cultured in normal serum (S: 10% FBS) or deprived of serum for 5 hrs (SD: 0,02% FBS). Thereafter, cells were fixed with methanol and incubated with anti-HA antibody (red). DNA was stained with DAPI (blue). (b) Quantification of cells shown in (a) with cytoplasmic Tel2(S485D) fluorescence grown under serum containing or serum deprived conditions (n = 3, ± sd). Scale bars represent 10 µm.

In summary, CK2 activity is shown to be regulated on the level of subcellular localisation and is essential for Tel2/Tti1 degradation and mTOR signalling integrity upon serum withdrawal.

5.4 Fbxo9 preferentially targets mTORC1-bound Tel2/Tti1, thereby activating mTORC2 signalling

5.4.1 Fbxo9 targets mTORC1 associated Tel2/Tti1

Experimental evidence so far suggested differential effects of Fbxo9 on both mTOR complexes. This allowed hypothesising that Fbxo9 might preferentially target mTORC1-bound Tel2/Tti1 leading to its inactivation, which in turn, would activate the PI3K/mTORC2/Akt axis by relieving feedback inhibition (s. chapter 3.3.4). Starting to investigate this possibility, an analysis of Tel2/Tti1 bound to either mTORC1-specific component Raptor (s. chapter 3.3.2.1) or mTORC2-specific Rictor (s. chapter 3.3.5) in serum starved cells was performed. Therefore, MYC-tagged Raptor or Rictor were immunoprecipitated from cells either depleted of Fbxo9 by shRNA or the respective control cells

(Ctrl) (Figure 46) by Dr. V.Fernández-Sáiz. An empty vector (EV) was used to control MYC-IP specificity (lanes 1). As shown before (s. chapter 3.3.5), binding of Tel2 and Tti1 could be detected for both mTOR complex components; however, upon serum withdrawal (SD) signal intensities are only decreased in the Raptor-bound fraction, coinciding with increased phosphorylation signals of Tel2/Tti1 degrons (compare lanes 3+5/Ctrl). This effect can be abrogated by depletion of Fbxo9 with shRNA: Upon SD, no decreased signals for Tel2 and Tti1 are detected following Raptor IPs, yet the enhancement degron phosphorylation was unchanged (lane 3+5/Fbxo9_shRNA), suggesting intact CK2 phosphorylation, but absent ubiquitylation. Of note also association of Fbxo9 to Raptor, but not Rictor is enhanced in response to serum withdrawal as detected by a stronger immunoblot signal.

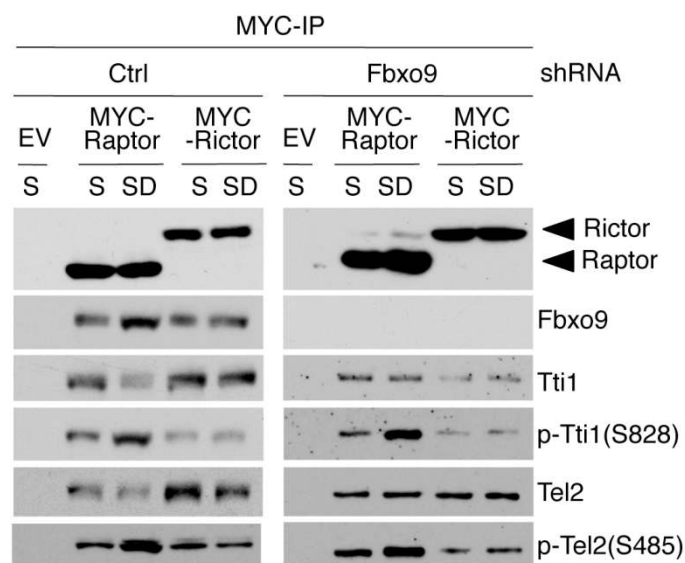


Figure 46: mTORC1-bound Tel2 and Tti1 are degraded in an Fbxo9-dependent and phospho-degron specific manner. Cell lines treated to downregulate Fbxo9 or mock (Ctrl) were transfected with empty vector (EV) or plasmids encoding MYC-Raptor or MYC-Rictor, serum starved (SD: 0.1% FBS) for 48 hrs or left untreated (S: 10% FBS), and subjected to anti-MYC immunoprecipitations (IP). Bound protein fractions were analysed by immunoblotting for the indicated proteins. [Data provided by Dr. V.Fernández-Sáiz]

These data strongly suggest degron-specific phosphorylation and Fbxo9 dependent degradation of Tel2 and Tti1 only within mTORC1, while the mTORC2 associated fraction of Tel2/Tti1 remains unaffected. Further, if a complex specific degradation of Tel2/Tti1 was indeed the reason for the observed results, specific inhibition mTORC1 or mTORC2 signalling in the setting of Fbxo9 deletion should recapitulate the differential responses detected. To this end, in experiments conducted by Dr. V.Fernández-Sáiz, mTORC1 specific changes in cell size and apoptosis induced via mTORC2 were assessed upon Rapamycin (Rapa) and Akt inhibitor IV (Akt-Inh.) treatment, respectively (Figure 47). Rapamycin specific inhibition of mTORC1 pathways diminished the enlarged cells as observed for cells depleted of Fbxo9 (Figure 47a), and reduced the concurrent increase in apoptosis (Figure 47b). In contrast, Akt inhibitor IV treatment to selectively modulate mTORC2 signalling displayed

apoptosis induction to similar levels for both control and Fbxo9 knockdown cells, a tendency, which is recapitulated in combination with Rapamycin treatment. This indicates that while specific mTORC1 inhibition signalling can counteract loss of Fbxo9, further inhibiting mTORC2 signalling can restore the apoptosis phenotype of Fbxo9 loss, invariant of Rapamycin treatment.

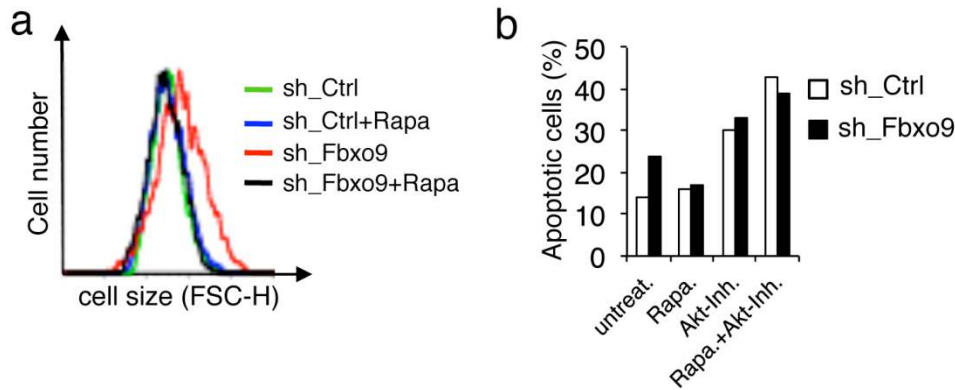


Figure 47: mTORC1 and mTORC2 inhibitors reverse Fbxo9 depletion phenotypes. T98G cells expressing either control or Fbxo9 shRNA were serum starved for 48 hrs in the presence of vehicle or mTORC1 inhibitor Rapamycin (Rapa) and Akt-inhibitor IV (Akt-Inh.), as specified. Cells were then subjected to forward scatter analyses (FSC-H) of G1-phase gated cells to determine cell size (a) or FACS analyses (PI) to determine apoptosis (b) (n =2). [Data provided by Dr. V.Fernandez-Sáiz]

As the presented results identified Fbxo9 and CK2 mediated degradation of Tel2/Tti1 to be specific for mTORC1 complex associated proteins, further characterisation of the role of Tel2 and Tti1 in regulating serum deprivation response was performed for Raptor-bound proteins. To clarify whether degradation of Tel2/Tti1 contributes to the immediate response to growth factor withdrawal or rather functions to maintain this response, time course experiments using Cycloheximide to inhibit protein biosynthesis (s. chapter 4.2.5.7) were performed by Dr. V.Fernandez-Sáiz. While a decrease in S6K1 and Akt phosphorylation was observed within 30 min, Tel2/Tti1 (within mTORC1) became unstable within three hours post serum withdrawal in control cells (lanes 1-5) (Figure 48). This effect was predictably not detected upon Fbxo9 depletion (lanes 6-10). Furthermore increased phosphorylation of Tel2 and Tti1 degrons could readily be detected after initial starvation. Of note, in Figure 48b similar effects on Tel2 and Tti1 could be shown by Dr. V.Fernandez-Sáiz even in the absence of Cycloheximide. These data suggest that degradation of Tel2/Tti1 via Fbxo9 and CK2 is required to establish a stable state of low mTORC1 and sustained mTORC2 activity during persistent starvation.

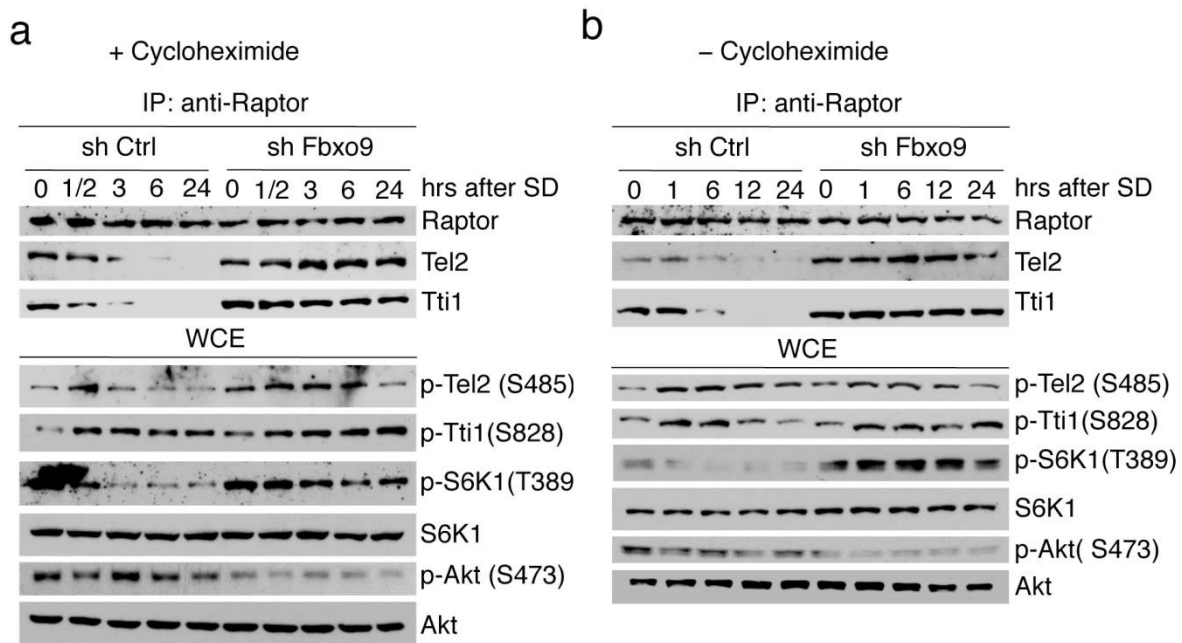
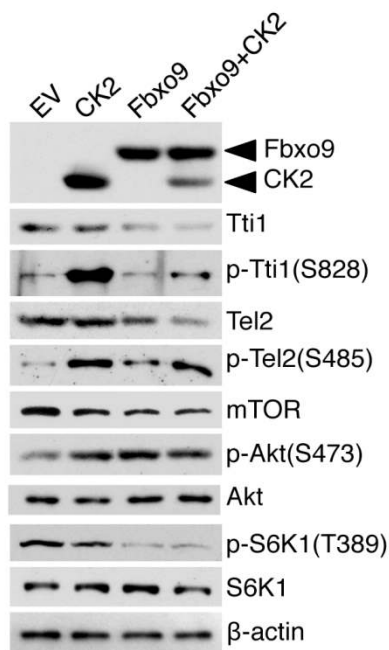


Figure 48: Degradation of Tel2/Tti1 is specific for Raptor-bound fraction. (a) T98G cells treated to downregulate Fbxo9 or control cells were deprived of serum (SD: 0.02% FBS) in the presence of Cycloheximide and harvested at the indicated time points. Endogenous Raptor was subsequently immunoprecipitated (IP) from whole cell extracts (WCE), and immunocomplexes and WCE were probed with antibodies to the indicated proteins. (b) The experiment was essentially performed as in (a), except that Cycloheximide was omitted. [Data provided by Dr. V.Fernández-Sáiz]

5.4.2 Overexpression of Fbxo9 and CK2 enhances mTORC2 signalling

Next experiments investigated if overexpressing Fbxo9 could reverse the effects on differential mTOR complex regulation observed for CK2 and Fbxo9 depletion (Figure 44 and Figure 19) as well as for



the stable Tti1(S828A) mutant (Figure 33). As shown, forced Fbxo9 expression led to a decrease in Tel2/Tti1 levels and inhibited phosphorylation of S6K1, and at the same time increased Akt phosphorylation (Figure 49). Overexpressing CK2 alone substantially enhanced levels of phosphorylated Tel2 and Tti1, but further reduction in signal intensity of Tel2 and Tti1 was only affected when CK2 was co-expressed with Fbxo9, emphasising that CK2 acts prior to SCF^{Fbxo9} to mark Tel2 and Tti1 proteins for subsequent ubiquitylation and degradation.

Figure 49: Overexpression of Fbxo9 and CK2 activates mTORC2 signalling. HEK293T cells were transiently transfected with empty vector (EV) or plasmids encoding FLAG-tagged CK2 and/or Fbxo9 as indicated. Whole cell lysates were analysed by immunoblotting for indicated antibodies.

The effects of forced expression of Fbxo9 on mTORC2 signalling were further monitored by 2D cell cycle analysis (Figure 50). While in the normal expression status (panels 1+3) proliferation and survival were reduced upon SD, overexpressing Fbxo9 in cells greatly limited apoptosis and growth restriction (panels 2+4). Of note, this effect was even seen in unstarved cells (panels 1+2); however, more pronounced upon growth factor withdrawal, with proliferative cells in S-Phase increasing from 11.4% to 26.7%, while sub-G1 fractions were reduced from 38.0% to 8.7% (panels 3+4). Thus, constant overexpression of Fbxo9 results in an increase of proliferation and survival, confirming sustained mTORC2 activity.

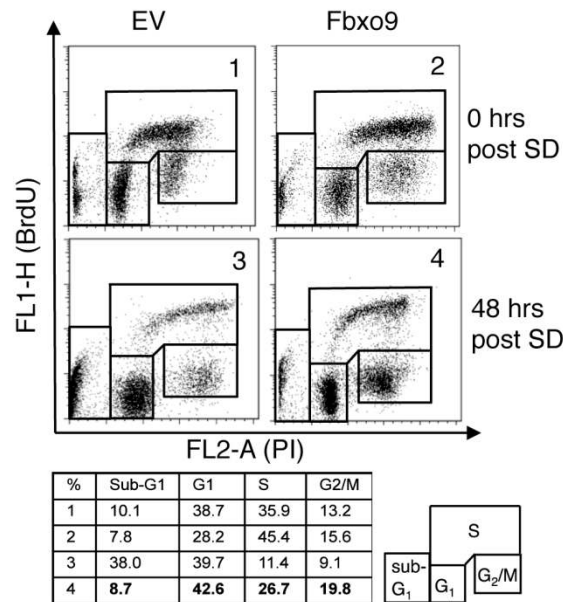


Figure 50: Fbxo9 overexpression increased cell survival and proliferation. U2OS cells were retrovirally infected with expression vector for FLAG-tagged Fbxo9 or empty vector (EV), fixed at the indicated times post serum deprivation (SD: 0.02% FBS), and subjected to 2D cell cycle analysis (BrdU/PI).

Taken together, overexpressing Fbxo9 results in impaired mTORC1 signalling, paralleled by an activation of the mTORC2 pathway.

In analogy to the function of Fbxo9 upon growth factor withdrawal described in chapter 5.1.4, forced expression of Fbxo9 was likely to result in constitutive mTORC1 specific degradation of Tel2/Tti1. Indeed, in IP experiments for endogenous Raptor or Rictor, which were essentially performed by Dr. V.Fernandez-Sáiz, a significant decrease in the amount of Raptor-bound Tel2/Tti1 could be observed upon Fbxo9 overexpression, while the levels of Rictor-bound Tel2/Tti1 remained largely unaffected (Figure 51). Of note, this effect was reversible upon proteasome inhibition (MG132), indicating an UPS dependent degradation of mTORC1 bound Tel2/Tti1. An increase in cyclin B signal served as a control for efficient proteasome inhibition. The Fbxo9 overexpression is depicted by a FLAG-immunoblot.

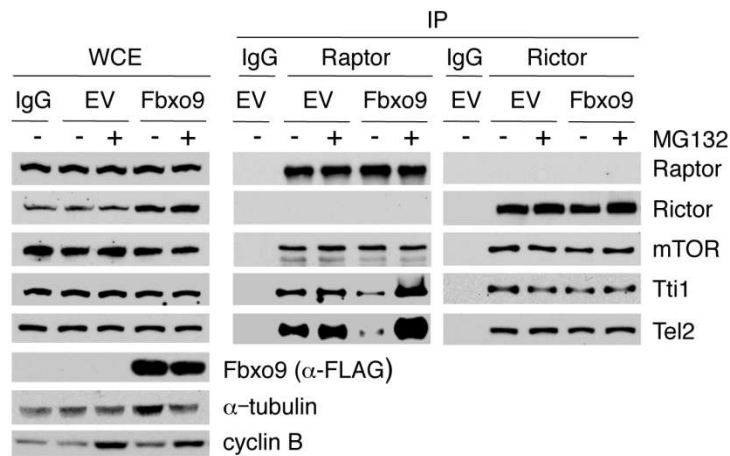


Figure 51: Fbxo9 preferentially targets mTORC1-bound Tel2/Tti1. HEK293T cells were transfected with FLAG-tagged Fbxo9 or empty vector (EV) and treated with MG132 where indicated. Endogenous Raptor and Rictor were immunoprecipitated (IP) from whole cell extracts (WCE), and immunocomplexes were probed with antibodies to the indicated proteins. Rabbit IgG was used as control for specificity of Raptor and Rictor IP. [Data provided by Dr. V.Fernandez-Sáiz]

In summary, experimental evidence could confirm a mTORC1-specific degradation of Tel2/Tti1 mediated by CK2 phosphorylation and SCF^{Fbxo9} ubiquitylation, which accounts for differential regulation of mTOR complex signalling.

5.4.3 Tel2/Tti1 degradation is relevant for mTOR signalling in vivo

In an attempt to verify the experimental data in an *in vivo* setting, mice were fed or fasted for 16 hrs and analysed. In accordance with the model, in liver extracts of fasted mice levels of Fbxo9 increased up to 7.5-fold (Figure 52a, b), indicative of an essential regulatory role during starvation response. Similarly, staining for phospho-degrons of Tel2 or Tti1 increased, while signal intensities for Tel2 and Tti1 proteins decreased (Figure 52a, b), essentially recapitulating the observed degradation-mediating priming phosphorylation event. Of special interest, coinciding with lower levels of mTOR, detection of phosphorylated S6K1 and S6 was reduced to 0.16 or 0.1 fold, respectively (Figure 52a, b). Furthermore, weight of the liver was significantly reduced from 1.43 g to 1.08 g, indicating a robust response to starvation (Figure 52c). Together, the *in vivo* data indicate that upon fasting attenuated mTORC1 signalling indeed involves phosphorylation dependent degradation of Tel2/Tti1 via Fbxo9.

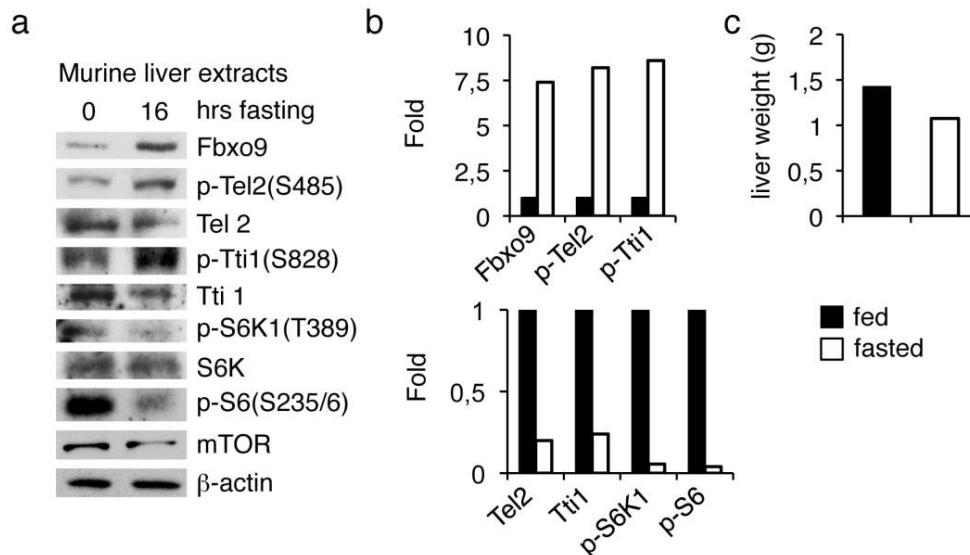


Figure 52: Tel2/Tti1 degradation *in vivo*. (a) Wildtype C57BL/6 mice were fed or fasted for 16 hrs and sacrificed. Thereafter, liver extracts were prepared and subjected to immunoblotting using the indicated antibodies. (b) Quantification of protein levels shown in (a) averaged with an additional independent experiment (n = 2). The values present in the fed samples were set as 1. (c) Panels show liver weights of sacrificed mice (n = 2). [Data provided by Ruth Eichner]

5.5 Fbxo9 is overexpressed in MM to promote survival

Together, the above experiments demonstrate that Fbxo9 and CK2 mediate phospho-degron dependent degradation of Tel2/Tti1 within mTORC1 to attenuate mTORC1 signalling and sustain PI3K/mTORC2/Akt activity in the setting of growth factor withdrawal. Moreover, the data indicate that this mechanism can be driven towards constitutive activation of mTORC2, when forced expression of Fbxo9 is present. Since upregulation of the PI3K/mTORC2/Akt pathway is commonly observed in malignancies and the FBXO9 locus was frequently found to be amplified in human multiple myeloma (MM) (s. chapter 3.1.4) the next investigations focussed on the role of Fbxo9 in this blood cell malignancy.

In a first approach, openly available Oncomine databases¹⁷⁶ of previous microarray studies were re-analysed for *Fbxo9* expression levels in MM patients (Figure 53). Indeed, with a significance of $p = 0.00017$ an increase of expression could be found for patients diagnosed in the premalignant state of the disease - monoclonal gammopathy of undetermined significance (MGUS) (22 samples) - compared to plasma cells from bone marrow of healthy donors (23 samples) (Figure 53a). As well, the further transformation from MGUS (seven patients) over MM (39 patients) to late stage extramedullary plasma cell leukaemia (six patients) is paralleled with a gain of *Fbxo9* mRNA expression levels (Figure 53b). Data evaluation indicates that Fbxo9 might be involved in both priming and progressive events during MM development.

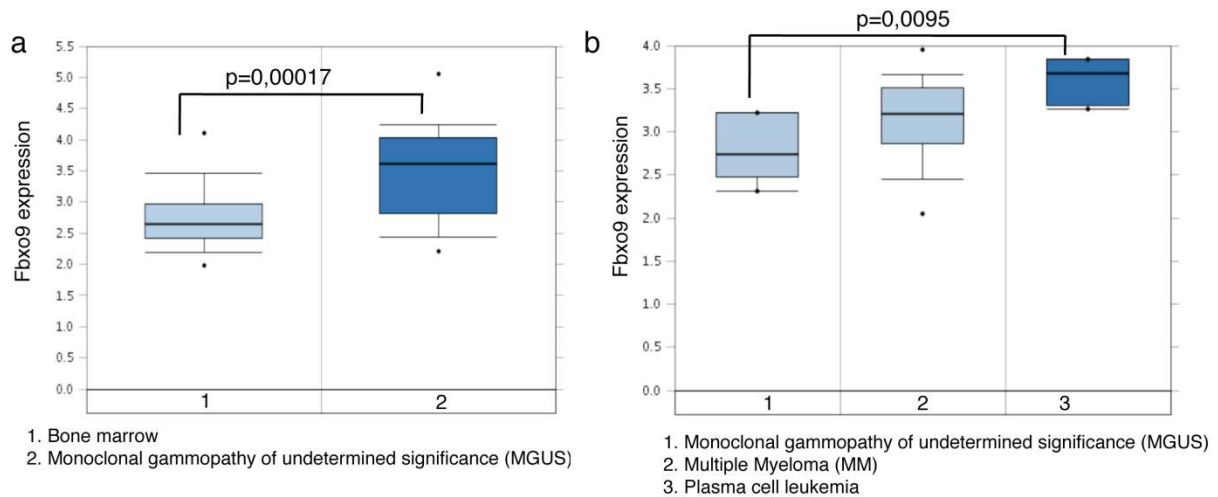


Figure 53: Elevated mRNA levels of *Fbxo9* in human MM at different clinical stages. All data was provided by the Oncomine database. The associated p-values are shown for each study. Box-and-whisker plots show the upper and lower quartiles (25–75%) with a line at the median, whiskers extend from the 10th to the 90th percentile, and dots correspond to minimal and maximal values. (a) Data from Mattioli, M. et al., 2005¹⁷⁷ reanalyzed to show expression levels of *Fbxo9* in normal bone marrow and monoclonal gammopathy of undetermined significance (MGUS) (n = 78). (b) Data from Zhan, F. et al., 2007¹⁷⁸ reanalysed to show expression levels of *Fbxo9* in MGUS, MM, and plasma cell leukaemia (n = 52).

To reliably correlate *Fbxo9* mRNA expression with disease status, a cohort of 180 human MM samples was analysed and normalised to mRNA levels of normal plasma cells of four individual

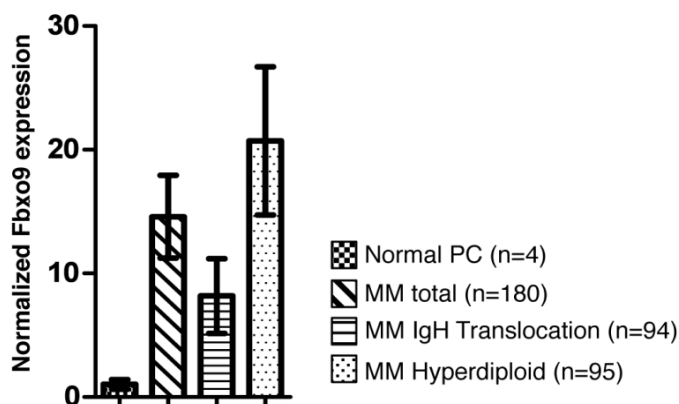


Figure 54: Relevance of *Fbxo9* overexpression in patients. Relative *Fbxo9* mRNA expression levels in 180 MM patient samples. Expression levels are normalised to the expression levels of normal plasma cells of four independent healthy donors. 54 of 180 cases (30%) show an at least five-fold increased expression compared to normal plasma cells. MM samples presenting with a hyperdiploid chromosome set express *Fbxo9* at significantly higher levels as compared to cases with a translocation involving the immunoglobulin heavy chain (IgH) locus. The mean *Fbxo9* expression levels are shown for each group (n = 180; p = 0.03; unpaired t-test) Error bars represent s.e.m. [Data provided by Dr. C.Langer]

healthy donors. These analyses, conducted in the Department of Internal Medicine III (University of Ulm) by Dr. C. Langer revealed an expression range covering five logarithmic ranks and overexpression of *Fbxo9* (defined as more than five-fold compared to normal plasma cells) in 30% (54 out of 180) of the investigated cases (Figure 54). Interestingly, patients harbouring a hyperdiploid chromosome set express *Fbxo9* to significantly higher levels than patients with an IgH translocation, indicative of a correlation with distinct genomic aberrations.

As Fbxo9 was characterised to mediate proteasomal degradation of its substrates, inhibiting the UPS was suspected to be beneficial for patients with elevated Fbxo9 expression levels. Therefore a previously published gene expression data set of 163 patients treated with the proteasome inhibitor Bortezomib was analysed in the Department of Internal Medicine III (University of Ulm) by Prof. L. Bullinger. Apparently, responders to Bortezomib treatment (R) showed significantly ($p = 0.0079$) higher Fbxo9 expression levels compared to non-responding patients (NR) (Figure 55a). In the course of time the progression-free survival of R positively correlated with high Fbxo9 expression as shown in Kaplan Maier curves (Figure 55b), suggesting that indeed Fbxo9 could promote survival of MM cells in these cases.

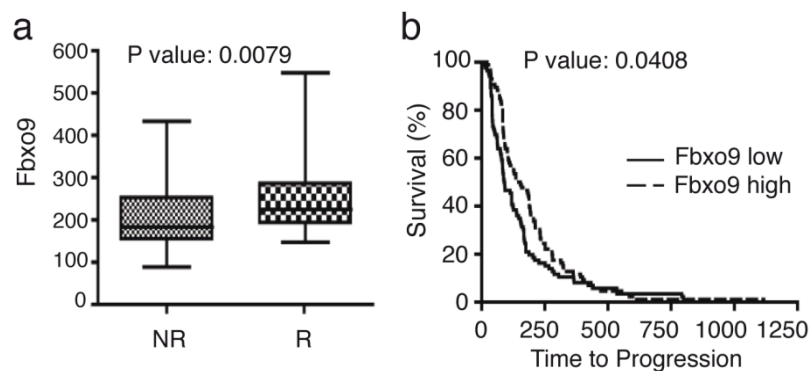


Figure 55: Response and survival correlate with Fbxo9 expression.(a) Normalized *Fbxo9* fluorescence intensities are shown for Bortezomib non-responders (NR) and responders (R). *Fbxo9* levels were significantly higher in R vs. NR ($n = 163$; $P = 0.0079$, unpaired t-test). (b) Kaplan Meier analyses for progression-free survival based on *Fbxo9* expression (data dichotomized at the median *Fbxo9* expression level; $n = 182$, $P = 0.041$, log-rank test). Gene expression data of this figure were derived from Mulligan et al., 2007¹⁷⁹ (GEO accession number: GSE9782). [Data provided by Prof. L.Bullinger]

Since Fbxo9 expression correlated with disease progression, further investigations tried to recapitulate the delineated mechanism of Fbxo9 action in patient samples. To this end, extracts derived from MM patient bone marrow samples, were subjected to reverse phase protein microarray analyses with antibodies specific to the phosphorylated forms of S6 and Akt (**Fehler! Verweisquelle konnte nicht gefunden werden.**) and analysed by Clemens Reiter (TUM). Since Fbxo9 antibody could not be utilised for this specific method, expression levels were obtained using quantitative PCR (qPCR) analyses (graphs on the left). **Fehler! Verweisquelle konnte nicht gefunden werden.** shows five representative MM cases (in grey), with either elevated (upper three panels) or normal (two lower panels) *Fbxo9* levels compared to a control sample (Ctrl; in black). Depicted in the middle are the immunoblot analyses of the protein array spotted with raising concentrations (in triplicate) and the respective whole protein extract control (Sypro ruby). Quantifications of signal intensities (right graphs), were performed in comparison to Ctrl signals. They reveal a correlation of high Fbxo9 expression with low phosphorylation of the mTORC1-specific S6 and high phosphorylation of the

mTORC2 target Akt (graphs on the right), indicating a role for Fbxo9 in the activation of PI3K/mTORC2/Akt axis via reduced mTORC1 activity in MM patients.

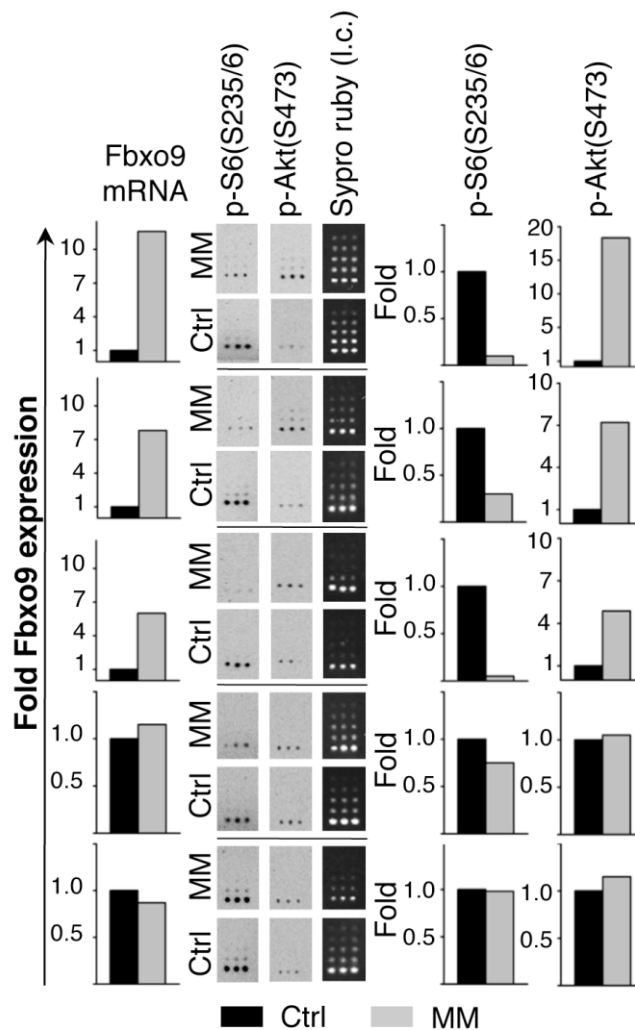


Figure 56: High Fbxo9 expression correlates with activation of Akt. Protein extracts were prepared from bone marrow biopsies of different MM cases and subjected to a reverse phase protein microarray (in triplicate) using the indicated validated antibodies. Sypro ruby was used to visualise equal amounts overall protein extract (middle panels). Microarray signal intensities were normalised to Ctrl and set as one (right graphs). *Fbxo9* mRNA levels of control (Ctrl) and MM cases were assessed by qPCR on extracted material (left graphs). [Data provided by Clemens Reiter]

To test the hypothesis further, different MM cell lines were characterised by immunoblot analyses. As expected cell lines with high levels of Fbxo9 displayed low expression signals of Tel2/Tti1 and mTOR, high phosphorylation levels of Akt and low phosphorylation levels of S6K1 (Figure 57), while overall levels of Akt and S6K1 were found to be equal. This result suggests that the differential deregulation of both mTOR pathways can be recapitulated in MM. Interestingly, five out of nine cell

lines tested displayed a strong signal of Fbxo9, indicating that its elevated expression is indeed favourable for survival of myeloma cells.

Nevertheless, taking into consideration that phosphorylated Akt is known to drive gene expression of a number of genes (s. chapter 3.3.3.3), it was still possible that hyperactivity of Akt could account for the observed elevated expression of Fbxo9 in those cell lines. To test this possibility, OPM2 – a cell line with high levels of both phosphorylated Akt and Fbxo9 (s. Figure 57) – were treated with Wortmannin, which could that effectively inhibit phosphorylation of Akt, as shown by immunoblot analyses (Figure 58). However, levels of Fbxo9 and controls (mTOR, Cul1) remained unaffected by this treatment, demonstrating that expression of Fbxo9 is not dependent on Akt activity.

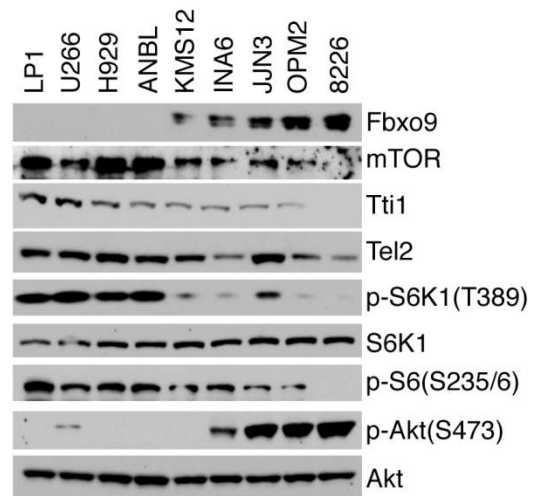


Figure 57: Fbxo9 expression correlates with asymmetric mTOR signalling in MM cell lines. Whole cell lysates of nine different human MM cell lines were subjected to immunoblot analysis for the indicated proteins.

As a significant number of MM cell lines were characterised to resemble good models for a deregulated Fbxo9-Tel2/Tti1-mTOR axis in the context of the disease, final approaches tried to re-establish physiological Tel2/Tti1 levels by manipulating activity of CK2 or levels of Fbxo9 expression. By inhibiting CK2, the effects of Fbxo9 overexpression should be counteracted. Indeed,

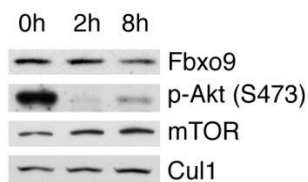


Figure 58: Fbxo9 expression is not driven by phosphorylated Akt. OPM2 cells with high levels of Fbxo9 expression were treated with Akt inhibitor Wortmannin (500 nM) for the indicated times and subjected to immunoblot analysis.

upon pharmacologic inhibition of CK2 with TBB in three different MM cell lines with high Fbxo9 expression, stabilised levels of Tel2, Tti1, and mTOR, and increased phosphorylation of S6K1 compared to untreated controls could be detected in collaboration with Ruth Eichner (Figure 59a). Conversely, stimulation of CK2 activity with Sorbitol could indeed minimise protein levels of Tel2 and Tti1 in MM cells with high levels of Fbxo9 (Figure 59b). As such, in line with the notion that CK2 dependent phosphorylation is a prerequisite for Tel2/Tti1 degradation, it could be shown that CK2-dependent phosphorylation can indeed modulate Tel2/Tti1 stability and mTOR pathway signalling in the context of MM.

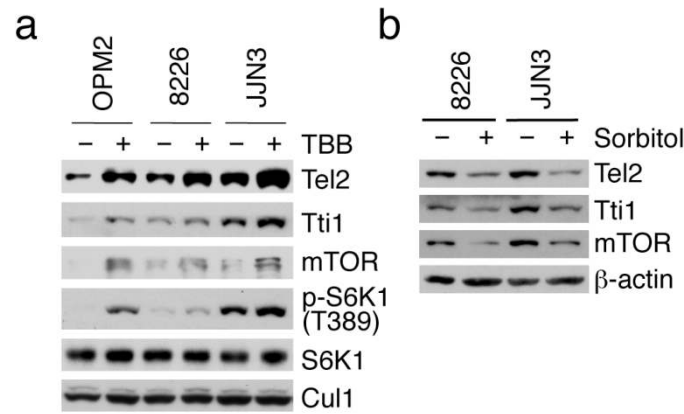


Figure 59: CK2 kinase activity modulates Tel2/Tti1 stability. (a) Inhibition of CK2 kinase stabilises Tel2/Tti1. The MM cell lines OPM2, RPMI-8226, and JJN3 were treated with TBB or vehicle to inhibit CK2 kinase, lysed and probed with antibodies to the indicated proteins [Data provided by Ruth Eichner]. (b) RPMI-8226 and JJN3 were treated with Sorbitol for 2 hrs to activate CK2 kinase. Immunoblot analyses to the indicated antibodies are shown.

To directly assess if Fbxo9 overexpression indeed confers a survival advantage to the MM cell lines, apoptosis induction upon Fbxo9 depletion was analysed. Lentiviral shRNA constructs against Fbxo9, coupled to a GFP expression marker, was applied in MM cell lines with either normal (U266)

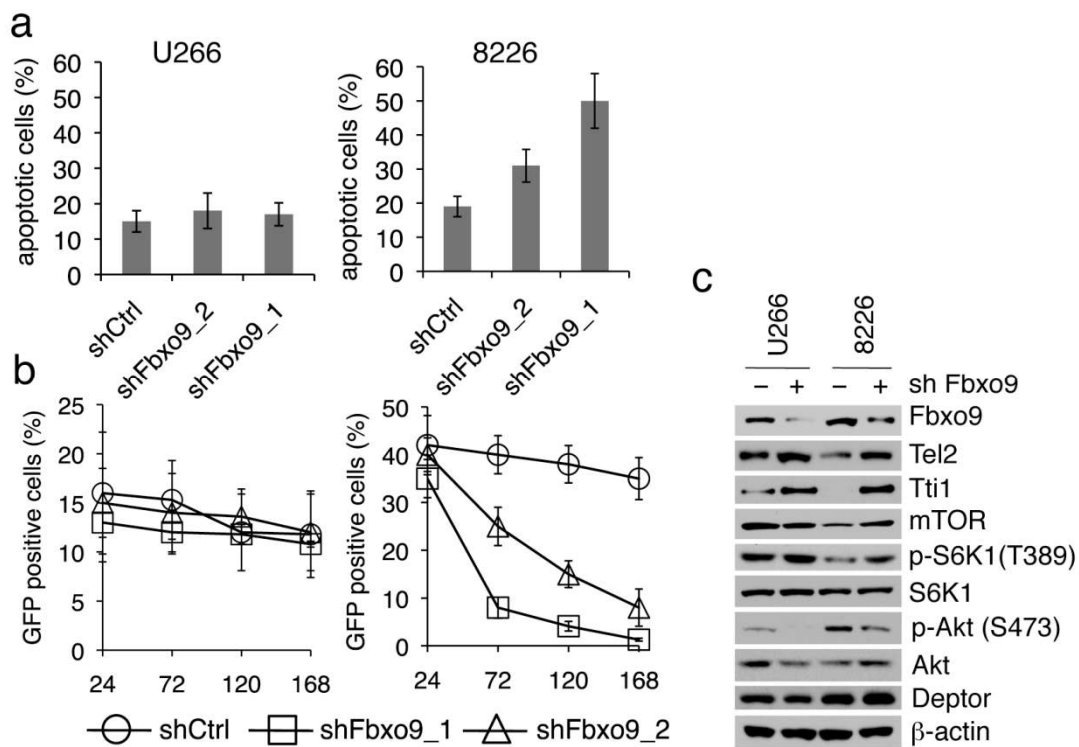


Figure 60: Survival of MM cells is dependent on Fbxo9 overexpression. U266 and RPMI-8226 (8226) were lentivirally infected with shRNA constructs directed against a non-relevant mRNA or *Fbxo9* mRNA coupled with expression of a GFP reporter, and processed for (a) two-colour FACS analyses (PI, GFP) in three independent experiments (n = 3, ±sd). The apoptotic fraction of GFP positive cells is shown. (b) cells as in (a) were subjected to FACS analyses for GFP-positive cells in three independent experiments (n = 3, ±sd). The x-axis depicts time [hrs] (c) Immunoblot analysis of whole cell lysates used in (a) and (b) to indicated proteins.

or high (RPMI-2886) Fbxo9 expression levels. In flow cytometric analyses of the infected GFP-positive fraction of cells, the inactivation of Fbxo9 strongly enhanced apoptosis induction in MM cells with high Fbxo9 expression (right graphs), with an almost 2.5 fold rise for the most efficient knockdown (Figure 60a). This effect was merely detectable in cells with initially low Fbxo9 expression (left graph). Likewise, survival - defined by the proportion of GFP positive cells after several generation times of U266 (left graph) was unaffected. In contrast in RPMI-8226 (right graph) treated to downregulate Fbxo9 (shFbxo9_1,2) survival was strongly reduced compared to control (shCtrl) treated cells (Figure 60b). Figure 60c shows effective downregulation of Fbxo9, subsequent stabilisation of Tel2/Tti1 and mTOR, decreased phosphorylation of Akt and an increase in S6K1 phosphorylation in Western Blot analyses. These effects were most prominent for RPMI-8226, underscoring that overexpression of Fbxo9 promotes survival via repression of mTORC1-mediated feedback inhibition of PI3K/mTORC2/Akt signalling.

6 Discussion

The present study shows that CK2 and SCF^{Fbxo9} regulate mTOR signalling in response to serum deprivation via targeted proteasomal degradation of Tel2/Tti1 specifically in mTORC1 to promote survival of multiple myeloma (MM). By differentially regulating mTORC1 and mTORC2 signalling, the so far uncharacterised F-box protein (FBP) Fbxo9 and the constitutively active kinase CK2 function to establish a steady state defined by maintained survival during minimised energy consumption. This elegant mechanism allows the cells to endure for prolonged periods until eventually better growth conditions arise, thereby greatly avoiding premature cellular apoptosis. Importantly, relevance of this UPS driven mechanism can be recapitulated in an *in vivo* setting. However, under non-physiological conditions, a hyperactivation of this mechanism caused by the overexpression of Fbxo9 leads to constant pro-survival signalling – a finding that applies to approximately one third of MM patients and correlates with increased responsiveness and survival upon treatment with proteasome inhibitor Bortezomib. Together, Fbxo9 and CK2 emerge as potential novel targets in MM with high expression of Fbxo9, and suggest that Fbxo9 levels may be a useful biomarker to predict clinical response to treatment, particularly proteasomal inhibition.

Mechanistically, the collective results propose a model in which under physiological conditions, SCF^{Fbxo9} and CK2 specifically target mTORC1-bound Tel2/Tti1 in a phospho-degron dependent man-

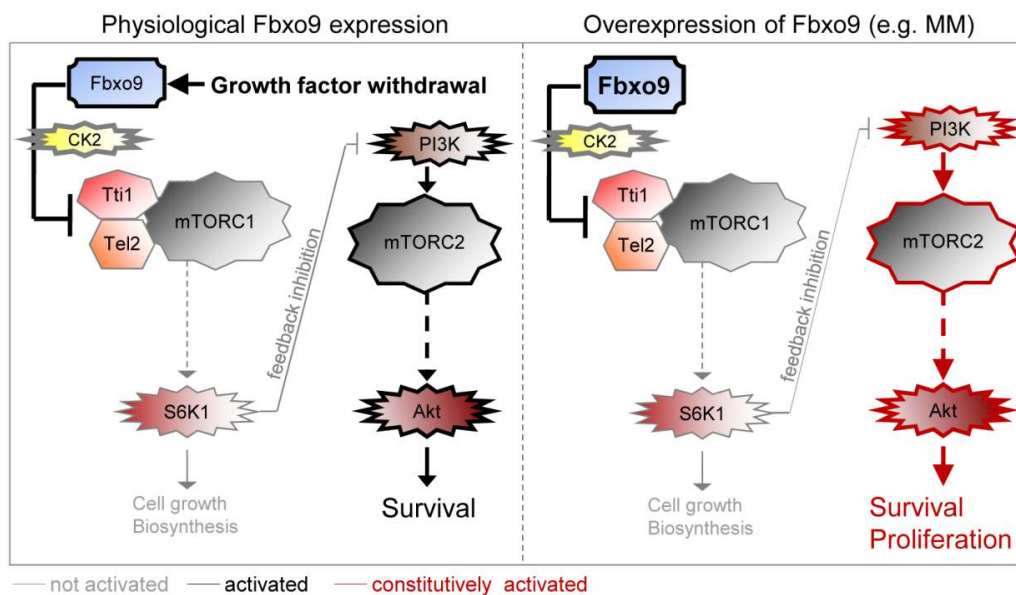


Figure 61: Schematic model for how Fbxo9 and CK2 orchestrate the cellular response to growth factor withdrawal (left). By degrading Tel2/Tti1 complex specifically in mTORC1 signalling via S6K1 is deactivated to minimise energy consumption through cell growth and biosynthesis. Reduced mTORC1 signalling further relieves the feedback inhibition on the mTORC2 pathway, thus activating anti-apoptotic Akt and prolonged cell survival. This elegant mechanism can be shifted to the constitutively active PI3K/mTORC2/Akt pro-survival signalling upon non-physiological overexpression of Fbxo9 (right).

ner for degradation by the proteasome (Figure 61). This entails cellular adaption to nutrient saving conditions, in which energy consuming processes – governed by mTORC1 and S6K1 – such as protein biosynthesis and growth are restrained whereas prolonged survival is granted via relief of feedback inhibition on the PI3K/mTORC2/Akt axis. Under non-physiological conditions, forced overexpression of Fbxo9 swings this normally stimulus dependent activation towards a constant pro-survival signalling via hyperactivation of the PI3K/mTORC2/Akt axis (Figure 61).

In the following, the roles of the newly identified mTOR pathway regulation will be discussed in the context of the physiological response to growth factor withdrawal and its impact on pathogenesis and treatment strategies of MM.

6.1 CK2 and SCF^{Fbxo9} regulate mTOR signalling in response to serum deprivation via targeted proteasomal degradation of Tel2/Tti1

The UPS is an effective cellular system regulating a diverse array of processes ranging from cell proliferation and death to circadian clock rhythms¹⁸⁰. By identifying for the first time substrates of the so far uncharacterised E3 ligase SCF^{Fbxo9} and demonstrating its implication within the cellular response to growth factor withdrawal, the present study adds another item to the growing list of UPS governed pathways. By negatively regulating mTORC1 activity, Fbxo9 is important to maintain anti-apoptotic signalling by mTORC2. Of note, a pro-survival function was also assigned to Hrt3p, the yeast homologue of Fbxo9 in *Saccharomyces cerevisiae*, where its overexpression confers resistance to environmental poisoning with methylmercury¹⁸¹. No substrates of Hrt3p have been defined so far, but the protective role of this FBP was clearly dependent on intact proteasome function in this context. It is therefore tempting to speculate that the yeast homologue of Fbxo9 might also have a regulatory role for cellular responses upon other diverse environmental perturbations. Furthermore, considering its conservedness up to plants, Fbxo9-mediated function in faithful protein degradation is putatively indispensable for cells. Responding to yet another external stimulus, the expression of AtFBP7 – the *Arabidopsis thaliana* counterpart of Fbxo9 – is increased upon cold and heat shock and required for protein synthesis during temperature stress³⁶. Since a mTOR homologue also exists in plants (TOR), which seems to recapitulate some key characteristics and functions described in mammals¹⁸², and the mTORC1 pathway is governing protein synthesis¹⁰⁹, it may be speculated, that mammalian Fbxo9 can mediate cellular responses to temperature stress in a similar fashion as delineated here for nutrient deprivation.

Overall, the present study suggests that the conserved protein Fbxo9 may very well be able to integrate other environmental cues to cellular responses, since its targets Tel2 and Tti1 are both integral components of not only mTOR complexes, but are also involved in the signalling cascades controlled

by ATM, ATR, DNA-PKcs, TRRAP and SMG1. Markedly, the stability of these PIKKs was to some degree also affected by Fbxo9 deletion in the initial starvation experiments (s. Figure 19), indicating that following a pathway specific stimuli, SCF^{Fbxo9} might be regulating stability and function of the respective protein kinases via targeted degradation of Tel2/Tti1, as well. On second thought, many of the so far characterised FBPs have more than one substrate and can be recruited or activated in a context specific fashion. For example, the E3 ligase SCF ^{β -TrCP} (β -transducin repeat containing protein) was shown to target PDCD4 and Deptor in response to serum repletion^{136, 183-185}, while after DNA damage its activity is directed against cell cycle regulator Cdc25A¹⁸⁶⁻¹⁸⁷ to stall the cell cycle and permit sufficient time for repair. As such, in future research for other cellular substrates and roles of Fbxo9, the identification of **pSDXDXE** (s. Figure 31) as canonical degron motif recognised by Fbxo9 in this study may facilitate further investigations.

Many biochemical and biological properties of the FBP regulating the Fbxo9-Tel2/Tti1-mTor axis were extensively studied. Considering its specialised role in a stimuli-dependent context, it may be speculated, if the cell regulates Fbxo9-mediated ubiquitylation activity apart from degron phosphorylation dependency. If SCF^{Fbxo9} may not be a constitutively active E3 enzyme, several regulatory measures are supposable. For example, dimerisation of two SCF complexes has been shown to promote activity of Fbxw7¹⁸⁸. Similarly, acetylation of certain residues within the RING domain of Mdm2 was reported to inhibit its E3 ligase activity towards its target p53¹⁸⁹. Furthermore different FBPs have been reported to regulate their own activity or abundance via autoubiquitylation⁹². As immunofluorescence-based localisation studies identified Fbxo9 to be constantly cytoplasmic (s. Figure 18), a compartmentalisation-mediated regulation of the protein is rather unlikely; however, an association to specific sub-structures within the cytosol might still represent a measure of sequestering the FBP from its substrates. Another plausible form of adjusting Fbxo9 reactivity accordingly could be on the level of transcriptional regulation. However, during starvation mRNA levels of Fbxo9 did not increase (s. Figure 15b), while protein expression seems to be augmented (s. Figure 19). While the increased signal intensity might simply reflect a higher abundance in a situation where most dispensable cellular components are being reduced to a minimum, there is still a likelihood that in these conditions, activation of Fbxo9 on a post-transcriptional level is at play. If this involves enhanced translation of *Fbxo9* mRNA or any other PTM described above, remains to be determined.

Degradation of SCF targets is mostly dependent on specific substrate modifications, such as phosphorylation of defined degron motifs⁴⁸. Thus, upon context specific stimulation, cells integrate environmental cues to distinct signalling, leading to controlled substrate phosphorylation, subsequent ubiquitylation and proteasomal degradation¹⁸⁰. This study identified the constitutively active CK2 as

the regulating kinase. It is a multifunctional and pleiotropic protein kinase targeting a myriad of substrates located in diverse cellular compartments, with crucial roles in cell differentiation, proliferation, and survival¹⁹⁰⁻¹⁹¹. The active kinase is assembled as a tetrameric protein complex consisting of the two catalytic subunits CK2 α and CK2 α' and a dimer of two regulatory β -subunits¹⁹². Localisation studies reported both catalytic subunits to be mostly nuclear in interphase and dispersed throughout the cell in mitosis¹⁹³. An independent nuclear import of all subunits at different kinetics suggests that formation of the active holoenzyme takes place in the nucleus¹⁹⁴. Moreover, in contrast to the majority of protein kinases, which are usually in an inactive state unless their activity is required in response to specific stimuli and effectors, CK2 is constitutively active¹⁹⁰. Still, even though not evident, the kinase can mediate stimuli-specific proteasomal degradation of target proteins in a phospho-degron dependent manner as identified here for Tel2 and Tti1. For example, expression of the cell cycle regulator Wee1 is tightly controlled by phospho-degron specific binding to its E3 ligase SCF ^{β -TrCP} at the transition to mitosis, which is, amongst other kinases, regulated by CK2¹⁹⁵. Further, in response to stress, an increased CK2 activity towards the tumor suppressor PML (promyelocytic leukaemia protein) was reported to lead to proteasomal degradation of PML¹⁹⁶. This suggests that CK2-specific degron sites are generally valid motifs for UPS-mediated cellular processes. In this respect, to allow substrate discrimination by the pleiotropic CK2, certain mechanisms for regulation of phosphorylation activity must exist; however, despite considerable investigations, an unifying model for a potential cellular regulation of CK2 has not yet been described¹⁹¹. Favourable and strongly debated hypotheses involve altered localisation, priming phosphorylation, and modifying protein-protein interactions^{175, 190-191, 197-200}. For example CK2 was shown to be phosphorylated in a CDK-dependent fashion²⁰¹ entailing association with the peptidyl-prolyl isomerase Pin1 during mitosis²⁰². These events generally enhance CK2 activity towards its mitotic substrates, but the exact mode of activation is not fully elucidated. Mitotic phosphorylation of CK2 does not directly affect its intrinsic kinase activity²⁰³, and Pin1 might actually rather regulate accessibility to substrates, than positively influencing CK2 activity¹⁹⁸. Along the same line, recent work suggested that mitotic Pin1 association represents a mechanism for CK2 recruitment to sites of action²⁰⁴, suggesting a synergistic interplay of several factors to regulate the directed CK2 activity.

Against this background, the present study could identify a nucleo-cytoplasmic translocation as the main regulatory means to direct CK2 activity towards Tel2 and Tti1 proteins following growth factor withdrawal. CK2 accumulates in the cytoplasm during serum deprivation (s. Figure 41), and is retained at its reaction sites, because a fully assembled holoenzyme cannot be imported to the nucleus¹⁹⁴. However, the initial underlying mechanism for CK2 shuttling remains obscure. A *de novo* formation of a cytoplasmic holoenzyme prior to the usual nuclear import is unlikely, considering the absence of nuclear CK2 staining after growth factor withdrawal (s. Figure 41). Hence, active export of CK2 via

well established shuttling proteins like CRM1 or via assistance of adaptor molecules is a more likely scenario²⁰⁵. Binding to those interactors could be putatively mediated by a stimulus-dependent PTM on CK2, thus integrating the external cue to directed transport. If such an export process occurs separately for all CK2 subunits in a concerted fashion, or if the complete holoenzyme is exported, will be subject of future investigations. By providing evidence for nucleo-cytoplasmic translocation of CK2 as regulatory means upon serum withdrawal, this study adds spatial control to the list of CK2 substrate specificity determination mechanisms.

Substrates of the CK2 mediated polyubiquitylation by SCF^{Fbxo9} are Tel2 and Tti1 – two integral components of the mTOR complexes. Their proteasomal degradation within the cell is characterised by two distinctive features: The process is triggered in the context of serum withdrawal and is specialised as to only the mTORC1-bound fraction of Tel2 and Tti1 proteins are effectively targeted. In combination with the recent evidences that Tel2/Tti1 are essential for stability of mTOR complexes¹²⁰, it is thus proposed that in response to unfavourable growth conditions, degradation of Tel2 and Tti1 entails disruption of mTORC1, which in turn lowers its kinase activities to minimise cellular energy consumption. However, mTORC2 integrity remains largely unaffected, and thus procures cell survival. Of interest, complex formation and PIKK association is also found in yeast cells²⁰⁶, where induction of cellular quiescence in *Schizosaccharomyces pombe* was suggested to depend on the Tel2/Tti1 complex²⁰⁷. Quiescence resembles in many aspects the starvation response with growth and cell cycle silencing during maintained survival, thus indicating an essential and conserved role for Tel2 and Tti1 regulating cellular metabolism.

With regard to the observed complex-specific targeting of Tel2/Tti1 in mTORC1 (s. Figure 48), this study convincingly shows that degradation is mediated by a priming phosphorylation through CK2. Only thereafter SCF^{Fbxo9} can ubiquitylate its substrates, in line with the the delayed degradation of Tel2/Tti1 following serum deprivation response (s. Figure 48). The molecular regulation, establishing such a preference for only one mTOR complex remains however speculative. The dynamics of its translocation might bear a possibility to direct CK2 only to mTORC1. If this involves the function of an active transport protein, a specific adaptor or a direct binding to one of the mTORC1 specific components (e.g. PRAS40¹²³ and Raptor¹²¹⁻¹²²) has yet to be defined. Targeted transport for CK2 has been reported¹⁹⁴ and specific adaptor molecules are widely used to improve reaction specificity²⁰⁸⁻²⁰⁹. Of note, Raptor can function as a scaffold protein for mTORC1 specific reaction partners¹³⁴ and alteration in the phosphorylation status of Raptor²¹⁰ might provide an dynamic motif for a context-based binding partner discrimination. In another scenario Tel2 and Tti1 in mTORC2 could be actively protected from phosphorylation by an opposing phosphatase to CK2. However, evidence for the existence of such an enzyme that must be either associated or recruited specifically to mTORC2 upon

SD is so far lacking and has to be experimentally provided. Moreover, the significance of spatial proximity and substrate accessibility for execution of a biochemical reaction within a crowded cellular environment could be considered. In this regard, absent targeting of Tel2 and Tti1 within mTORC2 may be explained by sterical hindrance of CK2, which could impair physical interaction. As such mTORC2 was described to be ribosome associated¹⁰⁸, which could be a way to sequester reaction partners even within the cytoplasm. Also for mTORC1, a specialised subcellular localisation was described²¹¹. Stimulation with amino acids induces movement of mTORC1 to lysosomal membranes²¹¹. While further investigations are needed to fully address these hypotheses, it is thus possible that differential substructure association of mTORC1 and mTORC2, respectively, might actually result in exclusive exposure of mTORC1-bound Tel2/Tti1 for phosphorylation and subsequent ubiquitylation reactions during starvation.

In discovering the complex-specific targeting of Tel2/Tti1, the present study provides a convincing model how differential regulation mTOR signalling can be established (s. Figure 61). A similar asymmetrical regulation was previously assigned to Deptor, an inhibitory protein associated and directly interfering with both mTOR complex signalling pathways¹¹⁹. Following nutrient deprivation Deptor expression was shown to be upregulated and subsequent reduction of mTOR signalling actually stabilised Deptor expression levels in a self-amplifying loop. This demonstrates how similar cellular responses can be achieved by completely different mechanisms, as exemplified here by either increasing abundance of inhibitory Deptor or decreasing levels of stabilising Tel2/Tti1. However, in contrast to the situation of Tel2/Tti1 where already under physiological conditions the two mTOR pathways are differentially affected in response to nutrient depletion, only forced expression of Deptor alleviates mTORC1 feedback inhibition on mTORC2, by an to date unexplained preference for mTORC1 inhibition¹¹⁹. While this deregulation becomes especially interesting in the context of MM (s. next chapter), the physiological role of Deptor may complement the sustaining function of Tel2/Tti1 in response to starvation by immediate action. It may be hypothesised that the two processes for attenuation of mTOR signalling share some redundancy and can even substitute each other, whereas an action in parallel might actually strengthen starvation response. Further investigations are needed to delineate the mode of interplay between Tel2/Tti1 and Deptor during nutrient deprivation.

The role of Tel2 and Tti1 proteins in maintaining cellular responses might not solely be restricted to growth factor withdrawal, since they can interact with all mammalian PIKKs and essentially regulate their abundance¹⁵⁰. Indeed, in starved conditions, once Tel2/Tti1 levels are abnormally high during Fbxo9 depletion, also other PIKKs are stabilised (s. Figure 19). This might be a mere effect of augmented intercellular concentration, but it might also point towards an active role of the SCF^{Fbxo9}-dependent degradation of Tel2/Tti1 associated with other PIKKs (see above). ATM, ATR and DNA-

PKCs are well-defined regulators of response to various forms of DNA-damage, inducing cell cycle arrest and lesion repair²¹²⁻²¹³. Considering the proposed stabilising effect of Tel2/Tti1, the interaction might be most valuable once such stresses are imposed on the cell. Concomitantly, depletion of Tti1 renders cells sensitive to damaging agents and results in checkpoint bypass¹⁵². Targeted degradation of Tel2/Tti1 within these complexes is then most likely to occur during damage stress recovery, when the kinases are no longer required. On the other hand, after treatment with damaging agents, Tti1 interaction with PIKKs is markedly reduced, suggesting a stimuli dependent dissociation, which might be explained by degradation¹⁵². In turn, this would lead to the hypothesis that Tel2/Tti1 might act as scaffolds to sequester, yet stabilise PIKKs under normal conditions, and release them to sites of damaged DNA upon stimuli, reflecting of course a different mode of regulation compared to maintenance of mTOR signalling. Another interactor, TRRAP, which is a regulator of gene expression via its association with histone acetyltransferase complexes was also found to contribute to DDR²¹⁴ and might hence underlie a similar regulation. SMG1 which is generally an important factor during non-sense mediated decay, additionally functions as a sensor of DNA damage and oxidative stress²¹⁵ and it is speculative which cellular role of SMG1 is essentially governed by Tel2/Tti1 conferred stability. All these considerations would define an omnipotent role for Tel2/Tti1 to mediate a tightly connected crosstalk between all PIKKs upon various environmental influences. Future investigations will shed light onto the role of Tel2/Tti1 and the stability of PIKKs within the diverse cellular contexts and how members of the UPS are involved in these processes.

The identification of a novel process regulating cellular starvation response has added new UPS associated proteins and mechanisms to the current understanding of mTOR signalling. The next chapter will focus on how this tightly controlled physiological regulation can be driven towards a constitutively active survival pathway, which is frequently found during development of the hematologic malignancy MM.

6.2 Fbxo9 dependent degradation of Tel2/Tti1 is deregulated in MM to promote survival via asymmetric activation of mTOR pathways

The UPS has a crucial role in maintaining and regulating cellular homeostasis⁹⁸. Not surprisingly, as one of the main members of the UPS, the E3 ligases have been implicated in causing and sustaining malignant transformations in various cell types²¹⁶. This study shows overexpression of the FBP Fbxo9 in 30% of MM cases and better response to proteasome inhibition and subsequent PFS were correlated to elevated levels of Fbxo9. In these cases, survival was demonstrated to greatly depend on Fbxo9 overexpression, defining it as an oncogene in MM. Despite the effectiveness of proteasome inhibitors in clinical applications, myeloma-specific deregulated components of the UPS are to date only rarely defined. The only other FBP, reported to positively influence viability of MM cells is Fbxw7 α .

Regulating the nuclear p100 degradation, this E3-ligase promotes survival, by negatively interfering with physiological NF- κ B pathway inhibition in MM²¹⁷. While aberrant activation of the NF- κ B pathway has long been proposed to be an important mechanism underlying the successful application of proteasome inhibitors²¹⁸, this study additionally links the frequently hyperactivated PI3K/mTORC2/Akt signalling to an UPS-specific deregulation event in MM. Considering that the PI3K/mTORC2/Akt pathway also positively regulates the NF- κ B pathway²¹⁹ it is speculative that a deregulation of Fbxo9-Tel2/Tti1-mTOR axis may be the actual cause for the observed activation of the NF- κ B signalling cascade. To test this hypothesis, future investigations may focus on reanalysing MM patient data or cell lines with implications for NF- κ B pathway deregulation and a good responsiveness to proteasomal inhibition for levels of Fbxo9, Tel2 and Tti1, too. In this respect, it is possible that Fbxo9 will emerge as the key oncogenic protein deregulating a whole metabolic axis to promote survival of MM cells in many aspects.

Of note, inhibitory Deptor, which is regulated via the UPS-member SCF ^{β -TrCP} also has a role in mTOR signalling regulation¹⁸³⁻¹⁸⁵, and its overexpression has been shown to activate Akt via asymmetric mTOR complex inhibition in certain myeloma cells like RPMI-8226¹¹⁹. Thus, Deptor may contribute to the increased activity of Akt in MM observed in this study as well. However, presented results show that Deptor levels were not affected by Fbxo9 expression in MM cell lines examined (s. Figure 60c) and contrary to the prevalent enrichment of Fbxo9 in hyperdiploid MM cases, Deptor was enriched in MM patients presenting with IgH translocations¹¹⁹, indicating independent pathways (s. chapter 6.1). Thus, the present characterisation of Fbxo9 definitely demonstrates overexpression as frequent oncogenic event in the setting of MM. Transformation-promoting property of Fbxo9 might be not restricted to this malignancy, making it a promising candidate for expression analyses in other cancer types. In this respect, dependent on the underlying context, other already identified FBPs were shown to function as either oncogenes or tumorsuppressors²²⁰. For example, the SCF ^{β -TrCP} has been assigned mostly oncogenic functions with targets like inhibitory Deptor¹⁸³⁻¹⁸⁵, inhibitor of NF- κ B pathway (I κ B)²²¹, and DNA damage sensor Claspin²²²⁻²²³; however, in rare cases loss-of-function mutations caused accumulation of oncogenic targets like Wnt-signalling protein β -catenin^{62,224}. Thus, future investigations on putative substrates and aberrant expression in other cancer types may identify other essential functions for Fbxo9.

Nevertheless, considering the special context in which transformation of plasma cells to MM cells occurs, the oncogenic properties of Fbxo9 become essentially important during pathogenesis of this hematologic neoplasm. The differential regulation of mTOR signalling results in an usually disadvantageous status of reduced energy and growth with yet sustained and prolonged survival. As MM is a slowly developing disease¹³, such conditions might be particularly favourable for clonal

expansion of MM cells homing to the protective BMM²²⁵. The constant production of growth factors like IGF-1 and IL-6²²⁶ by the BMM was shown to further promote PI3K/mTORC2/Akt hyperactivation and thus survival²²⁷⁻²²⁸. The asymmetric deregulation of mTOR signalling by Fbxo9 overexpression is hence additionally shifted towards anti-apoptotic signalling via mTORC2 by external cues. This proposes a scenario, where residual mTORC1 activity is sufficient for the production of necessary biomass synthesis to allow MM cell expansion, but is however too little to establish effective feedback inhibition on the hyperactivated mTORC2 pathway. As such, MM cells can compensate for the minimal metabolic activity for extended periods, while profiting of the survival advantage. This may allow for an accumulation of further malignant genetic mutations, and thus disease progression.

The identification of deregulated Fbxo9-Tel2/Tti1-mTOR axis as a special tumor promoting mechanism in MM, incites further investigations on differential deregulation of mTOR signalling in an Fbxo9-dependent manner in other malignancies. As such, levels of inhibitory Deptor could be shown to inversely correlate with the activity of the mTOR signalling pathway in a panel of breast cancer cell lines¹⁸⁴. This suggests that other cell types might be prone to non-physiological relief of feed-back inhibition between mTORC1 and mTORC2, as well. Moreover, considering its many and versatile functions in almost every aspect of cellular life, aberrant mTOR signalling can be found at the heart of tumorigenesis in many other neoplasms and upregulation of the PI3K/mTORC2/Akt pathway is commonly observed in malignancies²²⁹. Hence, inhibition of this pathway has been subject of drug development²³⁰. In other cases hyperphosphorylation of S6 was found to correlate with disease in cases of malignant melanoma, clear cell renal carcinoma, and head and neck carcinoma, indicative of mTORC1 axis hyperactivation²³¹. However, inhibition of mTORC1 with Rapamycin-like compounds (rapalogues) yielded only moderate success²³². Regarding the data of this study, this effect can in all likelihood be explained by a one-sided attenuation of mTOR signalling that eventually leads to hyperactivation of the PI3K/mTORC2/Akt axis. Consequently, cell survival is promoted, probably causing more harm than curtailing the original cancerous deregulation. Thus, to circumvent the influence of feedback inhibition relief, recently developed inhibitors that target catalytic domains of both mTOR complexes or of mTOR and PI3K simultaneously were tested to be more promising therapeutic compounds²³³⁻²³⁴. Furthermore, the results of the present data suggest that inhibition of the proteasome might also be a promising option for treatment of cancer patients presenting with hyperactivated PI3K/mTORC2/Akt signalling. Indeed, clinical data show that although Bortezomib treatment was most successfully applied in hematologic diseases, it was also partially beneficial for patients with solid tumors²³⁵. As such, future investigations might be able to correlate this responsiveness to a deregulation of Fbxo9-Tel2/Tti1-mTOR axis and thus provide a rationale for choice of medication.

The identification of targeted strategies to treat cancer patients has become a central goal over the last decades¹²⁵. Because cancer cells originate from intact normal cells, any treatment targeting cellular components or pathways of malignant cells can greatly disturb intact and balanced biological mechanisms within the healthy cells, as well. Clinically, this situation manifests in many adverse effects observed upon drug administration. In the case of MM, for example, treatment with proteasome inhibitor Bortezomib, can be associated with side-effects such as hypotension, shingles, fatigue, nausea and vomiting, and in most cases, peripheral neuropathy and gastrointestinal symptoms^{235,236}. As such prediction of the most promising drug treatment based on distinct molecular biomarkers is an important means to increase anti-tumor effectivity and minimise suffering for patients. This study suggests that elevated Fbxo9 levels are a reliable biomarker for better responsiveness and outcome upon administration of Bortezomib (s. Figure 55), which can be assessed from bone marrow aspirates. Of note, the FBP Fbxw7 α favours MM survival via the NF- κ B pathway in a dose-independent manner²¹⁷ and thus its expression has no prognostic value. In contrast, elevated levels of Deptor were found to favour survival in MM cells¹¹⁹. However, this rather represents a contra-indicator for proteasome inhibition, because Deptor is a target for degradation by the UPS¹⁸³⁻¹⁸⁵. Thus, Fbxo9 levels might emerge as the first UPS-related biomarker recommending proteasome inhibitor treatment in MM.

Another novel finding of the present study, which might be useful as a future predictive marker is that subcellular localisation of CK2 directly correlates with its activity towards Tel2/Tti1. Considering that stability of Tel2/Tti1 is greatly dependent on CK2 kinase activity in certain MM cell lines (s. Figure 59), such cells might conceivably also display increased cytoplasmic localisation of CK2. In this regard, if CK2 localisation can be specifically detected in MM cells of patient samples and further correlated to effectiveness of proteasome inhibitor treatment, another clinically relevant biomarker would be defined. Also, the abundance of CK2 might be a useful biomarker, because abnormally high levels of CK2, which were shown to promote asymmetric deregulation of mTOR signalling in this study, were reported to be implicated in cancer progression in a broad variety of solid tumors as well as hematologic malignancies²³⁷⁻²³⁸. Considering its growth promoting, proliferative, pro-survival, and anti-apoptotic functions, CK2 activity can provide and maintain an environment that favours cancer progression²³⁹. Consistently, CK2 overexpression is protective against drug-induced apoptosis²⁴⁰, and apoptosis-induction resistant cell lines often display elevated CK2 levels²⁴¹. On a molecular level, the pro-survival function by CK2 was assigned to regulation of several prominent pathways. For example, CK2 is important for the phosphorylation-dependent stabilisation of c-Myc, which was shown to promote lymphomagenesis²⁴². With respect to MM, there is evidence that both elevated protein levels and activity of CK2 implicate attenuated responsiveness to cell death induction, since depletion of CK2 increases the cytotoxic effects of drug treatment on MM cells²⁴³. Interestingly, similarly to the

nutrient independent activation of pro-apoptotic signalling upon CK2 depletion observed in this study (s. Figure 44), stimulation with growth factors could not reverse the phenotype caused by CK2 depletion in these MM cells²⁴³. It is thus conceivable that in the context of MM, deregulation of the Fbxo9-Tel2/Tti1-mTOR axis represents another important cellular pathway that is essentially dependent not only on CK2 activity but also expression levels. In the future, a correlation between CK2 expression and responsiveness to proteasome inhibition in MM remains to be demonstrated, to reliably define CK2 levels as a biomarker.

Further, clinicians and patients might not only profit from a better response prediction based on the suggested novel biomarkers, but this study also provides targets and rationales for development of new treatment strategies. This is of particular interest in MM, since owing to their high genomic instability these tumors are often relapsing and/or become resistant to treatment¹³. Firstly, a putative, novel target structure is CK2. Specific inhibitors of this kinase are already widely available and applicable for cancer treatment²⁴⁴ and could be used to treat MM patients with high Fbxo9 (or CK2) expression, which became refractory to proteasome inhibitors. On the other hand, a general administration in combination with proteasom inhibitors could considerably re-establish apoptosis signalling in MM cells. Of note, also ubiquitylation of p100 by SCF^{Fbxw7 α} is degraon-dependent, and inhibitory drugs directed against the priming kinase could dramatically reduce viability of MM cell lines²¹⁷, indicating that this strategy might also prove to be effective to interfere with CK2 mediated Tel2/Tti1 degradation by SCF^{Fbxo9}. Secondly, directly targeting the deregulated mTOR signalling pathway in parallel to the UPS or as secondary treatment for proteasome inhibitor resistant MM cases, might be beneficial in patients analysed with Fbxo9 overexpression. Considering its hyperactivation in the case of Fbxo9 overexpression, interfering with the PI3K/mTORC2/Akt pathway in combination with UPS inhibition should efficiently induce apoptosis in MM cells. Indeed, in a recent study combining Bortezomib/Dexamethasone treatment with Perifosine, an Akt inhibitory agent has shown good overall response rates of 65% in MM patients that were relapsing from Bortezomib/Dexamethasone treatment²⁴⁵. In line with the finding that inhibition of mTORC1 alone was not sufficient to re-establish the apoptotic phenotype of serum deprived cells (s. Figure 47) studies that have attempted the use of rapalogues for treatment of MM patients were also less successful²⁴⁶, whereas in combination with inhibition of the PI3K/mTORC2/Akt pathway, an enhanced anti-myeloma activity was observed in pre-clinical models²⁴⁷. Obviously, targeting both mTOR complexes may establish more robust responses, and ongoing studies aim to develop more specialised drugs²³³. Already, in MM cell lines an inhibitor of both mTORC1 and mTORC2, pp242, led to synergistic anti-MM effects in combination with Bortezomib²⁴⁷. Thus, the availability of second generation mTOR inhibitors could improve treatment strategies of MM with deregulated Fbxo9-Tel2/Tti1-mTOR signalling.

To further advance therapies, individualised cancer care of patients has long been hypothesised to replace the common systemic and unspecific chemotherapeutic treatment strategies¹²⁵. However, despite promising better success in both cancer remission and patient well-being, the search for reliable, potent and specific target structures associated with a malignancy has not yet been completed. A well-established example is the personalised care for breast cancer patients. Only those patients displaying high levels of the Her2/neu oncogene, will respond to administration of the specific Her2/neu inhibitor and can be treated accordingly²⁴⁸. With respect to MM, such treatment options are not yet available. As such, the MM-specific oncogene Fbxo9 might emerge as a promising candidate for individualised treatment, because manipulating Fbxo9 levels to low abundance, strongly reduced viability selectively in MM cell lines with high Fbxo9 expression (s. Figure 60). This indicates two promising prerequisites for future drug development: targeting Fbxo9 on its own is potent enough to induce cytotoxicity; albeit the effectiveness is specifically restricted to cells with abnormally high expression levels. As a first step towards personalised medicine in MM, this study can define a subpopulation of MM patients with remarkably high Fbxo9 expression levels, suggesting that almost a third of MM patients might benefit from such a novel drug design. Future clinical and pharmacologic studies will have to investigate whether compounds specifically inhibiting Fbxo9 and hence progression of MM can be found.

In the future, it will be interesting to follow, if the novel underlying mechanism of genesis and development of multiple myeloma delineated in this study will indeed prove to provide valuable information to clinicians for improved treatment of patients.

6.3 Summary

High clinical response rates have established proteasome inhibitors in the first line therapy of MM. Therefore, the identification of ubiquitylation pathways whose MM specific deregulation favours survival is critical to gain further insights into the disease. As such, the present study defines Fbxo9 and CK2 mediated degradation of Tel2/Tti1 as a mechanism for regulating mTOR signalling. By identifying Fbxo9 overexpression as a means to selectively and constitutively activate the PI3K/mTORC2/Akt axis in MM, this study links a specifically deregulated UPS-dependent event to pathogenesis of MM that may serve to predict response to proteasomal inhibitors and provide novel target structures (Fbxo9, CK2) in MM with high expression of Fbxo9.

7 Literature

1. Bassermann, F. & Pagano, M. Dissecting the role of ubiquitylation in the DNA damage response checkpoint in G2. *Cell death and differentiation* **17**, 78-85 (2010).
2. Palumbo, A. & Anderson, K. Multiple myeloma. *The New England journal of medicine* **364**, 1046-1060 (2011).
3. Harousseau, J.L., Dreyling, M. & Group, E.G.W. Multiple myeloma: ESMO clinical recommendations for diagnosis, treatment and follow-up. *Annals of oncology : official journal of the European Society for Medical Oncology / ESMO* **20 Suppl 4**, 97-99 (2009).
4. Klein, B., Zhang, X., Lu, Z. & Bataille, R. Interleukin-6 in human multiple myeloma. *Blood* **85**, 863-872 (1995).
5. Schmidlin, H., Diehl, S. & Blom, B. New insights into the regulation of human B-cell differentiation. *Trends in immunology* **30**, 277-285 (2009).
6. O'Connor, B., Gleeson, M., Noelle, R. & Erickson, L. The rise and fall of long-lived humoral immunity: terminal differentiation of plasma cells in health and disease. *Immunological reviews* **194**, 61-76 (2003).
7. Manier, S., Sacco, A., Leleu, X., Ghobrial, I. & Roccaro, A. Bone marrow microenvironment in multiple myeloma progression. *Journal of biomedicine & biotechnology* **2012**, 157496 (2012).
8. Sirohi, B. & Powles, R. Multiple myeloma. *Lancet* **363**, 875-887 (2004).
9. Kyle, R. & Rajkumar, S. Multiple myeloma. (2004).
10. Fonseca, R. *et al.* Genetics and cytogenetics of multiple myeloma: a workshop report. *Cancer research* **64**, 1546-1558 (2004).
11. Gadó, K., Silva, S., Pálóczi, K., Domján, G. & Falus, A. Mouse plasmacytoma: an experimental model of human multiple myeloma. *Haematologica* **86**, 227-236 (2001).
12. Raab, M., Podar, K., Breitkreutz, I., Richardson, P. & Anderson, K. Multiple myeloma. *Lancet* **374**, 324-339 (2009).
13. Dimopoulos, M. & Terpos, E. Multiple myeloma. *Annals of oncology : official journal of the European Society for Medical Oncology / ESMO* **21 Suppl 7**, 50 (2010).
14. Kumar, S. *et al.* Expression of VEGF and its receptors by myeloma cells. *Leukemia : official journal of the Leukemia Society of America, Leukemia Research Fund, U.K* **17**, 2025-2031 (2003).
15. Giuliani, N., Storti, P., Bolzoni, M., Palma, B. & Bonomini, S. Angiogenesis and multiple myeloma. *Cancer microenvironment : official journal of the International Cancer Microenvironment Society* **4**, 325-337 (2011).
16. Durie, B. *et al.* Myeloma management guidelines: a consensus report from the Scientific Advisors of the International Myeloma Foundation. *The hematology journal : the official journal of the European Haematology Association / EHA* **4**, 379-398 (2003).
17. Giuliani, N., Rizzoli, V. & Roodman, G. Multiple myeloma bone disease: Pathophysiology of osteoblast inhibition. *Blood* **108**, 3992-3996 (2006).
18. Dimopoulos, M., Kastritis, E., Rosinol, L., Bladé, J. & Ludwig, H. Pathogenesis and treatment of renal failure in multiple myeloma. *Leukemia : official journal of the Leukemia Society of America, Leukemia Research Fund, U.K* **22**, 1485-1493 (2008).
19. Greipp, P. *et al.* International staging system for multiple myeloma. *Journal of clinical oncology : official journal of the American Society of Clinical Oncology* **23**, 3412-3420 (2005).
20. Kyle, R. & Rajkumar, S. Criteria for diagnosis, staging, risk stratification and response assessment of multiple myeloma. *Leukemia : official journal of the Leukemia Society of America, Leukemia Research Fund, U.K* **23**, 3-9 (2009).
21. Kyle, R. & Rajkumar, S. Monoclonal gammopathy of undetermined significance. *British journal of haematology* **134**, 573-589 (2006).
22. Kuehl, W. & Bergsagel, P. Multiple myeloma: evolving genetic events and host interactions. *Nature reviews. Cancer* **2**, 175-187 (2002).

23. Anderson, K. & Carrasco, R. Pathogenesis of myeloma. *Annual review of pathology* **6**, 249-274 (2011).
24. Mele, G., Pinna, S., Melpignano, A. & Quarta, G. Retrospective case series of three patients with plasma cell leukemia treated with bortezomib-based regimens. *Clinical therapeutics* **32**, 915-919 (2010).
25. Kumar, S. *et al.* Improved survival in multiple myeloma and the impact of novel therapies. *Blood* **111**, 2516-2520 (2008).
26. Kelly, K., Rowe, J., Padmanabhan, S., Nawrocki, S. & Carew, J. Mammalian target of rapamycin as a target in hematological malignancies. *Targeted oncology* **6**, 53-61 (2011).
27. Shah, J. & Orłowski, R. Proteasome inhibitors in the treatment of multiple myeloma. *Leukemia : official journal of the Leukemia Society of America, Leukemia Research Fund, U.K* **23**, 1964-1979 (2009).
28. Quach, H. *et al.* Mechanism of action of immunomodulatory drugs (IMiDS) in multiple myeloma. *Leukemia : official journal of the Leukemia Society of America, Leukemia Research Fund, U.K* **24**, 22-32 (2010).
29. Morgan, G. *et al.* Thalidomide combinations improve response rates; results from the MRC IX study. *BLOOD-NEW YORK-* **110**, 3593 (2007).
30. Mitsiades, C., Hayden, P., Anderson, K. & Richardson, P. From the bench to the bedside: emerging new treatments in multiple myeloma. *Best practice & research. Clinical haematology* **20**, 797-816 (2007).
31. Giuliani, N. *et al.* The proteasome inhibitor bortezomib affects osteoblast differentiation in vitro and in vivo in multiple myeloma patients. *Blood* **110**, 334-338 (2007).
32. Stewart, A. Novel therapies for relapsed myeloma. *Hematology / the Education Program of the American Society of Hematology. American Society of Hematology. Education Program*, 578-586 (2009).
33. Carrasco, D. *et al.* High-resolution genomic profiles define distinct clinico-pathogenetic subgroups of multiple myeloma patients. *Cancer cell* **9**, 313-325 (2006).
34. Scanlan, M.J. *et al.* Antigens recognized by autologous antibody in patients with renal-cell carcinoma. *Int J Cancer* **83**, 456-464 (1999).
35. Katayama, S., Kitamura, K., Lehmann, A., Nikaido, O. & Toda, T. Fission yeast F-box protein Pof3 is required for genome integrity and telomere function. *Mol.Biol.Cell* **13**, 211-224 (2002).
36. Calderón-Villalobos, L., Nill, C., Marrocco, K., Kretsch, T. & Schwechheimer, C. The evolutionarily conserved Arabidopsis thaliana F-box protein AtFBP7 is required for efficient translation during temperature stress. *Gene* **392**, 106-116 (2007).
37. Glotzer, M., Murray, A. & Kirschner, M. Cyclin is degraded by the ubiquitin pathway. *Nature* **349**, 132-140 (1991).
38. Hershko, A., Ganoth, D., Pehrson, J., Palazzo, R. & Cohen, L. Methylated ubiquitin inhibits cyclin degradation in clam embryo extracts. *The Journal of biological chemistry* **266**, 16376-16385 (1991).
39. Kouranti, I. & Peyroche, A. Protein degradation in DNA damage response. *Seminars in cell & developmental biology* (2012).
40. Motegi, A., Murakawa, Y. & Takeda, S. The vital link between the ubiquitin-proteasome pathway and DNA repair: impact on cancer therapy. *Cancer letters* **283**, 1-10 (2009).
41. Rock, K. & Goldberg, A. Degradation of cell proteins and the generation of MHC class I-presented peptides. *Annual review of immunology* **17**, 739-818 (1999).
42. Heo, J.-M. & Rutter, J. Ubiquitin-dependent mitochondrial protein degradation. *The international journal of biochemistry & cell biology* **43**, 1422-1428 (2011).
43. Liu, C.-H., Goldberg, A. & Qiu, X.-B. New insights into the role of the ubiquitin-proteasome pathway in the regulation of apoptosis. *Chang Gung medical journal* **30**, 469-548 (2007).
44. Löw, P. The role of ubiquitin-proteasome system in ageing. *General and comparative endocrinology* **172**, 39-82 (2011).

45. Spataro, V., Norbury, C. & Harris, A. The ubiquitin-proteasome pathway in cancer. *British journal of cancer* **77**, 448-503 (1998).
46. Hegde, A. & Upadhyaya, S. Role of ubiquitin-proteasome-mediated proteolysis in nervous system disease. *Biochimica et biophysica acta* **1809**, 128-168 (2011).
47. Finkbeiner, S. & Mitra, S. The ubiquitin-proteasome pathway in Huntington's disease. *TheScientificWorldJournal* **8**, 421-454 (2008).
48. Powell, S. & Divald, A. The ubiquitin-proteasome system in myocardial ischaemia and preconditioning. *Cardiovascular research* **85**, 303-314 (2010).
49. Tisdale, M. The ubiquitin-proteasome pathway as a therapeutic target for muscle wasting. *The journal of supportive oncology* **3**, 209-226 (2005).
50. Fukasawa, H., Fujigaki, Y., Yamamoto, T., Hishida, A. & Kitagawa, M. Protein degradation by the ubiquitin-proteasome pathway and organ fibrosis. *Current medicinal chemistry* **19**, 893-1793 (2012).
51. Fukasawa, H. The role of the ubiquitin-proteasome system in kidney diseases. *Clinical and experimental nephrology* (2012).
52. Wing, S. The UPS in diabetes and obesity. *BMC biochemistry* **9 Suppl 1** (2008).
53. http://www.nobelprize.org/nobel_prizes/chemistry/laureates/2004/.
54. Goldstein, G. *et al.* Isolation of a polypeptide that has lymphocyte-differentiating properties and is probably represented universally in living cells. *Proceedings of the National Academy of Sciences of the United States of America* **72**, 11-16 (1975).
55. Schlesinger, D., Goldstein, G. & Niall, H. The complete amino acid sequence of ubiquitin, an adenylate cyclase stimulating polypeptide probably universal in living cells. *Biochemistry* **14**, 2214-2222 (1975).
56. Wilkinson, K., Urban, M. & Haas, A. Ubiquitin is the ATP-dependent proteolysis factor I of rabbit reticulocytes. *The Journal of biological chemistry* **255**, 7529-7561 (1980).
57. Ciechanover, A. & Ben-Saadon, R. N-terminal ubiquitination: more protein substrates join in. *Trends in cell biology* **14**, 103-109 (2004).
58. Chen, Z. & Sun, L. Nonproteolytic functions of ubiquitin in cell signaling. *Molecular cell* **33**, 275-361 (2009).
59. Ikeda, F. & Dikic, I. Atypical ubiquitin chains: new molecular signals. 'Protein Modifications: Beyond the Usual Suspects' review series. *EMBO reports* **9**, 536-578 (2008).
60. Hicke, L. & Dunn, R. Regulation of membrane protein transport by ubiquitin and ubiquitin-binding proteins. *Annual review of cell and developmental biology* **19**, 141-213 (2003).
61. Bremm, A. & Komander, D. Emerging roles for Lys11-linked polyubiquitin in cellular regulation. *Trends in biochemical sciences* **36**, 355-418 (2011).
62. Komander, D. & Rape, M. The ubiquitin code. *Annual review of biochemistry* **81**, 203-232 (2012).
63. Deng, L. *et al.* Activation of the I κ B kinase complex by TRAF6 requires a dimeric ubiquitin-conjugating enzyme complex and a unique polyubiquitin chain. *Cell* **103**, 351-412 (2000).
64. Song, L. & Rape, M. Regulated degradation of spindle assembly factors by the anaphase-promoting complex. *Molecular cell* **38**, 369-451 (2010).
65. Chau, V. *et al.* A multiubiquitin chain is confined to specific lysine in a targeted short-lived protein. *Science (New York, N.Y.)* **243**, 1576-1659 (1989).
66. Thrower, J., Hoffman, L., Rechsteiner, M. & Pickart, C. Recognition of the polyubiquitin proteolytic signal. *The EMBO journal* **19**, 94-196 (2000).
67. Pickart, C. & Fushman, D. Polyubiquitin chains: polymeric protein signals. *Current opinion in chemical biology* **8**, 610-616 (2004).
68. Wójcik, C. & DeMartino, G. Intracellular localization of proteasomes. *The international journal of biochemistry & cell biology* **35**, 579-668 (2003).
69. Coux, O., Tanaka, K. & Goldberg, A. Structure and functions of the 20S and 26S proteasomes. *Annual review of biochemistry* **65**, 801-848 (1996).

70. Xie, Y. Structure, assembly and homeostatic regulation of the 26S proteasome. *Journal of molecular cell biology* **2**, 308-325 (2010).
71. Gallastegui, N. & Groll, M. The 26S proteasome: assembly and function of a destructive machine. *Trends in biochemical sciences* **35**, 634-676 (2010).
72. Kisselev, A., Songyang, Z. & Goldberg, A. Why does threonine, and not serine, function as the active site nucleophile in proteasomes? *The Journal of biological chemistry* **275**, 14831-14838 (2000).
73. Nandi, D., Tahiliani, P., Kumar, A. & Chandu, D. The ubiquitin-proteasome system. *Journal of biosciences* **31**, 137-192 (2006).
74. Zwickl, P. *et al.* Primary structure of the Thermoplasma proteasome and its implications for the structure, function, and evolution of the multicatalytic proteinase. *Biochemistry* **31**, 964-1036 (1992).
75. Groll, M. *et al.* Structure of 20S proteasome from yeast at 2.4 Å resolution. *Nature* **386**, 463-534 (1997).
76. Finley, D. Recognition and processing of ubiquitin-protein conjugates by the proteasome. *Annual review of biochemistry* **78**, 477-990 (2009).
77. Rubin, D., Glickman, M., Larsen, C., Dhruvakumar, S. & Finley, D. Active site mutants in the six regulatory particle ATPases reveal multiple roles for ATP in the proteasome. *The EMBO journal* **17**, 4909-4928 (1998).
78. Liu, C.-W. *et al.* ATP binding and ATP hydrolysis play distinct roles in the function of 26S proteasome. *Molecular cell* **24**, 39-89 (2006).
79. Yao, T. & Cohen, R. A cryptic protease couples deubiquitination and degradation by the proteasome. *Nature* **419**, 403-410 (2002).
80. Hershko, A., Heller, H., Elias, S. & Ciechanover, A. Components of ubiquitin-protein ligase system. Resolution, affinity purification, and role in protein breakdown. *The Journal of biological chemistry* **258**, 8206-8214 (1983).
81. Weissman, A. Themes and variations on ubiquitylation. *Nature reviews. Molecular cell biology* **2**, 169-247 (2001).
82. Ciechanover, A. The ubiquitin-proteasome proteolytic pathway. *Cell* **79**, 13-34 (1994).
83. de Bie, P. & Ciechanover, A. Ubiquitination of E3 ligases: self-regulation of the ubiquitin system via proteolytic and non-proteolytic mechanisms. *Cell death and differentiation* **18**, 1393-1795 (2011).
84. Hershko, A. & Ciechanover, A. The ubiquitin system. *Annual review of biochemistry* **67**, 425-504 (1998).
85. Hoppe, T. Multiubiquitylation by E4 enzymes: 'one size' doesn't fit all. *Trends in biochemical sciences* **30**, 183-187 (2005).
86. Willems, A., Schwab, M. & Tyers, M. A hitchhiker's guide to the cullin ubiquitin ligases: SCF and its kin. *Biochimica et biophysica acta* **1695**, 133-170 (2004).
87. Jackson, P. *et al.* The lore of the RINGs: substrate recognition and catalysis by ubiquitin ligases. *Trends in cell biology* **10**, 429-439 (2000).
88. Varshavsky, A. Naming a targeting signal. *Cell* **64**, 13-18 (1991).
89. Carrano, A., Eytan, E., Hershko, A. & Pagano, M. SKP2 is required for ubiquitin-mediated degradation of the CDK inhibitor p27. *Nature cell biology* **1**, 193-202 (1999).
90. Peters, J.-M. The anaphase promoting complex/cyclosome: a machine designed to destroy. *Nature reviews. Molecular cell biology* **7**, 644-656 (2006).
91. Duda, D. *et al.* Structural regulation of cullin-RING ubiquitin ligase complexes. *Current opinion in structural biology* **21**, 257-264 (2011).
92. Weissman, A., Shabek, N. & Ciechanover, A. The predator becomes the prey: regulating the ubiquitin system by ubiquitylation and degradation. *Nature reviews. Molecular cell biology* **12**, 605-620 (2011).
93. Deshaies, R. & Joazeiro, C. RING domain E3 ubiquitin ligases. *Annual review of biochemistry* **78**, 399-434 (2009).

94. Verma, R. *et al.* Phosphorylation of Sic1p by G1 Cdk required for its degradation and entry into S phase. *Science (New York, N.Y.)* **278**, 455-460 (1997).
95. Zimmerman, E., Schulman, B. & Zheng, N. Structural assembly of cullin-RING ubiquitin ligase complexes. *Current opinion in structural biology* **20**, 714-721 (2010).
96. Bai, C. *et al.* SKP1 connects cell cycle regulators to the ubiquitin proteolysis machinery through a novel motif, the F-box. *Cell* **86**, 263-274 (1996).
97. Skaar, J., D'Angiolella, V., Pagan, J. & Pagano, M. SnapShot: F Box Proteins II. *Cell* **137** (2009).
98. Frescas, D. & Pagano, M. Deregulated proteolysis by the F-box proteins SKP2 and beta-TrCP: tipping the scales of cancer. *Nature reviews. Cancer* **8**, 438-449 (2008).
99. Inuzuka, H. *et al.* SCF(FBW7) regulates cellular apoptosis by targeting MCL1 for ubiquitylation and destruction. *Nature* **471**, 104-109 (2011).
100. Koepp, D. *et al.* Phosphorylation-dependent ubiquitination of cyclin E by the SCFFbw7 ubiquitin ligase. *Science (New York, N.Y.)* **294**, 173-177 (2001).
101. Song, L. & Rape, M. Reverse the curse--the role of deubiquitination in cell cycle control. *Current opinion in cell biology* **20**, 156-163 (2008).
102. Nijman, S. *et al.* A genomic and functional inventory of deubiquitinating enzymes. *Cell* **123**, 773-786 (2005).
103. Larsen, C., Krantz, B. & Wilkinson, K. Substrate specificity of deubiquitinating enzymes: ubiquitin C-terminal hydrolases. *Biochemistry* **37**, 3358-3368 (1998).
104. Gallery, M. *et al.* The JAMM motif of human deubiquitinase Poh1 is essential for cell viability. *Molecular cancer therapeutics* **6**, 262-268 (2007).
105. Popov, N. *et al.* The ubiquitin-specific protease USP28 is required for MYC stability. *Nature cell biology* **9**, 765-774 (2007).
106. Komander, D., Clague, M. & Urbé, S. Breaking the chains: structure and function of the deubiquitinases. *Nature reviews. Molecular cell biology* **10**, 550-563 (2009).
107. Reyes-Turcu, F., Ventii, K. & Wilkinson, K. Regulation and cellular roles of ubiquitin-specific deubiquitinating enzymes. *Annual review of biochemistry* **78**, 363-397 (2009).
108. Zinzalla, V., Stracka, D., Oppliger, W. & Hall, M. Activation of mTORC2 by association with the ribosome. *Cell* **144**, 757-768 (2011).
109. Ma, X. & Blenis, J. Molecular mechanisms of mTOR-mediated translational control. *Nature reviews. Molecular cell biology* **10**, 307-318 (2009).
110. Laplante, M. & Sabatini, D. mTOR signaling in growth control and disease. *Cell* **149**, 274-293 (2012).
111. Heitman, J., Movva, N. & Hall, M. Targets for cell cycle arrest by the immunosuppressant rapamycin in yeast. *Science (New York, N.Y.)* **253**, 905-909 (1991).
112. Cutler, N., Heitman, J. & Cardenas, M. TOR kinase homologs function in a signal transduction pathway that is conserved from yeast to mammals. *Molecular and cellular endocrinology* **155**, 135-142 (1999).
113. Wullschleger, S., Loewith, R. & Hall, M. TOR signaling in growth and metabolism. *Cell* **124**, 471-484 (2006).
114. Chang, M. & Lingner, J. Cell signaling. Tel2 finally tells one story. *Science (New York, N.Y.)* **320**, 60-61 (2008).
115. Bosotti, R., Isacchi, A. & Sonnhammer, E. FAT: a novel domain in PIK-related kinases. *Trends in biochemical sciences* **25**, 225-227 (2000).
116. Brown, E. *et al.* A mammalian protein targeted by G1-arresting rapamycin-receptor complex. *Nature* **369**, 756-758 (1994).
117. Sabatini, D., Erdjument-Bromage, H., Lui, M., Tempst, P. & Snyder, S. RAFT1: a mammalian protein that binds to FKBP12 in a rapamycin-dependent fashion and is homologous to yeast TORs. *Cell* **78**, 35-43 (1994).
118. Kim, D.-H. *et al.* GbetaL, a positive regulator of the rapamycin-sensitive pathway required for the nutrient-sensitive interaction between raptor and mTOR. *Molecular cell* **11**, 895-904 (2003).

119. Peterson, T. *et al.* DEPTOR is an mTOR inhibitor frequently overexpressed in multiple myeloma cells and required for their survival. *Cell* **137**, 873-886 (2009).
120. Kaizuka, T. *et al.* Tti1 and Tel2 are critical factors in mammalian target of rapamycin complex assembly. *The Journal of biological chemistry* **285**, 20109-20116 (2010).
121. Kim, D.-H. *et al.* mTOR interacts with raptor to form a nutrient-sensitive complex that signals to the cell growth machinery. *Cell* **110**, 163-175 (2002).
122. Hara, K. *et al.* Raptor, a binding partner of target of rapamycin (TOR), mediates TOR action. *Cell* **110**, 177-189 (2002).
123. Sancak, Y. *et al.* PRAS40 is an insulin-regulated inhibitor of the mTORC1 protein kinase. *Molecular cell* **25**, 903-915 (2007).
124. Jacinto, E. *et al.* Mammalian TOR complex 2 controls the actin cytoskeleton and is rapamycin insensitive. *Nature cell biology* **6**, 1122-1128 (2004).
125. Abou-Jawde, R., Choueiri, T., Alemany, C. & Mekhail, T. An overview of targeted treatments in cancer. *Clinical therapeutics* **25**, 2121-2137 (2003).
126. Ma, L., Chen, Z., Erdjument-Bromage, H., Tempst, P. & Pandolfi, P. Phosphorylation and functional inactivation of TSC2 by Erk implications for tuberous sclerosis and cancer pathogenesis. *Cell* **121**, 179-193 (2005).
127. Lee, D.-F. *et al.* IKK beta suppression of TSC1 links inflammation and tumor angiogenesis via the mTOR pathway. *Cell* **130**, 440-455 (2007).
128. Manning, B. & Cantley, L. Rheb fills a GAP between TSC and TOR. *Trends in biochemical sciences* **28**, 573-576 (2003).
129. Düvel, K. *et al.* Activation of a metabolic gene regulatory network downstream of mTOR complex 1. *Molecular cell* **39**, 171-183 (2010).
130. Laplante, M. & Sabatini, D. An emerging role of mTOR in lipid biosynthesis. *Current biology : CB* **19**, 52 (2009).
131. Mayer, C., Zhao, J., Yuan, X. & Grummt, I. mTOR-dependent activation of the transcription factor TIF-IA links rRNA synthesis to nutrient availability. *Genes & development* **18**, 423-434 (2004).
132. Shor, B. *et al.* Requirement of the mTOR kinase for the regulation of Maf1 phosphorylation and control of RNA polymerase III-dependent transcription in cancer cells. *The Journal of biological chemistry* **285**, 15380-15392 (2010).
133. Settembre, C. *et al.* A lysosome-to-nucleus signalling mechanism senses and regulates the lysosome via mTOR and TFEB. *The EMBO journal* **31**, 1095-1108 (2012).
134. Schalm, S. & Blenis, J. Identification of a conserved motif required for mTOR signaling. *Current biology : CB* **12**, 632-639 (2002).
135. Hay, N. & Sonenberg, N. Upstream and downstream of mTOR. *Genes & development* **18**, 1926-1945 (2004).
136. Dorrello, N. *et al.* S6K1- and betaTRCP-mediated degradation of PDCD4 promotes protein translation and cell growth. *Science (New York, N.Y.)* **314**, 467-538 (2006).
137. Sarbassov, D. *et al.* Rictor, a novel binding partner of mTOR, defines a rapamycin-insensitive and raptor-independent pathway that regulates the cytoskeleton. *Current biology : CB* **14**, 1296-1302 (2004).
138. Jacinto, E. *et al.* SIN1/MIP1 maintains rictor-mTOR complex integrity and regulates Akt phosphorylation and substrate specificity. *Cell* (2006).
139. Pearce, L. *et al.* Identification of Protor as a novel Rictor-binding component of mTOR complex-2. *The Biochemical journal* **405**, 513-522 (2007).
140. Sarbassov, D. *et al.* Prolonged rapamycin treatment inhibits mTORC2 assembly and Akt/PKB. *Molecular cell* **22**, 159-168 (2006).
141. Pearce, L., Komander, D. & Alessi, D. The nuts and bolts of AGC protein kinases. *Nature reviews. Molecular cell biology* **11**, 9-22 (2010).
142. García-Martínez, J. & Alessi, D. mTOR complex 2 (mTORC2) controls hydrophobic motif phosphorylation and activation of serum- and glucocorticoid-induced protein kinase 1 (SGK1). *The Biochemical journal* **416**, 375-385 (2008).

143. Lawlor, M. & Alessi, D. PKB/Akt: a key mediator of cell proliferation, survival and insulin responses? *Journal of cell science* **114**, 2903-2910 (2001).
144. Sarbassov, D., Guertin, D., Ali, S. & Sabatini, D. Phosphorylation and regulation of Akt/PKB by the rictor-mTOR complex. *Science (New York, N.Y.)* **307**, 1098-1101 (2005).
145. Datta, S. *et al.* Akt phosphorylation of BAD couples survival signals to the cell-intrinsic death machinery. *Cell* **91**, 231-241 (1997).
146. Harrington, L. *et al.* The TSC1-2 tumor suppressor controls insulin-PI3K signaling via regulation of IRS proteins. *The Journal of cell biology* **166**, 213-223 (2004).
147. Tzatsos, A. & Kandror, K. Nutrients suppress phosphatidylinositol 3-kinase/Akt signaling via raptor-dependent mTOR-mediated insulin receptor substrate 1 phosphorylation. *Molecular and cellular biology* **26**, 63-76 (2006).
148. Yu, Y. *et al.* Phosphoproteomic analysis identifies Grb10 as an mTORC1 substrate that negatively regulates insulin signaling. *Science (New York, N.Y.)* **332**, 1322-1326 (2011).
149. Hsu, P. *et al.* The mTOR-regulated phosphoproteome reveals a mechanism of mTORC1-mediated inhibition of growth factor signaling. *Science (New York, N.Y.)* **332**, 1317-1322 (2011).
150. Takai, H., Wang, R., Takai, K., Yang, H. & de Lange, T. Tel2 regulates the stability of PI3K-related protein kinases. *Cell* **131**, 1248-1307 (2007).
151. Takai, H., Wang, R., Takai, K., Yang, H. & de Lange, T. Tel2 regulates the stability of PI3K-related protein kinases. *Cell* **131**, 1248-1259 (2007).
152. Hurov, K., Cotta-Ramusino, C. & Elledge, S. A genetic screen identifies the Triple T complex required for DNA damage signaling and ATM and ATR stability. *Genes & development* **24**, 1939-1950 (2010).
153. Takai, H., Xie, Y., de Lange, T. & Pavletich, N. Tel2 structure and function in the Hsp90-dependent maturation of mTOR and ATR complexes. *Genes & development* **24**, 2019-2030 (2010).
154. Horejsí, Z. *et al.* CK2 phospho-dependent binding of R2TP complex to TEL2 is essential for mTOR and SMG1 stability. *Molecular cell* **39**, 839-850 (2010).
155. Boulton, S. Differential regulation of the PIKK kinase family by Tel2. *Cell cycle (Georgetown, Tex.)* **7**, 3617 (2008).
156. Kaizuka, T. *et al.* Tti1 and Tel2 are critical factors in mammalian target of rapamycin complex assembly. *The Journal of biological chemistry* **285**, 20109-20125 (2010).
157. Gloeckner, C., Boldt, K., Schumacher, A., Roepman, R. & Ueffing, M. A novel tandem affinity purification strategy for the efficient isolation and characterisation of native protein complexes. *Proteomics* **7**, 4228-4262 (2007).
158. <http://www.quantprime.de/>.
159. <http://rsbweb.nih.gov/ij/ImageJ>.
160. Lowry, O., Rosebrough, N., Farr, A. & Randall, R. Protein measurement with the Folin phenol reagent. *The Journal of biological chemistry* **193**, 265-340 (1951).
161. Gloeckner, C., Boldt, K., Schumacher, A. & Ueffing, M. Tandem affinity purification of protein complexes from mammalian cells by the Strep/FLAG (SF)-TAP tag. *Methods in molecular biology (Clifton, N.J.)* **564**, 359-431 (2009).
162. Becker, K.F. *et al.* Quantitative protein analysis from formalin-fixed tissues: implications for translational clinical research and nanoscale molecular diagnosis. *J Pathol* **211**, 370-378 (2007).
163. Wolff, C., Schott, C., Malinowsky, K., Berg, D. & Becker, K.F. Producing reverse phase protein microarrays from formalin-fixed tissues. *Methods Mol Biol* **785**, 123-140 (2011).
164. http://embnet.vital-it.ch/software/COILS_form.html.
165. <http://blast.ncbi.nlm.nih.gov/Blast.cgi>.
166. Meredith, M. Rat hepatocytes prepared without collagenase: prolonged retention of differentiated characteristics in culture. *Cell biology and toxicology* **4**, 405-425 (1988).

167. Felgner, P. *et al.* Lipofection: a highly efficient, lipid-mediated DNA-transfection procedure. *Proceedings of the National Academy of Sciences of the United States of America* **84**, 7413-7420 (1987).
168. Davis, H., Rosinski, M., Morgan, J. & Yarmush, M. Charged polymers modulate retrovirus transduction via membrane charge neutralization and virus aggregation. *Biophysical journal* **86**, 1234-1276 (2004).
169. Bassermann, F. *et al.* NIPA defines an SCF-type mammalian E3 ligase that regulates mitotic entry. *Cell* **122**, 45-102 (2005).
170. www.ncbi.nlm.nih.gov/geo/.
171. www.oncomine.org.
172. Liu, E., Knutzen, C., Krauss, S., Schweiger, S. & Chiang, G. Control of mTORC1 signaling by the Opitz syndrome protein MID1. *Proceedings of the National Academy of Sciences of the United States of America* **108**, 8680-8685 (2011).
173. Musgrove, E., Caldon, C., Barraclough, J., Stone, A. & Sutherland, R. Cyclin D as a therapeutic target in cancer. *Nature reviews. Cancer* **11**, 558-572 (2011).
174. Cardozo, T. & Pagano, M. The SCF ubiquitin ligase: insights into a molecular machine. *Nat Rev Mol Cell Biol* **5**, 739-751 (2004).
175. Olsen, B., Guerra, B., Niefind, K. & Issinger, O.-G. Structural basis of the constitutive activity of protein kinase CK2. *Methods in enzymology* **484**, 515-529 (2010).
176. Rhodes, D. *et al.* ONCOMINE: a cancer microarray database and integrated data-mining platform. *Neoplasia (New York, N.Y.)* **6**, 1-6 (2004).
177. Mattioli, M. *et al.* Gene expression profiling of plasma cell dyscrasias reveals molecular patterns associated with distinct IGH translocations in multiple myeloma. *Oncogene* **24**, 2461-2473 (2005).
178. Zhan, F. *et al.* Gene-expression signature of benign monoclonal gammopathy evident in multiple myeloma is linked to good prognosis. *Blood* **109**, 1692-1700 (2007).
179. Mulligan, G. *et al.* Gene expression profiling and correlation with outcome in clinical trials of the proteasome inhibitor bortezomib. *Blood* **109**, 3177-3188 (2007).
180. Silverman, J., Skaar, J. & Pagano, M. SCF ubiquitin ligases in the maintenance of genome stability. *Trends in biochemical sciences* **37**, 66-73 (2012).
181. Hwang, G.-W., Ishida, Y. & Naganuma, A. Identification of F-box proteins that are involved in resistance to methylmercury in *Saccharomyces cerevisiae*. *FEBS letters* **580**, 6813-6818 (2006).
182. Robaglia, C., Thomas, M. & Meyer, C. Sensing nutrient and energy status by SnRK1 and TOR kinases. *Current opinion in plant biology* **15**, 301-307 (2012).
183. Duan, S. *et al.* mTOR generates an auto-amplification loop by triggering the β TrCP- and CK1 α -dependent degradation of DEPTOR. *Molecular cell* **44**, 317-324 (2011).
184. Gao, D. *et al.* mTOR drives its own activation via SCF(β TrCP)-dependent degradation of the mTOR inhibitor DEPTOR. *Molecular cell* **44**, 290-303 (2011).
185. Zhao, Y., Xiong, X. & Sun, Y. DEPTOR, an mTOR inhibitor, is a physiological substrate of SCF(β TrCP) E3 ubiquitin ligase and regulates survival and autophagy. *Molecular cell* **44**, 304-316 (2011).
186. Busino, L. *et al.* Degradation of Cdc25A by beta-TrCP during S phase and in response to DNA damage. *Nature* **426**, 87-91 (2003).
187. Jin, J. *et al.* SCFbeta-TRCP links Chk1 signaling to degradation of the Cdc25A protein phosphatase. *Genes & development* **17**, 3062-3074 (2003).
188. Welcker, M. & Clurman, B. Fbw7/hCDC4 dimerization regulates its substrate interactions. *Cell division* **2**, 7 (2007).
189. Wang, X., Taplick, J., Geva, N. & Oren, M. Inhibition of p53 degradation by Mdm2 acetylation. *FEBS letters* **561**, 195-201 (2004).
190. Meggio, F. & Pinna, L. One-thousand-and-one substrates of protein kinase CK2? *FASEB journal : official publication of the Federation of American Societies for Experimental Biology* **17**, 349-368 (2003).

191. Filhol, O. & Cochet, C. Protein kinase CK2 in health and disease: Cellular functions of protein kinase CK2: a dynamic affair. *Cellular and molecular life sciences : CMLS* **66**, 1830-1839 (2009).
192. Thornburg, W. & Lindell, T. Purification of rat liver nuclear protein kinase NII. *The Journal of biological chemistry* **252**, 6660-6665 (1977).
193. Martel, V. *et al.* Visualization and molecular analysis of nuclear import of protein kinase CK2 subunits in living cells. *Molecular and cellular biochemistry* **227**, 81-90 (2001).
194. Filhol, O. *et al.* Live-cell fluorescence imaging reveals the dynamics of protein kinase CK2 individual subunits. *Molecular and cellular biology* **23**, 975-987 (2003).
195. Watanabe, N. *et al.* Cyclin-dependent kinase (CDK) phosphorylation destabilizes somatic Wee1 via multiple pathways. *Proceedings of the National Academy of Sciences of the United States of America* **102**, 11663-11668 (2005).
196. Scaglioni, P. *et al.* A CK2-dependent mechanism for degradation of the PML tumor suppressor. *Cell* **126**, 269-283 (2006).
197. Pinna, L. The raison d'être of constitutively active protein kinases: the lesson of CK2. *Accounts of chemical research* **36**, 378-384 (2003).
198. St-Denis, N. & Litchfield, D. Protein kinase CK2 in health and disease: From birth to death: the role of protein kinase CK2 in the regulation of cell proliferation and survival. *Cellular and molecular life sciences : CMLS* **66**, 1817-1829 (2009).
199. Battistutta, R. & Lolli, G. Structural and functional determinants of protein kinase CK2 α : facts and open questions. *Molecular and cellular biochemistry* **356**, 67-73 (2011).
200. Olsten, M., Weber, J. & Litchfield, D. CK2 interacting proteins: emerging paradigms for CK2 regulation? *Molecular and cellular biochemistry* **274**, 115-124 (2005).
201. Litchfield, D. *et al.* Phosphorylation of the beta subunit of casein kinase II in human A431 cells. Identification of the autophosphorylation site and a site phosphorylated by p34cdc2. *The Journal of biological chemistry* **266**, 20380-20389 (1991).
202. Messenger, M. *et al.* Interactions between protein kinase CK2 and Pin1. Evidence for phosphorylation-dependent interactions. *The Journal of biological chemistry* **277**, 23054-23064 (2002).
203. Bosc, D., Lüscher, B. & Litchfield, D. Expression and regulation of protein kinase CK2 during the cell cycle. *Molecular and cellular biochemistry* **191**, 213-222 (1999).
204. St-Denis, N., Bailey, M., Parker, E., Vilk, G. & Litchfield, D. Localization of phosphorylated CK2 α to the mitotic spindle requires the peptidyl-prolyl isomerase Pin1. *Journal of cell science* **124**, 2341-2348 (2011).
205. Turner, J., Dawson, J. & Sullivan, D. Nuclear export of proteins and drug resistance in cancer. *Biochemical pharmacology* **83**, 1021-1032 (2012).
206. Hayashi, T. *et al.* Rapamycin sensitivity of the *Schizosaccharomyces pombe* tor2 mutant and organization of two highly phosphorylated TOR complexes by specific and common subunits. *Genes to cells : devoted to molecular & cellular mechanisms* **12**, 1357-1370 (2007).
207. Yanagida, M. Cellular quiescence: are controlling genes conserved? *Trends in cell biology* **19**, 705-715 (2009).
208. Carnegie, G., Means, C. & Scott, J. A-kinase anchoring proteins: from protein complexes to physiology and disease. *IUBMB life* **61**, 394-406 (2009).
209. Mackintosh, C. Dynamic interactions between 14-3-3 proteins and phosphoproteins regulate diverse cellular processes. *The Biochemical journal* **381**, 329-342 (2004).
210. Gwinn, D. *et al.* AMPK phosphorylation of raptor mediates a metabolic checkpoint. *Molecular cell* **30**, 214-226 (2008).
211. Sancak, Y. *et al.* Ragulator-Rag complex targets mTORC1 to the lysosomal surface and is necessary for its activation by amino acids. *Cell* **141**, 290-303 (2010).
212. Collis, S., DeWeese, T., Jeggo, P. & Parker, A. The life and death of DNA-PK. *Oncogene* **24**, 949-961 (2005).
213. Kastan, M. & Bartek, J. Cell-cycle checkpoints and cancer. *Nature* **432**, 316-323 (2004).

214. Murr, R., Vaissière, T., Sawan, C., Shukla, V. & Herceg, Z. Orchestration of chromatin-based processes: mind the TRRAP. *Oncogene* **26**, 5358-5372 (2007).
215. Nicholson, P. *et al.* Nonsense-mediated mRNA decay in human cells: mechanistic insights, functions beyond quality control and the double-life of NMD factors. *Cellular and molecular life sciences : CMLS* **67**, 677-700 (2010).
216. Lipkowitz, S. & Weissman, A. RINGs of good and evil: RING finger ubiquitin ligases at the crossroads of tumour suppression and oncogenesis. *Nature reviews. Cancer* **11**, 629-643 (2011).
217. Busino, L. *et al.* Fbxw7 α - and GSK3-mediated degradation of p100 is a pro-survival mechanism in multiple myeloma. *Nature cell biology* **14**, 375-385 (2012).
218. Keats, J. *et al.* Promiscuous mutations activate the noncanonical NF-kappaB pathway in multiple myeloma. *Cancer cell* **12**, 131-144 (2007).
219. Bai, D., Ueno, L. & Vogt, P. Akt-mediated regulation of NFkappaB and the essentialness of NFkappaB for the oncogenicity of PI3K and Akt. *International journal of cancer. Journal international du cancer* **125**, 2863-2870 (2009).
220. Lau, A., Fukushima, H. & Wei, W. The Fbw7 and betaTRCP E3 ubiquitin ligases and their roles in tumorigenesis. *Frontiers in bioscience : a journal and virtual library* **17**, 2197-2212 (2012).
221. Wu, C. & Ghosh, S. beta-TrCP mediates the signal-induced ubiquitination of IkappaBbeta. *The Journal of biological chemistry* **274**, 29591-29594 (1999).
222. Mailand, N., Bekker-Jensen, S., Bartek, J. & Lukas, J. Destruction of Claspin by SCFbetaTrCP restrains Chk1 activation and facilitates recovery from genotoxic stress. *Molecular cell* **23**, 307-318 (2006).
223. Peschiaroli, A. *et al.* SCFbetaTrCP-mediated degradation of Claspin regulates recovery from the DNA replication checkpoint response. *Molecular cell* **23**, 319-329 (2006).
224. Latres, E., Chiaur, D. & Pagano, M. The human F box protein beta-Trcp associates with the Cull1/Skp1 complex and regulates the stability of beta-catenin. *Oncogene* **18**, 849-854 (1999).
225. Kuehl, W. & Bergsagel, P. Molecular pathogenesis of multiple myeloma and its premalignant precursor. *The Journal of clinical investigation* **122**, 3456-3463 (2012).
226. Kawano, M. *et al.* Autocrine generation and requirement of BSF-2/IL-6 for human multiple myelomas. *Nature* **332**, 83-85 (1988).
227. Hideshima, T., Mitsiades, C., Tonon, G., Richardson, P. & Anderson, K. Understanding multiple myeloma pathogenesis in the bone marrow to identify new therapeutic targets. *Nature reviews. Cancer* **7**, 585-598 (2007).
228. Ferlin, M. *et al.* Insulin-like growth factor induces the survival and proliferation of myeloma cells through an interleukin-6-independent transduction pathway. *British journal of haematology* **111**, 626-634 (2000).
229. Vivanco, I. & Sawyers, C. The phosphatidylinositol 3-Kinase AKT pathway in human cancer. *Nature reviews. Cancer* **2**, 489-501 (2002).
230. Hennessy, B., Smith, D., Ram, P., Lu, Y. & Mills, G. Exploiting the PI3K/AKT pathway for cancer drug discovery. *Nature reviews. Drug discovery* **4**, 988-1004 (2005).
231. Hardt, M., Chantaravisoot, N. & Tamanoi, F. Activating mutations of TOR (target of rapamycin). *Genes to cells : devoted to molecular & cellular mechanisms* **16**, 141-151 (2011).
232. Meric-Bernstam, F. & Gonzalez-Angulo, A. Targeting the mTOR signaling network for cancer therapy. *Journal of clinical oncology : official journal of the American Society of Clinical Oncology* **27**, 2278-2287 (2009).
233. Vilar, E., Perez-Garcia, J. & Tabernero, J. Pushing the envelope in the mTOR pathway: the second generation of inhibitors. *Molecular cancer therapeutics* **10**, 395-403 (2011).
234. Brachmann, S. *et al.* Specific apoptosis induction by the dual PI3K/mTor inhibitor NVP-BEZ235 in HER2 amplified and PIK3CA mutant breast cancer cells. *Proceedings of the National Academy of Sciences of the United States of America* **106**, 22299-22304 (2009).

235. Caravita, T., de Fabritiis, P., Palumbo, A., Amadori, S. & Boccadoro, M. Bortezomib: efficacy comparisons in solid tumors and hematologic malignancies. *Nature clinical practice. Oncology* **3**, 374-387 (2006).
236. Oakervee, H. *et al.* PAD combination therapy (PS-341/bortezomib, doxorubicin and dexamethasone) for previously untreated patients with multiple myeloma. *British journal of haematology* **129**, 755-762 (2005).
237. Trembley, J., Wang, G., Unger, G., Slaton, J. & Ahmed, K. Protein kinase CK2 in health and disease: CK2: a key player in cancer biology. *Cellular and molecular life sciences : CMLS* **66**, 1858-1867 (2009).
238. Piazza, F. *et al.* Protein kinase CK2 in hematologic malignancies: reliance on a pivotal cell survival regulator by oncogenic signaling pathways. *Leukemia : official journal of the Leukemia Society of America, Leukemia Research Fund, U.K* **26**, 1174-1179 (2012).
239. Ruzzene, M., Di Maira, G., Tosoni, K. & Pinna, L. Assessment of CK2 constitutive activity in cancer cells. *Methods in enzymology* **484**, 495-514 (2010).
240. Guo, C. *et al.* A potential role of nuclear matrix-associated protein kinase CK2 in protection against drug-induced apoptosis in cancer cells. *The Journal of biological chemistry* **276**, 5992-5999 (2001).
241. Di Maira, G. *et al.* Comparative analysis of CK2 expression and function in tumor cell lines displaying sensitivity vs. resistance to chemical induced apoptosis. *Molecular and cellular biochemistry* **316**, 155-161 (2008).
242. Channavajhala, P. & Seldin, D. Functional interaction of protein kinase CK2 and c-Myc in lymphomagenesis. *Oncogene* **21**, 5280-5288 (2002).
243. Piazza, F. *et al.* Multiple myeloma cell survival relies on high activity of protein kinase CK2. *Blood* **108**, 1698-1707 (2006).
244. Battistutta, R. Protein kinase CK2 in health and disease: Structural bases of protein kinase CK2 inhibition. *Cellular and molecular life sciences : CMLS* **66**, 1868-1889 (2009).
245. Richardson, P. *et al.* Perifosine plus bortezomib and dexamethasone in patients with relapsed/refractory multiple myeloma previously treated with bortezomib: results of a multicenter phase I/II trial. *Journal of clinical oncology : official journal of the American Society of Clinical Oncology* **29**, 4243-4249 (2011).
246. Wan, X., Harkavy, B., Shen, N., Grohar, P. & Helman, L. Rapamycin induces feedback activation of Akt signaling through an IGF-1R-dependent mechanism. *Oncogene* **26**, 1932-1940 (2007).
247. Hoang, B. *et al.* Targeting TORC2 in multiple myeloma with a new mTOR kinase inhibitor. *Blood* **116**, 4560-4568 (2010).
248. Lohrisch, C. & Piccart, M. HER2/neu as a predictive factor in breast cancer. *Clinical breast cancer* **2**, 129 (2001).

8 List of figures and tables

8.1 Figures

Figure 1: Different stages of MM.....	3-12
Figure 2: Ribbon diagrams of Ub and two forms of di-ubiquitin.....	3-16
Figure 3: The structure of the proteasome.....	3-17
Figure 4: The ubiquitin-proteasome system.....	3-19
Figure 5: The SCF complex.....	3-20
Figure 6: The many functions of deubiquitylating enzymes.....	3-21
Figure 7: Domains in mTOR.....	3-23
Figure 8: Schematic illustration of the mTORC1 and the mTORC2 components.....	3-26
Figure 9: Silver Gel of TAP- purified Fbxo9 for mass spectrometry analysis. [Data provided by Dr. V.Fernández-Sáiz].....	5-57
Figure 10: Fbxo9 is the only F-box protein that interacts with Tel2 and Tti1. [Data provided by Dr. V.Fernández-Sáiz].....	5-59
Figure 11: Reciprocal co-immunoprecipitation of Fbxo9 with Tti1 and Tel2. [Data provided by Dr. V.Fernández-Sáiz].....	5-60
Figure 12: SCF ^{Fbxo9} specifically ubiquitylates Tel2 and Tti1. [Data provided by Dr. V.Fernández-Sáiz].....	5-60
Figure 13: SCF ^{Fbxo9} specifically ubiquitylates Tel2 and Tti1. [Data provided by Dr. V.Fernández-Sáiz].....	5-61
Figure 14: Cell cycle profile of Tel2 and Tti1.....	5-62
Figure 15: Effects of serum deprivation (SD) and serum addition (SA) in T98G..	5-63
Figure 16: Tel2/Tti1 degradation is mediated by the UPS in an Fbxo9-dependent manner..	5-64
Figure 17: Fbxo9 binding to Tel2/Tti1 upon SD.....	5-64
Figure 18: Co-localisation of Fbxo9 and Tel2/Tti1 under S and SD.....	5-65
Figure 19: Fbxo9 depletion in serum starvation.....	5-66
Figure 20: Fbxo9 promotes degradation of Tel2/Tti1 in response to SD in primary IMR90 cells..	5-67
Figure 21: <i>De novo</i> synthesis of mTOR and ATM is mediated by Fbxo9.....	5-67
Figure 22: Cell size is increased upon loss of Fbxo9.....	5-68
Figure 23: Elevated Cap-dependent translation during starvation upon depletion of Fbxo9.....	5-68
Figure 24: Proliferation is reduced upon Fbxo9 loss.....	5-69
Figure 25: Apoptosis induction is enhanced by Fbxo9 depletion.....	5-70
Figure 26: Tel2/Tti1 degradation via Fbxo9 specifically regulates differential mTOR signalling	5-70

Figure 27: Binding site for Fbxo9 to Tel2 or Tti1. [Data provided by Dr. V.Fernández-Sáiz].....	5-71
Figure 28: Silver gel of purified Tel2 and Tti1 proteins for comparative phosphopeptide enrichment. [Data provided by Dr. V.Fernández-Sáiz].....	5-72
Figure 29: Phosphorylation analysis of Tel2. [Data provided by Dr. S. Lemeer and Prof. Dr. B. Küster].....	5-72
Figure 30: Phosphorylation analysis of Tti1. [Data provided by Dr. S. Lemeer and Prof. Dr. B. Küster].....	5-73
Figure 31: Degrons in Tel2/Tti1 are evolutionary conserved. [Data provided by Dr. V.Fernández-Sáiz].....	5-74
Figure 32: Stability of Tti1 WT and Tti1(S828A) mutant and Tel2 WT and Tel2(S485A) mutant..	5-74
Figure 33: Effects of the non-degradable degron mutant of Tti1..	5-75
Figure 34: Expression of a non-degradable Tti1 mutant differentially affects mTOR signalling.....	5-76
Figure 35: <i>in vitro</i> ubiquitylation of Tel2 and Tti1 proteins is dependent on their phospho-degrons. [Data provided by Dr. V.Fernández-Sáiz].....	5-77
Figure 36: Kinase dependent ubiquitylation of Tel2 and Tti1 proteins. [Data provided by Dr. V.Fernández-Sáiz].....	5-77
Figure 37: CK2 phosphorylates Tel2 and Tti1 degrons <i>in vitro</i>	5-78
Figure 38: CK2 phosphorylation of Tel2/Tti1 mediates binding to Fbxo9 <i>in vitro</i>	5-79
Figure 39: CK2 activity enhances Tel2/Tti1 ubiquitylation by SCF ^{Fbxo9}	5-79
Figure 40: Intrinsic kinase activity of CK2 towards Tti1 and Tel2.....	5-80
Figure 41: CK2 translocates from nucleoplasm to cytosol upon serum starvation.....	5-81
Figure 42: CK2 associates with Tel2/Tti1 upon serum deprivation.....	5-81
Figure 43: The phosphorylation and stability Tel2/Tti1 in SD are influenced by CK2. [Data provided by Dr. V.Fernández-Sáiz].....	5-82
Figure 44: CK2 impacts on Tel2/Tti1 phosphorylation and stability.....	5-82
Figure 45: Localisation of phospho-mimic degron-mutant Tel2.....	5-83
Figure 46: mTORC1-bound Tel2 and Tti1 are degraded in an Fbxo9-dependent and phospho-degron specific manner. [Data provided by Dr. V.Fernández-Sáiz]	5-84
Figure 47: mTORC1 and mTORC2 inhibitors reverse Fbxo9 depletion phenotypes. [Data provided by Dr. V.Fernández-Sáiz].....	5-85
Figure 48: Degradation of Tel2/Tti1 is specific for Raptor-bound fraction. [Data provided by Dr. V.Fernández-Sáiz].....	5-86
Figure 49: Overexpression of Fbxo9 and CK2 activates mTORC2 signalling.....	5-86
Figure 50: Fbxo9 overexpression increased cell survival and proliferation.....	5-87

Figure 51: Fbxo9 preferentially targets mTORC1-bound Tel2/Tti1. [Data provided by Dr. V.Fernández-Sáiz].....	5-88
Figure 52: Tel2/Tti1 degradation <i>in vivo</i> . [Data provided by Ruth Eichner]	5-89
Figure 53: Elevated mRNA levels of <i>Fbxo9</i> in human MM at different clinical stages..	5-90
Figure 54: Relevance of Fbxo9 overexpression in patients. [Data provided by Dr. C.Langer]	5-90
Figure 55: Response and survival correlate with Fbxo9 expression. [Data provided by Prof. L.Bullinger]	5-91
Figure 56: High Fbxo9 expression correlates with activation of Akt. [Data provided by Clemens Reiter].....	5-92
Figure 57: Fbxo9 expression correlates with asymmetric mTOR signalling in MM cell lines.....	5-93
Figure 58: Fbxo9 expression is not driven by phosphorylated Akt.....	5-93
Figure 59: CK2 kinase activity modulates Tel2/Tti1 stability [Data was partly provided by Ruth Eichner]	5-94
Figure 60: Survival of MM cells is dependent on Fbxo9 overexpression.....	5-94
Figure 61: Schematic model.....	6-96

8.2 Tables

Table 1: List of primary rabbit antibodies.....	4-35
Table 2: List of primary mouse antibodies.....	4-36
Table 3: List of secondary antibodies.....	4-36
Table 4: List of plasmids.....	4-38
Table 5: List of cloning primer sequences	4-39
Table 6: List of sequencing oligos.....	4-40
Table 7: List of qPCR probe sequences	4-40
Table 8: List of siRNA target strand sequences	4-41
Table 9: List of cell lines.....	4-42
Table 10: Sequences and modifications of identified peptides corresponding toTel2. [Data provided by Dr. S. Lemeer and Prof. Dr. B. Küster].....	5-58
Table 11: Sequences of identified peptides corresponding toTti1. [Data provided by Dr. S. Lemeer and Prof. Dr. B. Küster].....	5-59

9 Publications

Fernández-Sáiz V^{*} and Targosz BS^{*}, Lemeer S, Eichner R, Langer C, Bullinger L, Reiter C, Slotta-Huspenina J, Schroeder S, Knorn AM, Kurutz J, Peschel C, Pagano M, Kuster B, Bassermann F: *SCF-Fbxo9 and CK2 direct the cellular response to growth factor withdrawal via Tel2 and Tti1 degradation and promote survival in multiple myeloma*. Nature Cell Biology (2013)

*Equal contribution

Palagyi A, Neveling K, Plinninger U, Ziesch A, Targosz BS, Denk GU, Ochs S, Rizzani A, Meier D, Thasler WE, Hanenberg H, De Toni EN, Bassermann F, Schäfer C, Göke B, Schindler D, Gallmeier E: *Genetic inactivation of the Fanconi anemia gene FANCC identified in the hepatocellular carcinoma cell line HuH-7 confers sensitivity towards DNA-interstrand crosslinking agents*. Molecular Cancer (2010)

10 Danksagung

Bekanntermaßen ist es die Summe der vielen kleinen Dinge, die erst ein großes Ganzes hervorbringen können. Deshalb möchte ich mich hier bei allen Menschen, die direkt oder indirekt zum Gelingen meiner Doktorarbeit beigetragen haben von Herzen bedanken.

Besonders danken möchte zuallererst Dr. Florian Bassermann, der mich als seine erste Doktorandin in seinem neugegründeten Labor trotz vieler anderer Verpflichtungen stets intensiv betreut, unterstützt und motiviert hat. Seine begeisternde, positive Art hat maßgeblich zum Erfolg dieser Arbeit beigetragen.

Bei Prof. Dr. Claus Schwegheimer möchte ich mich für die freundliche Bereitschaft bedanken, meine Doktorarbeit als Vertreter von Seiten des Wissenschaftszentrums Weihenstephan für Ernährung, Landnutzung und Umwelt der Technischen Universität München zu betreuen.

Desweiteren möchte ich mich bei Prof. Dr. Christian Peschel für die Möglichkeit bedanken, meine Dissertation am haematologischen Forschungslabor am Klinikum rechts der Isar anzufertigen.

Spezieller Dank geht an Prof. Dr. Bernhard Küster und Dr. Simone Lemeer, die mit ihrer massenspektrometischen Analyse unserer Kandidaten-Proteine die Arbeit erst in Gang gebracht haben. Desweiteren möchte ich mich bei allen wissenschaftlichen Kooperationspartnern; Prof. Dr. Lars Bullinger, Dr. Christian Langer, Dr. Julia Slotta Huspenina, Dr. Moik und Dr. Michele Pagano für die erfolgreiche Zusammenarbeit bedanken.

A very special thank goes to Dr. Vanesa Fernández-Sáiz for teaching me how to be water, where I can always find help and how to avoid to become grey (and some spanish swearing...) Muchas Gracias!

Ganz herzlich bedanken möchte ich mich bei Sonja Schröder, die mit stoischer Ruhe und großer Genauigkeit in unermüdlicher Hilfe zum Gelingen meiner Experimente beigetragen hat, ohne dass ihr dabei der ansteckende Humor vergangen wäre. Ein weiterer Dank geht an Julia Kurutz, die mich auf der letzten Teilstrecke der Arbeit tatkräftig unterstützt hat.

Vielen Dank auch an Ruth Eichner und Clemens Reiter, die der Arbeit noch den nötigen Schliff von studierten Medizinerinnen verpasst haben.

Selbstverständlich möchte ich auch der gesamten AG Bassermann für die kollegiale und tolerante Arbeitsatmosphäre, die aufbauenden Worte in den schlechten Phasen und die ehrliche Freude in den guten Phasen danken. Ihr habt's ja auch net immer leicht gehabt.

Ebenfalls bedanken möchte ich mich bei der AG Duyster, die mit so einigen Materialien, Vorschlägen und Diskussionen meine Arbeit erleichtert haben. Ich danke hierbei auch Frau Budak, die mein geniales Chaos nicht zu oft „beseitigt“ hat.

Ein ganz persönlicher Dank geht an meine Eltern, die mich immer ermutigt haben zu lernen und an mich selbst zu glauben. Vielen Dank auch an meine Schwester, die wohl die Einzige ist, die auch dann an mich glauben würde, wenn ich versuchen würde den Mond vom Himmel zu holen – oder Spitzensportlerin zu werden. Nicht vergessen möchte ich auch die Weigells, die Foltmans, und den Barabend, die mich mit Rat und Tat gerne von meinen wissenschaftlichen Sorgen abgelenkt haben.

Und das Wichtigste am Schluss: An der Seite jeder erfolgreichen Wissenschaftlerin steht ein starker Mann, der möglichst nix über die Thematik weiß. Ein riesiger Dank an meinen Robert, für all die endlose, geduldige und selbstlose Unterstützung während der letzten Jahre.